Fall 2021

Transport, species-specific resource competition, and shallow water effects in coupled bio-physical ecosystem models for C. polykrikoides harmful algal blooms off the coast of Korea

Jang-Geun Choi
University of New Hampshire, Durham

Transport, species-specific resource competition, and shallow water effects in coupled bio-physical ecosystem models for *C. polykrikoides* harmful algal blooms off the coast of Korea

By

Jang-Geun Choi

BA, Pusan National University, 2015

MS, Pusan National University, 2016

DISSERTATION

Submitted to the University of New Hampshire

In Partial Fulfillment of

The Requirements for the Degree of

Doctor of Philosophy

in

Oceanography

September 2021

This dissertation has been examined and approved in partial fulfillment of the requirements for the degree of Doctor of Philosophy in Oceanography by

Dissertation Director, Thomas Lippmann, PhD

James Pringle, PhD

Robert Letscher, PhD

Joseph Salisbury, PhD

Elizabeth Harvey, PhD

Young-Heon Jo, PhD

On 9 August

Original approval signatures are on file with the University of New Hampshire Graduate School.

ACKNOWLEDGEMENTS

First, I would like to express my sincere thanks and gratitude to my advisor Tom Lippmann for his full support and dedication, and to James Pringle, Robert Letscher, Joseph Salisbury, Elizabeth Harvey, and Young-Heon Jo for being committee members and great discussions and comments for my studies. Also, thanks to Salme Cook, Josh Humberston, Katie Kirk, Will Lush, Patrick Hampson, Eunsang Cho, Jinjin Ha, SaeWon Kim, and Mingcheng Ren for their support. Finally, I would like to thank my family.

TABLE OF CONTENTS

LIST OF TABLES

LIST OF FIGURES

ABSTRACT

This thesis examines the role of transport and environmental variables in determining the occurrence or suppression of harmful algal blooms (HABs). In the first part, a simple 2-D diagnostic model is used to hindcast HABs occurring off the coast of Korea using observations of averaged environmental factors including nutrient concentration. Hindcasting results using the model show that physical transport of HABs is of the same order of importance as the environmental conditions in controlling HABs. The model reproduces the interannual variability of the observe HABs off the coast of Korea. The relative importance of the environmental factors based on limiting functional analysis suggest that phosphate, ammonium, and temperature are the most important (in that order), and that nitrate and light limitations have very little influence on the behavior of HABs.

In the second part, a modified version of the NPZD ecosystem model is used to examine the effects of species competition and nutrient limitation in the development of HABs. Solutions to the NPZD system of equations show that steady state (equilibrium) conditions cannot occur for two phytoplankton groups (one normal and one HAB) without the presence of zooplankton which effectively acts to replenish the nitrogen pool. When the zooplankton prefer different phytoplankton groups, different equilibrium states are found and depend on a threshold for nitrogen level that depends on functional group parameters (like growth and mortality rates). Solutions explain details of population dynamics underlying HABs and should be useful to find best-fit mode coefficients.

In the third part, the NPZD model is modified to include a bottom boundary condition describing sediment nitrification-denitrification process that necessitates both the inclusion of a functional phytoplankton group that fixes nitrogen, and the phosphorus cycle. The model shows why previous models that do not include specified bottom boundary conditions

unrealistically predict oligotrophic water in coastal regions, whereas inclusions of denitrification and nitrogen fixing group lead to phytoplankton spatial distributions consistent with observations.

INTRODUCTION

Harmful Algae Blooms (HABs), also referred to as red tides, indicate excessive blooms of monospecific phytoplankton in the ocean. Blooms of ichthyotoxic species significantly increase fish mortality, so can hamper fishery and aquaculture industries. Over the past several decades HABs have become more frequent and intense (Hallegraeff, 1993; Anderson et al., 2012). In Korea, in any given year, economic losses from *Cochlodinium polykrikoides* HABs amount to about US $1-60M for the aquaculture industries (Park et al., 2013). Complicating the Korean problem (and certainly elsewhere) is that the dominant species responsible for coastal HABs is shifting. In the 1980s, phytoplankton blooms along the Korean coast were fostered primarily by the diatom *Skeletonema costatum*; however, over the past two decades, the dinoflagellate *C. polykrikoides* has become much more dominant than the diatoms (Lee et al., 2013). Both quantitative and qualitative changes to HABs indicate that the ecosystem off the coast of Korea has changed considerably, and often attributed to factors related to global warming or excessive nutrient loading from human activity (Davidson et al., 2014; Gobler et al., 2017). The Korean problem is not unique; HABs in U.S. coastal waters have also become more frequent and qualitatively different with previous decades (Anderson, 1995; Lewitus et al., 2012).

In general, HABs are not fully understood, largely owing to the complex coupling of biological and geochemical processes with physical oceanography. Introduction of nutrients from river discharge, advection of nutrient rich water by ocean currents, favorable water temperature, and light intensity are all important factors that contribute to HABs (Lee, 2006; Kim et al., 2016; Lee et al., 2016). HABs are also influenced by ambient ecosystem and biogeochemical cycles, especially, interspecific competition. Lim et al. (2014) explored the

interspecific competition between the *C. polykrikoides* and diatom species (including *S. costatum*) in laboratory experiments and showed that the presence of diatoms inhibits growth of *C. polykrikoides*. Jeong et al. (2017) reported the succession of species in HABs and concluded that the dominant species causing blooms is determined by water temperatures and the nitrogen uptake ability of the species. Oh et al. (2015) developed a resource competition model between *C. polykrikoides* and diatom *Skeletonema sp.* that included resolving the nitrogen and phosphorous cycle. They argue that the absence of *C. polykrikoides* blooms over parts of the south coast of Korea is caused by a dominant diatom which defeats *C. polykrikoides* in the resource competition.

Although various factors contributing to HABs have been suggested, the quantitative contribution by each factor is difficult to ascertain and poorly understood. The problem is exacerbated by the recognition that some of the factors (and findings) compete or contradict each other. For example, Lee (2008) suggested downwelling favorable wind triggers HABs by aggregating cells, whereas Kim et al. (2016) suggested upwelling favorable winds fosters HABs by supplying nutrients. To understand such a complex system objectively, dynamics models that resolve both hydrodynamics and biogeochemical cycles are required.

In this work, we approach the problem in a hierarchal sense by starting from a simple 2-D diagnostic model to addressing more complex interactions with fully 3-D models that include biogeochemical processes. Our approach will specifically consider the HAB processes believed to be present along the south coast of Korea, but the results should be applicable to HABs generally. We first examine the limiting factors of HABs and relative importance between physical transport and biological activities using simple diagnostic model. The results shows that both have identical order of contribution to HABs. Secondly, we modify traditional ecosystem model describing nitrogen cycle to consider HABs and discuss internal dynamics of the model including interspecies competition between species in a conservative nitrogen

situation. Thirdly, we add complexity into the traditional ecosystem model to resolve complex biogeochemical mechanisms, such as interaction between settled detritus and sediment layer (nitrification-denitrification process) and additional phytoplankton functional groups that fix nitrogen utilized in support of the coastal ecosystem. The thesis develops a model that can resolve realistic conditions surrounding HABs and uses the model for understanding details of internal ecosystem dynamics.

CHAPTER 1

DEVELOPMENT OF PHYSICAL-BIOLOGICAL COUPLED DIAGNOSTIC MODEL FOR HABS

Abstract

Cochlodinium polykrikoides (*C. polykrikoides*) is one of the most notorious species causing Harmful Algae Blooms and result in enormous economic damage for aquaculture industries off the coast of Korea. The *C. polykrikoides* blooms are closely linked to not only biological environments but also physical phenomenon governed by transport process. To resolve and understand the interdisciplinary interaction of their bloom, we develop simple physical-biological coupled population dynamics model for *C. polykrikoides*. We analyze forcing fields and the growth rate theoretically. Using the model, contributions from biological and physical factors which contribute to the *C. polykrikoides* blooms are quantified, and then the mechanisms that determine blooms by the species are discussed.

The model successfully distinguishes blooming and non-blooming years from 2010 to 2017 and shows the occurrence of excessive blooms during 2013 to 2015 that agree well with field observations. Furthermore, simulated maximum cell concentrations of the blooms in 2013 and 2015 are quantitatively comparable with in situ observation. However, in 2014, the model overestimates bloom intensity and failed to resolve its termination. This implies the presence of an additional reduction mechanism that is not resolved by the model. Our result suggests that phosphate and ammonium, rather than nitrate, are the most important biological factors that contributes to the blooms, and that sea water temperature is the second most important factor.

Simulated *C. polykrikoides* blooms off the coast of Korea are terminated by transport to offshore regions where the food sources are greatly reduced. To quantify contributions by

the transport process, flushing rates are estimated from passive tracer experiments conducted for a simplified box model. When the waters off the south coast of Korea are rapidly flushed, *C. polykrikoides* blooms do not occur, a consequence of insufficient dwell time along the nutrient-rich south coast indicating that transport by currents acts as a sinking mechanism of blooms. Results from the diagnostic model indicate that: (1) contribution by physical transport is of the same order as biological activities of the bloom, and (2) phosphate, ammonium concentrations, and temperature are the important factors contribute to the *C. polykrikoides* blooms.

1.1. Introduction

As in many areas worldwide, over the past several decades the seas off the coast of Korean Peninsula have been increasingly adversely affected by Harmful Algal Blooms (HABs; Wang and Wu, 2009; Lee et al., 2013). Because HABs significantly increase fish mortality, they bring lasting damage to aquaculture industries in Korean waters (Tang et al., 2003; Park et al., 2013; Jeong et al., 2017). *Cochlodinium polykrikoides* is one of the most notorious species causing fish-killing blooms, and near Korea have become the most dominant species causing HABs since the 1970s (Lee et al., 2013). In 1998, economic losses caused by *C. polykrikoides* blooms occurring over two-month period exceeded USD $70 million (Kim and Shin, 1997). As a result, many studies were conducted from various points of view to better understand the triggers for *C. polykrikoides* blooms. For instance, monitoring systems were incorporated to observe the HABs (Wang and Wu, 2009; Lee et al., 2013), and there were many laboratory experiments to analyze physiological characteristics of *C. polykrikoides* (Kim et al., 2001; Lee et al., 2001; Kim et al., 2004; Yamatogi et al., 2005; Oh et al., 2006; Oh et al., 2010; Gobler et al., 2012; Cho and Cho, 2014). Algorithms applied to ocean color satellite images were developed to detect HABs (Son et al., 2011; Noh et al., 2018).

Figure 1.1 shows the study area and general circulation system for the month of August. The *C. polykrikoides* blooms initiated off the south coast of Korea are transported by the Tsushima Warm Current (TWC), East Korea Warm Current (EKWC), and Nearshore Branch (NB), each of which head toward the East/Japan Sea (Choi et al., 2014; Kim et al., 2016). Onitsuka et al. (2010) suggested that the transported *C. polykrikoides* blooms influence the blooms in the San-in coastal region of Japan. In this way, HABs are closely connected with physical transport mechanisms. Lee (2008) showed that *C. polykrikoides* blooms are initiated by intrusion of offshore waters toward onshore regions off the south coast of Korea. In addition, Kim et al. (2016) assessed the physical factors that contributed to *C. polykrikoides* blooms in 2013 in the East/Japan Sea: advection of *C. polykrikoides* from the south coast of Korea, upwelling (providing nutrients), suitable sea surface temperature (SST), and photosynthetically available radiation (PAR). Lee et al. (2016) also discussed physical factors causing *C. polykrikoides* blooms off the south coast of Korea and concluded that the blooms are governed by inflow of offshore sea water from the East China Sea, rather than discharge from land. They also mentioned the existence of a thermohaline front and inflow of the Changjiang diluted water containing high nutrient as key factors for the *C. polykrikoides* blooms. Jeong et al. (2017) investigated with observations the succession of dominant species causing HABs and suggested that vertical mixing of the water column determines the dominant species. Numerical modeling approaches can simulate complex physical-biological interactions and are skillful tools that can help understand the dynamics underlying HABs. Kwon and Cho (2002) developed an individual-based physical-biological coupled model for the *C. polykrikoides* and tried to simulate transport of the *C. polykrikoides* blooms observed off the south coast of Korea in 1998. However, their model was not verified in terms of bloom intensity such as cell concentration of the species.

The purpose of this study is to develop a simple physical-biological coupled diagnostic

model, and from numerical experiments quantify the contribution of ecological and physical factors for *C. polykrikoides* blooms. Several simplifications are made to reduce complexity of the diagnostic model, including time-independent environmental factors, dominant geostrophic velocity component, and calibration of biological coefficients as parameterization for unresolved biological mechanisms. Despite these simplifying assumptions, it will be shown that the model compares well with observations and reasonably describes interannual variability of HAB occurrence. In Section 1.2, we describe the governing equation for the *C. polykrikoides* diagnostic model and the observations that are used as model inputs. In Section 1.3, the model is verified by hindcasting *C. polykrikoides* blooms from 2013 to 2015, and ideal interannual experiments are conducted to assess whether the model can resolve the presence or absence of blooms from 2010 to 2017. In Section 1.4, simulation results are discussed to determine what kind of factors stimulate or suppress the growth of *C. polykrikoides* during the study periods. Conclusions from this study are summarized in Section 1.5.

1.2. Data and method

Advection of the *C. polykrikoides* population is simulated with geostrophic currents fields estimated from altimetry. Spatial resolution of the velocity field is $0.25^{\circ} \times 0.25^{\circ}$, and temporal resolution is 1 day but we linearly interpolate the velocity field to 0.2 days to satisfy the stability condition of the advection term. Ekman current component is not considered because geostrophic current in the study area (Figure 1.1) outperforms the Ekman current (Choi et al., 2018). Kim et al. (2016) also showed that the geostrophic current fields can explain the distribution of the tracers in the study area. They also simulated transport from the south coast of Korea to the East/Japan Sea using particle tracking experiments based on the geostrophic current fields, and the simulated trajectories of the particles based on geostrophic currents

corresponded to ocean color satellite images showing a *C. polykrikoides* bloom in the East/Japan Sea.

Biological growth influenced by nutrient concentration is resolved with in situ observations obtained by the Korean National Institute of Fisheries Science (NIFS) and Korean Oceanographic Data Center (KODC). For the onshore regions, nutrient data were collected from the fishery environmental monitoring system operated by NIFS. For the offshore region, the serial oceanographic observation dataset from KODC was used, except for ammonium data which were not available. Offshore ammonium concentration is known to be less than 15% of the nitrate concentration (Choi et al., 2005; Kim et al., 2013), so we simply assume that offshore ammonium concentration is 15% of the nitrate concentration. Because the bimonthly sampling interval of the NIFS and KODC environmental monitoring system is too course to resolve the expected temporal variability, we use the observations for the month of August when most *C. polykrikoides* blooms have occurred (Lee et al., 2013). As a consequence, herein it is assumed that environmental fields are do not change with time. Scattered observations were gridded using optimal interpolation methods. Model input nutrient fields are shown in Figure 1.2.

Sea water temperature and light intensity for August were obtained from monthly mean SST and PAR estimated from MODIS Aqua satellite images. Spatial resolution of the MODIS satellite image is 4 km but was downgraded to match the spatial resolution of the geostrophic velocity fields by averaging pixels of the ocean color satellite images within a grid cell (Figure 1.2). Simulation results were verified with observations obtained from the NIFS red tide information system that reports various species causing HABs and their cell concentrations off the coast of Korea.

1.2.1. Governing equation of biological *C. polykrikoides* population model

Here we design a simple diagnostic physical-biological coupled model which has structure similar to the model of Stock et al. (2005) who developed a diagnostic model for *Alexandrium fundyense* blooms in the Gulf of Maine coupled with a hydrodynamics circulation model. Their model was able to diagnose environmental conditions that resulted in *A. fundyense* blooms. He et al. (2008) also coupled the biological model for *A. fundyense* with the Regional Ocean Modeling System (ROMS) and graded major factors causing HABs through model sensitivity experiments. These studies show that diagnostic models can be used for quantitative assessment of the factors causing HABs. The difference between our model and Stock et al. (2005) is that our model is entirely based on observations. Although Stock et al. (2005) and He et al. (2008) used observations for nutrient fields, the other environmental factors, such as velocity fields and water temperature, were based on outputs from hydrodynamic models. On the other hand, our model uses geostrophic velocity fields estimated from altimetry measurements and water temperature from ocean color satellite images.

The governing equation for our physical-biological coupled model for *C. polykrikoides* population is defined as

$$\frac{\partial C}{\partial t} + \nabla \cdot \left(u_g C\right) = K\nabla^2 C + (g - m)C \tag{1.1}$$

where C is cell concentration of *C. polykrikoides*, u_g is geostrophic velocities, K is a lateral diffusion coefficient, g is growth rate, and m is mortality rate. The last two terms on the right-hand-side indicate a simple biological sink and source. Although there are more complex equations to describe the biological activities for HABs (Franks, 1997; Jeong et al., 2015), the simple source/sink form in (1.1) has been shown to be a skillful model with proper coefficient adjustment (Stock et al., 2005; He et al., 2008). It is worth noting that this single equation model does not simulate other state variables such as nutrient concentration and predator density; the governing equation for nutrient concentration is replaced with in situ observational

fields assumed to be time-independent (as we mentioned above). Similarly, predation is parameterized by a higher mortality rate. The advantage of this strategy is that the model requires fewer inputs and coefficients than more complex models, greatly reducing the uncertainties from the inputs and coefficients (Fulton et al., 2003; Soetaert and Herman, 2009). We expect that this diagnostic approach based on observations will be more realistic than using simulated output from numerical models which might include discrepancies with actual conditions. The lateral diffusion coefficient is arbitrarily chosen, but it is set so that the diffusion process becomes negligible relative to advection, consistent with satellite observations that show blooms follows streamlines of the velocity field (Kim et al., 2016).

1.2.1.1. Growth rate and model coefficient optimization

Growth rate g is a function of various environmental limiting factors. Herein we consider five factors: light intensity (I), sea water temperature (T), nitrate (N), ammonium (A), and phosphate (P) concentration. Limiting functions for *C. polykrikoides* have been well developed by many previous studies based on laboratory culturing experiments. Cho and Cho (2014) summarized previous studies for the limiting functions and suggested an optimized growth rate given by

$$g = g_{max}\, f_I(I) \cdot f_T(T) \cdot f_{Nutrient}(N, A, P) \tag{1.2}$$

where g_{max} indicates the constant maximum growth rate, and f_x is a limiting function that depends on any given factor x. We take limiting functions for water temperature and light intensity from Cho and Cho (2014) without modification which are given as

$$f_I = \frac{I - I_0}{I + I_1} \tag{1.3}$$

$$f_T = \left(\frac{T}{T_{opt}}\right)^{\alpha} exp\left[1 - \left(\frac{T}{T_{opt}}\right)^{\alpha}\right]. \tag{1.4}$$

On the other hand, nutrient limiting functions are defined as the Monod function given by

$$f_N = \frac{N}{N + K_N}\frac{A}{A + K_A}\frac{P}{P + K_P}. \quad (1.5)$$

Half saturation concentrations, K_x, for each nutrient limitation function x and constant mortality rate coefficient are determined using a genetic algorithm approach to find the best-fit model coefficients. It is worth noting that the HAB model developed by Stoke et al. (2005) also optimized theses coefficients. A cost function is defined as root-mean-square difference between modeled and measured maximum *C. polykrikoides* cell concentration off the coast of Korea. Only observations during 2013 are used for the optimization, and the other observations are used to validate the model. Table 1.1 summarizes the model coefficients used in this study.

1.2.2. Hindcasting experiment for massive *C. polykrikoides* blooms from 2013 to 2015

From 2013 to 2015, the NIFS red tide information system reported massive *C. polykrikoides* blooms covering both the south and east coasts of Korea. To simulate the *C. polykrikoides* blooms, we set initial conditions in each year by filling the south coast of Korea (red box in Figure 1) using constant *C. polykrikoides* cell concentration observed on 15 July 2013, 27 July 2014, and 3 August 2015. The cell concentrations for each population are 1,700, 130, and 960 cell/mL, respectively. These initial intensities of the bloom and launching times are based on the observations from the NIFS red tide information system. Hindcasting results are later compared with observations to verify the model in Section 1.3.1.

1.2.3. Ideal interannual experiment from 2010 to 2017

C. polykrikoides populations with 10,000 cell/mL concentration were launched along the south coast of Korea (red box in Figure 1.1) on 10 July in each year from 2010 to 2017 to test whether the model can distinguish blooming and non-blooming years. These

concentrations have identical distribution with the hindcast experiments. The time of the bloom initiation is the same as used in particle tracking experiments by Kim et al. (2016). Results are compared with observations in Section 1.3.2, and the factors that contribute to the growth of *C. polykrikoides* are examined by analyzing forcing fields in Section 1.4.

1.2.4. Passive tracer experiment and simplified box model

To quantify contributions from physical transport by ocean currents, we estimate flushing rate by conducting passive tracer experiments. The governing equation for the passive tracer is given by

$$\frac{\partial P}{\partial t} + \nabla \cdot \left(u_g P\right) = K\nabla^2 P \tag{1.6}$$

where P is the concentration of the passive tracer. Initial concentrations are defined as one along the south coast of Korea (red box in Figure 1.1) and zero in the other areas. This distribution is identical with initial conditions of *C. polykrikoides* population in the other experiments. Equation (1.6) can be simplified to represent total mass of the passive tracer in the area, and given by

$$\frac{d(VP)}{dt} = Q_{in}P_{in} - Q_{out}P_{out} \tag{1.7}$$

where Q_{in}, Q_{out}, P_{in}, P_{out}, and V indicate inward or outward water discharge, passive tracer concentrations of inflow and outflow water, and the volume of the area, respectively. We assume that $Q_{in} = Q_{out} = Q$, $P_{in} = 0$, and $P_{out} = P$, corresponding to the configuration of initial and boundary conditions of the ideal interannual experiments discussed in the previous section. The flushing rate, Q/V, can be given as

$$Q/V = -\frac{1}{P}\frac{dP}{dt}. \tag{1.8}$$

We calculate flushing rate using time series of spatially averaged P in the area (red box in Figure 1.1) from the passive tracer experiments. The flushing rate can be considered as an index describing the contribution of physical transport for the tracer concentration within the box. Similarly, the governing equation for averaged *C. polykrikoides* concentration in the box can be expressed as

$$\frac{dC}{dt} = (g - m)C - \frac{Q}{V}C \tag{1.9}$$

The first term on the right-hand-side indicates the change rate owing to biological activity, and the second term indicates the change rate caused by physical transport. The flushing rate term in (1.9) implies that the physical transport acts as a sinking mechanism for *C. polykrikoides* concentration (from the Eulerian point of view). Because flushing rate (Q/V) has the same units as the growth or mortality rate ($g - m$), contributions from biological effects and those by physical transport (Q/V) can be directly compared. Results are discussed in Section 1.4.2.

1.3. Results

1.3.1. Hindcasted large *C. polykrikoides* blooms from 2013 to 2015

Figure 1.3 shows observed and modeled time series for maximum *C. polykrikoides* cell concentration off the coast of Korea from 2013 to 2015. In 2013 and 2015, the model reasonably reproduces the observed evolution of the *C. polykrikoides* bloom, including both increasing and decreasing phases. In 2014, although the model plausibly describes an exponential increase of the cell concentration until beginning of September, the termination of the bloom is not captured by the model, and cell concentration continuously increases. We suppose that the mismatch with observations in 2014 is due to structural errors inherent to the diagnostic model which assumes time-independent environmental factors. Because the model uses time-independent environmental forcing fields, it cannot resolve changes to the

environment caused by the bloom, such as depletion of nutrients. Furthermore, the model parameterizes all possible sinking mechanisms as a first order reaction with constant coefficients but does not consider sinking mechanisms varying with time such as an increase in predation or virus population as pray increases (Brussaard, 2004; Mitra and Flynn, 2006). The failure of the model to describe the bloom in 2014 clearly shows the limitation of our simple diagnostic model and presence of additional sinking mechanisms.

The skill of the model is not high enough to precisely hindcast blooms of *C. polykrikoides* (Figure 1.3). In addition to the unresolved termination of the observed HAB in 2014, the high frequency variability (including spiky-like observations of extremely high cell concentration) observed in 2013 and 2015 is not resolved. This is perhaps not surprising since it is inevitable that observed cell concentrations for the HABs species have high variability and the measurements range 5 orders of magnitude (from 10 to 10^5). Moreover, the model has much lower spatial resolution than real phenomenon, and thus renders spatially averaged quantities that cannot resolve the high spatial variability of the observations. It should be noted that although initial distributions of *C. polykrikoides* are quite arbitrary, the maximum cell concentrations of the initial conditions are based on observations. These uncertainties in the initial conditions also contribute to the mismatch with observations, and result in modeled blooms that are much smoother than the observations. This smoothing was also experienced by the model from Stock et al. (2005). Nevertheless, we conclude that the hindcast results from 2013 and 2015 indicates plausibility of the model, and further note that even though the termination is not simulated, the initial net change rate of the cell concentration in 2014 before September agrees with observations.

1.3.2. Simulation results of ideal interannual experiment from 2010 to 2017

Figure 1.4 shows the growth rate g, simulated distribution of *C. polykrikoides* in the ideal interannual experiments, and observations of *C. polykrikoides* blooms off the coast of Korea for each year. Simulated distribution of *C. polykrikoides* shows large *C. polykrikoides* blooms from 2013 to 2015, but that the intensity of the blooms in the other years are remarkably weaker (Figure 1.4). These results correspond to observations showing the large blooms from 2013 to 2015, and absence of blooms in 2010, 2011, 2016, and 2017 (Figure 1.4). This suggests that the key dynamics causing *C. polykrikoides* blooms are included in the model and show that interannual variability predicted by the model is plausible. However, the model does not accurately reproduce blooms of small intensity along the south coast of Korea; for example, discrepancies between the simulations and observations in 2012.

1.4. Discussion

1.4.1. Contribution of environmental factors

Figure 1.5 shows the calculated limiting functions for each of the environmental factors. All limiting functions were designed to have non-dimensional values ranging 0 to 1 and multiplied by the constant maximum growth rate. Consequently, values of limiting functions indicate how much growth of *C. polykrikoides* is stimulated by the factor. Moreover, contributions from an environmental factor to the *C. polykrikoides* bloom cannot be compared with those from another factor because each environmental factor itself has different units. In contrast, because the limiting functions are nondimensional, they can be compared to each other. Table 1.2 shows the spatially averaged value of each limiting function for the south coast of Korea (red box in Figure 1.1). Limitation from light intensity did not occur in any year from 2010 to 2017, and its deviation is negligible compared with the other functions indicating that light intensity is not a key factor contributing to interannual variability of the *C. polykrikoides* blooms. In contrast, the variation of temperature limitation is an order of magnitude larger than

for light intensity (Table 1.2). In particular, anomalous high sea surface temperature in 2016 (Figure 1.2) significantly limited growth of *C. polykrikoides* (Figure 1.5). The average value for the temperature limiting function from 2010 to 2017 was 0.88, but it was 0.75 in 2016 (Table 1.2), which indicates that about 25% of the growth rate was additionally suppressed by the high sea temperature occurring in 2016.

Limitations from phosphate and ammonium are more considerable than that of temperature, including interannual variability (Figure 1.5). The phosphorous limitation agrees with recent observations reporting that considerable phosphate limitation exists off the marginal coastal ocean around the Korean Peninsula (Jang et al., 2019). As a nitrogen resource, the model shows that *C. polykrikoides* bloom is limited by ammonium more so than nitrate. This may be a result of *C. polykrikoides* having flexible nitrogen nutrient availability (Kim et al., 2001; Kudela et al., 2008; Gobler et al., 2012). Furthermore, Kim et al. (2001) showed that *C. polykrikoides* in Korean waters have preference for ammonium based on laboratory experiments.

1.4.2. Contribution of transport

Although *C. polykrikoides* growth rates are mainly suppressed by nutrient concentration and temperature, there are still higher growth rates than mortality rates along the south coast of Korea in every year from 2010 to 2017 (Figure 1.4 and Table 1.2). Therefore, the biological sinking and source term in equation (1.1) is positive, and blooming conditions for *C. polykrikoides* occur (section 2.1.2). Consequently, in term of biological aspects alone, *C. polykrikoides* blooms should be simulated in every year. However, in spite of the larger growth than mortality rates, the blooms are not simulated every year. This result is attributed to the physical transport mechanisms that contributes to reduction locally of *C. polykrikoides*. From the Eulerian point of view, the advection term in equation (1.1) acts as a sinking term for *C.*

polykrikoides cell concentration off the south coast of Korea. The governing equation (1.9) for time series of *C. polykrikoides* cell concentration off the coast of Korea, can be driven by spatially integrating (1.1) (Cushman-Roisin and Beckers, 2011); that is, the flushing term in (1.9) is induced by the advection term in (1.1). As a result, (1.9) shows new blooming ($g - m - Q/V > 0$) and non-blooming ($g - m - Q/V < 0$) conditions that take into account the influence by physical transport (or flushing rate). The physical consequence of the flushing rate is how rapidly water within a given area is replaced by new water from outside. The reciprocal of the flushing rate is known as residence time, which indicates the time required to replace old water in an area with new water. Accordingly, low flushing rates indicate long residence time, so waters will remain for a longer time along the south coast of Korea where the bloom can exponentially increase due to larger growth than mortality rates (Figure 1.4). On the other hand, high flushing rates indicate that waters along the south coast of Korea are quickly discharged to offshore regions. From the Eulerian point of view, cell concentration is removed in the area of interest by the transport. From the Lagrangian prospective, cell concentrations still exist in the waters that are transported away by the surface flow, but the transported cell concentration exponentially decreases in time due to reduced growth rates that fall below the mortality rate (Figure 1.4).

Table 1.2 shows flushing rates calculated by passive tracer experiments for each year. In 2013 and 2014, much lower flushing rates were estimated (Table 1.2) than in other years, a time period that corresponds to large blooms in the simulation results (Figure 1.4). Flushing rate in 2015 was not significantly low, but relatively higher biological growth rates were estimated due to favorable nutrient concentrations and temperature condition than other non-blooming years (Table 1.2). Consequently, in 2015 there was positive net growth rate ($g - m - Q/V$) indicating blooming conditions that coincides with simulation results indicating the presence of blooms that year (Figure 1.7). Table 1.2 also shows that negative net growth rates

were estimated in the years when blooms were not simulated. In 2010 and 2012, temperature conditions were similar to those of blooming years, but there were relatively high flushing rates along with heightened phosphate limitation (Table 1.2), resulting in net growth rate that was negative consistent with the absence of a bloom. In 2011, the flushing rate was comparable to that of 2014 when blooms were simulated, but the ammonium condition was notably lower than the other years (Table 1.2). Similarly, in 2016 the most dominant flushing rate and temperature limitation suppressed growth of *C. polykrikoides*. Significant growth suppression existed from both phosphate and flushing in 2017. All together, these results show that the growth of *C. polykrikoides* is stimulated or inhibited mainly by three factors: nutrient concentration, temperature, and flushing rate, and that the contribution from each factor is different each year. As a nutrient limitation, the influence of phosphate is likely to be more dominant than that of ammonium.

As previously mentioned, the units of flushing rate are equivalent to those of growth or mortality rate, so we can determine the relative importance between biological activity ($g - m$) and physical transport (Q/V). Although averaged flushing rate, $Q/V = 0.114$, is larger than biological source, $g - m = 0.112$, they are of the same order (Table 1.2). This implies that the growth of *C. polykrikoides* off the coast of Korea is usually suppressed by physical transport, and the bloom is triggered when the condition is perturbed by an increase in biological source or decrease in physical ventilation. Consequently, the Damköhler number (ratio between biological source and flushing rate) is of order one off the south coast of Korea (Table 1.2), which indicates that both biological and physical process are important. The fact that flushing rates from geostrophic current fields plausibly describe the presence of *C. polykrikoides* bloom along the south coast of Korea implies that the geostrophic current component plays an important role in determining residence time for the region. Furthermore, as previously mentioned, hindcasting results (Section 1.2.1) showed that the *C. polykrikoides* blooms off the

coast of Korea are terminated by waters off the south coast being ventilated and transported toward the East/Japan Sea by the TWC. This suggests the importance of the TWC in determining flushing rate and the termination of blooms off the coast of Korea.

It should be noted that the model assumes that environmental factors are time-independent and that the velocity fields are governed by geostrophic balance; each of these approximations influences the model results. In particular, the model failed to resolve the termination of the bloom in 2014 suggesting the presence of other sinking mechanisms that are not considered by model. We presume that time-dependent ecological conditions, including depletion of nutrient or grazing from predators, are possible candidates. *C. polykrikoides* is known to have significant interspecific competition (Lim et al., 2014; Jeong et al., 2015; Jeong et al., 2017), so it too can act as a possible sinking mechanism. To resolve time-dependent ecological sinking mechanisms, the model in this study should be coupled to other ecosystem models. In addition, *C. polykrikoides* blooms can be triggered by cysts of the species (Kim et al., 2007). He et al. (2008) reported that cyst concentration was the most important factor causing *A. fundyense* blooms in 2005. Unfortunately, the excystment mechanism of the *C. polykrikoides* is poorly understood, and more detailed descriptions for excystment are required to improve model performance.

1.5. Conclusion

In this work we present a simple coupled physical-biological diagnostic model for *C. polykrikoides* along the south coast of Korea that is initiated entirely by observations: nutrients fields from in situ measurements, temperature and light intensity from ocean color satellite, and velocity fields estimated from altimetry. Despite errors in initial conditions, model coefficients, and assumptions, the model reasonably well simulates *C. polykrikoides* blooms comparable with observed cell concentrations (Figure 1.3 and 1.4). This implies that the

governing equation is appropriate for describing the behavior of the *C. polykrikoides* blooms. Although the simple model cannot perfectly resolve *C. polykrikoides* blooms, the model reveals important dynamics of the bloom. Damköhler numbers of *C. polykrikoides* blooms are found to be of order one off the south coast of Korea, indicating that both biological activities and physical transport contribute equally to blooms. The numerical experiments using the simple model show that lateral transport by geostrophic currents can act as a considerable local sink of *C. polykrikoides* and contributes to blooming and non-blooming conditions each year between 2010 and 2017. The hindcast experiments reveal that the large blooms occurring in 2013 and 2015 are terminated by an increase in transport out of the region.

In summary, a coupled physical-biological diagnostic model for *C. polykrikoides* blooms successfully simulates the presence and absence of blooms from 2010 to 2017 off the coast of Korea. Moreover, simulated maximum cell concentrations are consistent with observations. Detailed physical-biological interaction mechanisms based on modeling results and a simplified box model show that flushing of coastal waters inhibits growth of *C. polykrikoides* and terminates their blooms. Contributions to net growth by flushing rate is of the same order as biological activities. Environmental factors that cause the blooms from 2010 to 2017 were examined by analyzing forcing functions: nitrate, ammonium, phosphate, temperature, light intensity, and flow fields. Consequently, modeling results suggest that (1) physical transport is important as much as biological activities and (2) considerable environmental factors influencing the biological activities are phosphate, ammonium concentration, and temperature.

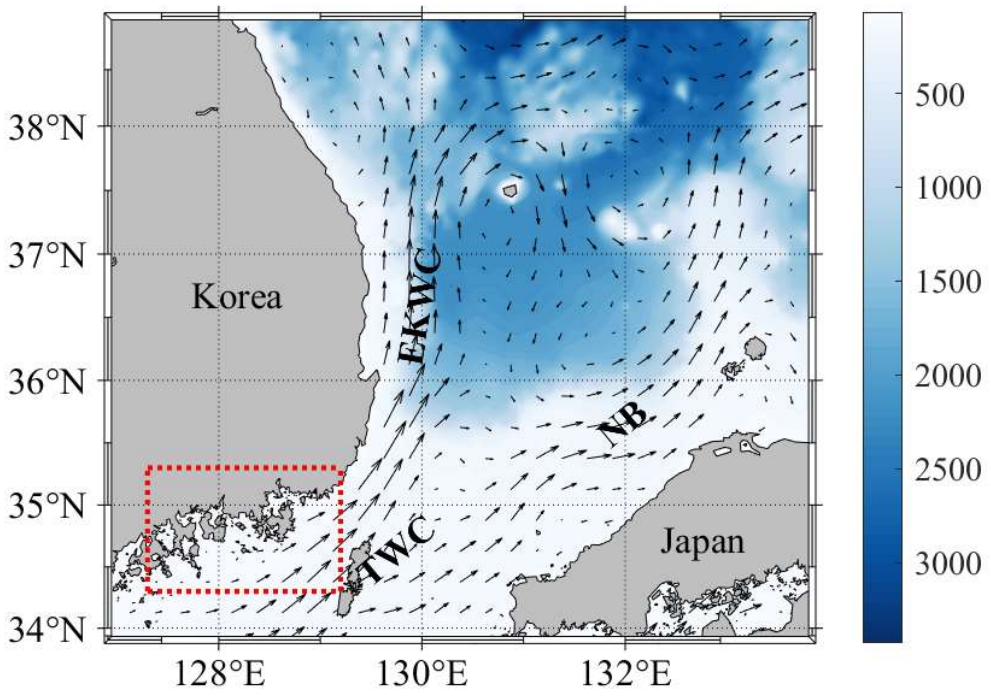

Figure 1.1. Study area and current system. The velocity field is climatological geostrophic currents in August from 2010 to 2017. Red box indicates the south coast region where *C. polykrikoides* bloom is initiated.

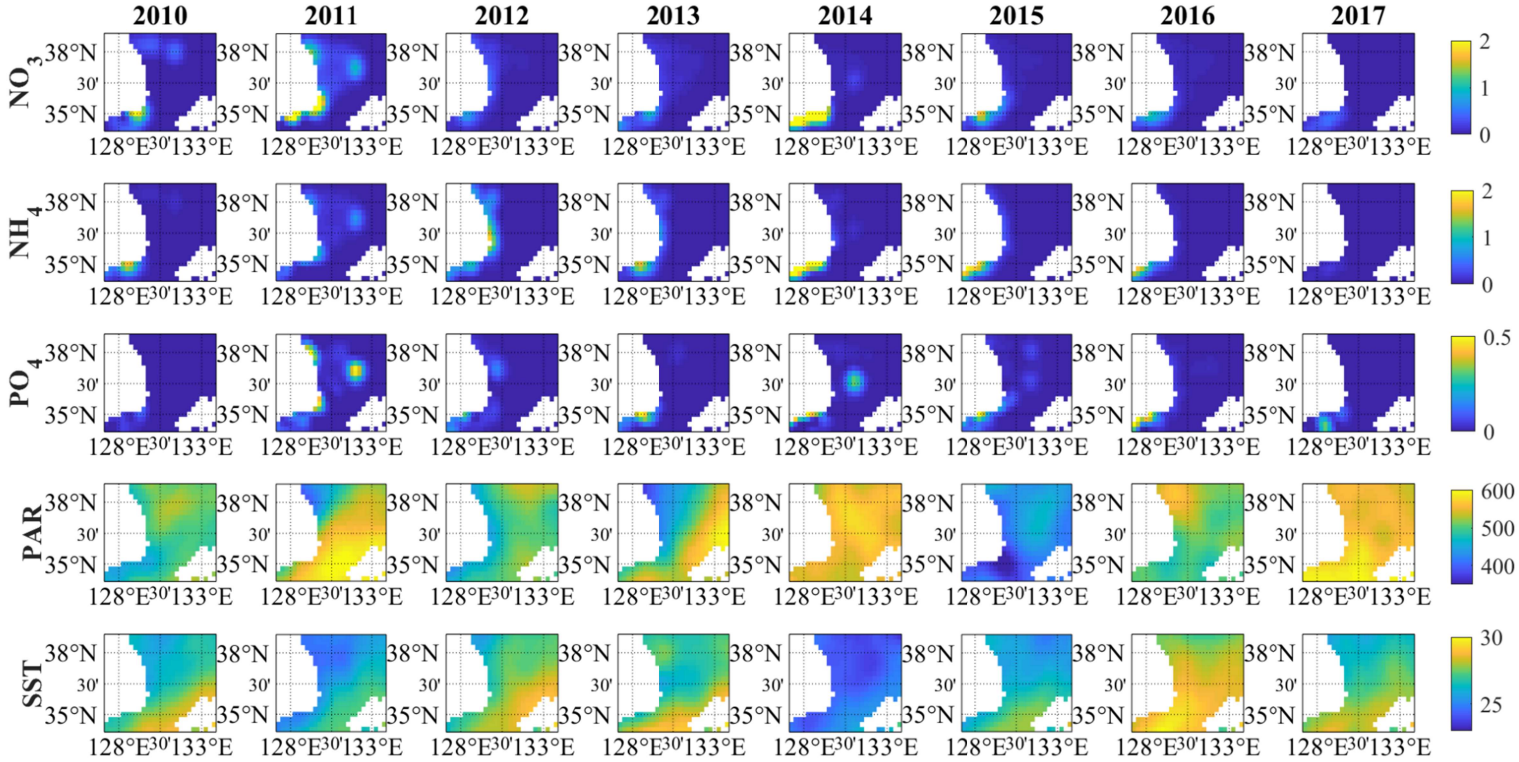

Figure 1.2. Nitrate, ammonium, phosphate, light intensity, and sea surface temperature from 2010 to 2017 in each August, which are used as model inputs.

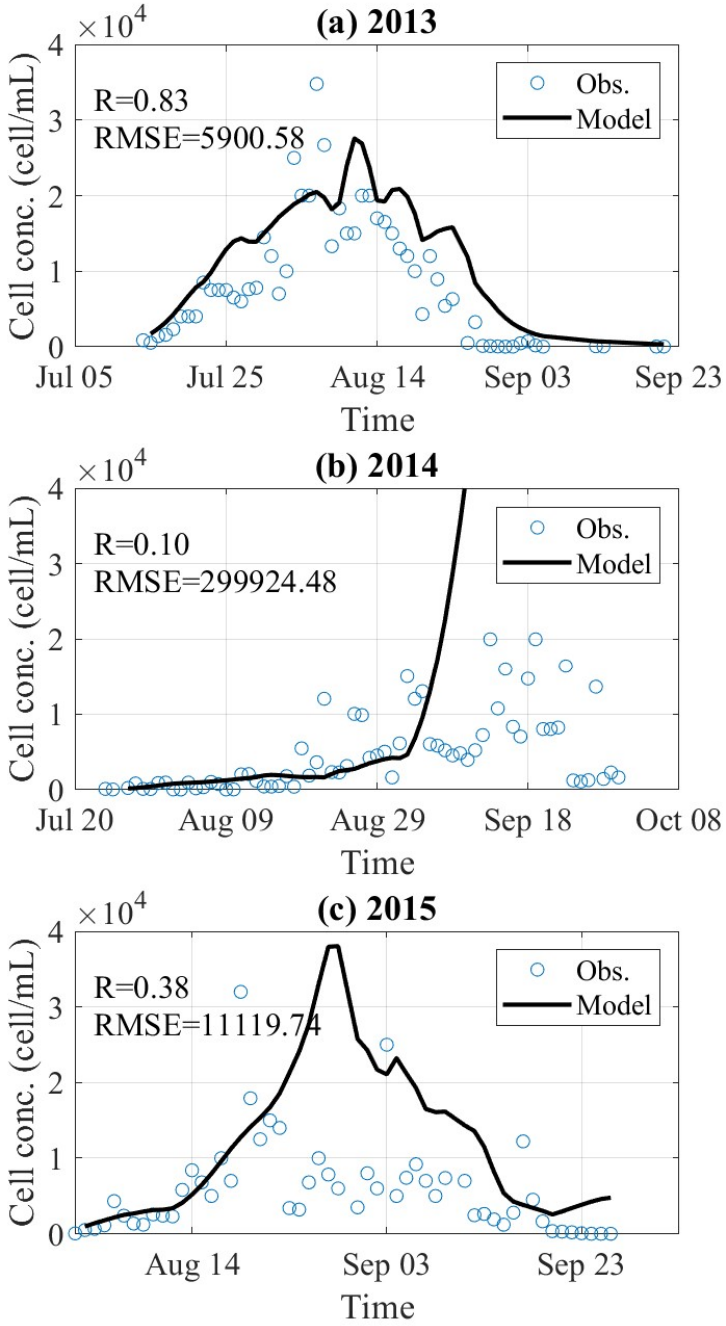

Figure 1.3. Simulated (solid lines) and observed (blue dots) maximum cell concentration of *C. polykrikoides* blooms from 2013 to 2015. The model reasonably describes bloom of *C. polykrikoides* but termination of the bloom in 2014 is not resolved.

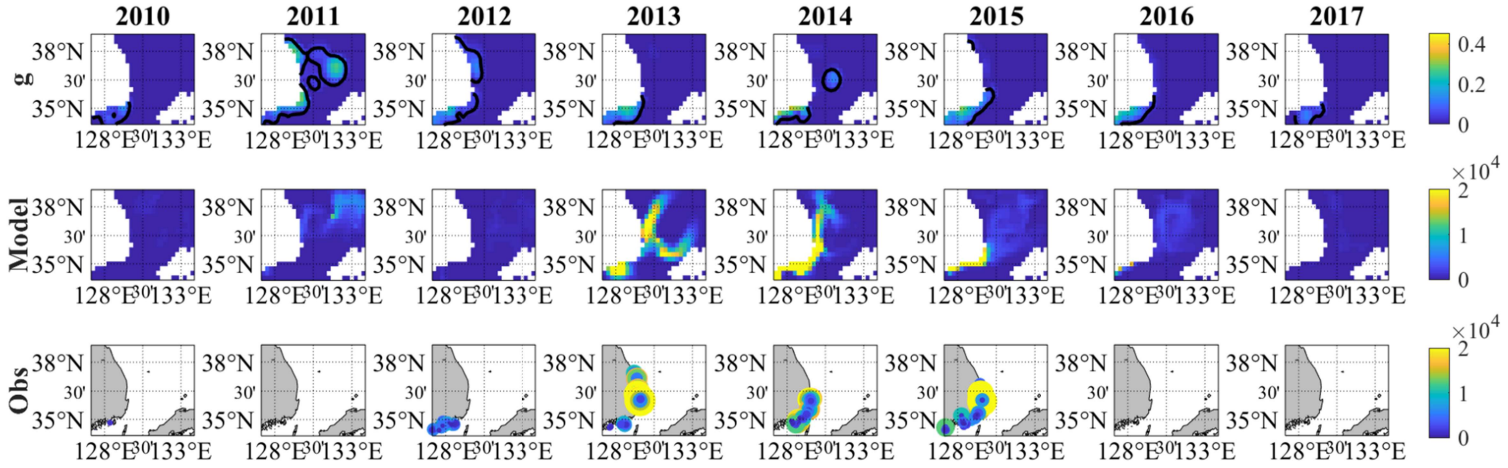

Figure 1.4. Calculated growth rate of *C. polykrikoides*, simulated bloom distribution by the interannual experiment, and corresponding observations. In terms of presence and absence of the bloom, the model well match with observations. Solid line indicates where the growth rate is equal to mortality rate.

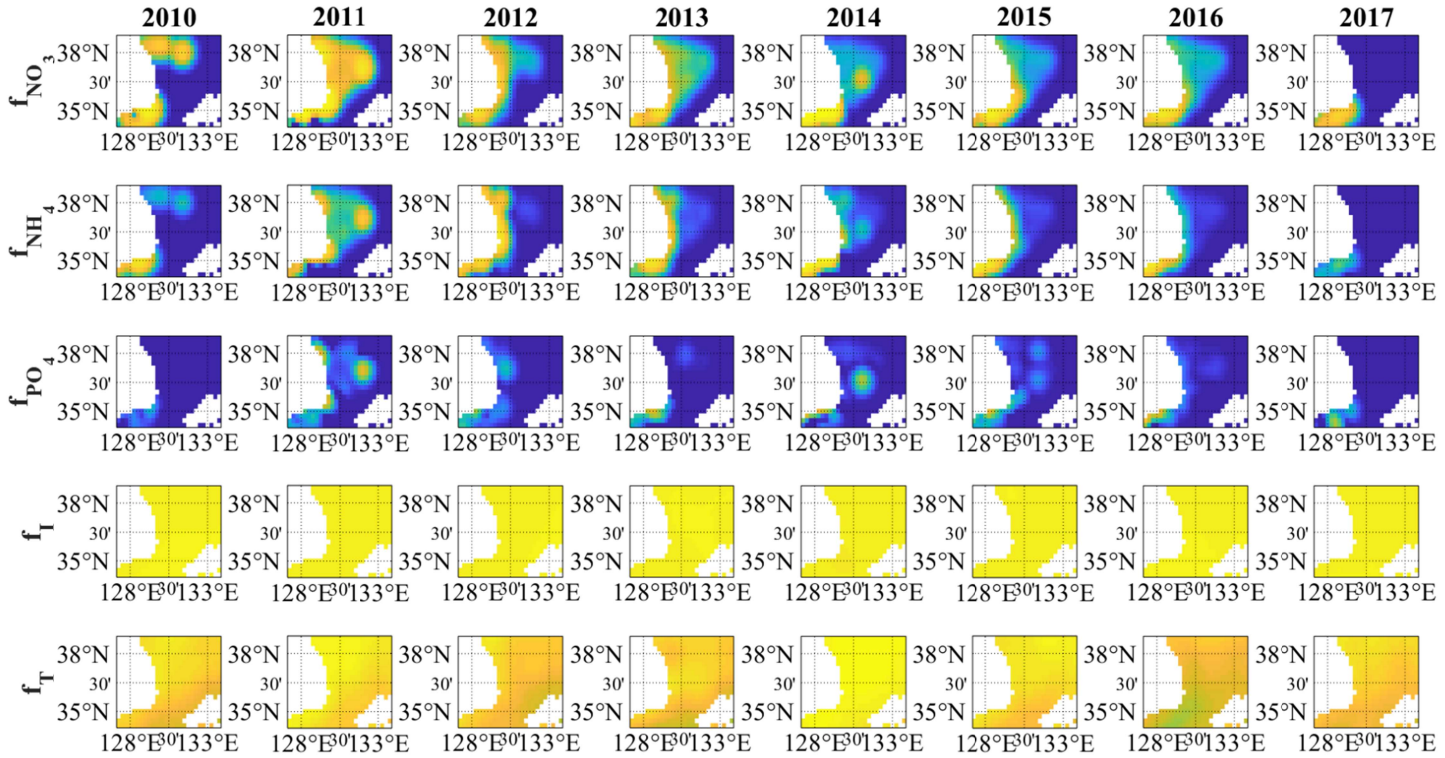

Figure 1.5. Calculated limiting functions of environmental factor: nitrate, ammonium, phosphate, light intensity, and sea surface temperature.

Symol	Parameter name	Value	Unit
g_{max}	maximum growth rate	0.45	1/day
I_0	Light intensity threshold	11.54	μmol/m^2/s
I_I	Light sensitivity coefficient	6.19	μmol/m^2/s
T_{opt}	Optimal temperature	23.12	℃
α	Temperature sensitivity coefficient	2.93	-
K_N	Half saturation concentration of nitrate	0.054	μM-N
K_A	Half saturation concentration of nitrate	0.095	μM-N
K_P	Half saturation concentration of nitrate	0.13	μM-P
m	Mortality rate	0.035	1/day
K	Lateral diffusion coefficient	40	m^2/s

Table 1.1. Model coefficients for the diagnostic model for *C. polykrikoides*.

Year	f_I	f_T	f_N	f_A	f_P	g	Q/V	g_{net}	Da
2010	0.967	0.878	0.865	0.872	0.210	0.061	0.127	-0.102	0.476
2011	0.962	0.963	0.797	0.495	0.370	0.068	0.080	-0.047	0.853
2012	0.966	0.877	0.841	0.809	0.367	0.101	0.130	-0.064	0.774
2013	0.968	0.866	0.883	0.854	0.558	0.163	0.052	0.076	3.140
2014	0.955	0.989	0.978	0.867	0.392	0.151	0.068	0.047	2.206
2015	0.965	0.917	0.911	0.856	0.480	0.159	0.124	0.000	1.284
2016	0.970	0.749	0.910	0.787	0.515	0.132	0.210	-0.114	0.627
2017	0.968	0.827	0.854	0.488	0.354	0.059	0.120	-0.096	0.489
Mean	0.965	0.883	0.880	0.754	0.406	0.112	0.114	-0.037	1.231
STD	0.005	0.076	0.054	0.164	0.110	0.045	0.049	0.071	0.959

Table 1.2. Calculated limiting functions for each environmental factor (f_x), growth rate (g), flushing rate (Q/V), net growth rate ($g_{net} = g - m - Q/V$), and Damköhler number (Da).

CHAPTER 2

POPULATION DYNAMICS UNDERLAYING TOP-DOWN CONTROL FOR HARMFUL ALGAL BLOOM

Abstract

A modified version of the NPZD ecosystem model is used to examine the effects of resource competition and predation avoidance in the development of harmful algal bloom (HAB). One additional phytoplankton functional group, which has slower nutrient uptake kinetics and better predation avoidance than normal phytoplankton group, is considered to resolve HAB group in the model. Because the two phytoplankton groups (one normal and one HAB) compete for only one resource in the system, steady state (equilibrium) conditions cannot occur for coexisting two phytoplankton groups without the presence of zooplankton and only normal phytoplankton group, which defeats HAB group in the resource competition, can survive in the equilibrium. Sufficient zooplankton effectively acts to replenish the nutrient pool by consuming normal phytoplankton. When this occurs, two equilibrium states resolving HABs are found: one coexists both phytoplankton groups and the other includes only HAB group without normal phytoplankton. The condition of equilibrium is that total nitrogen in the system should be larger than a threshold determined by the model coefficients. The threshold and feasibility of the equilibrium are sensitive to HAB group feeding preference coefficient. If the coefficient is larger than ratio of net growth rates between HAB and the normal (non-harmful) phytoplankton group, the threshold become infinite and the equilibriums resolving HAB are not feasible. The presence of thresholds as a controlling factor may explain the regime shift of dominant species causing HABs. We expect that this analytical study could be useful to develop strategies for HAB modeling and provide guidance for the model coefficients setting to resolve HAB.

2.1. Introduction

Harmful algal blooms (HABs), also referred to as red-tides, are excessive blooms of mono-phytoplanktonic species that can significantly increase fish mortality and cause massive economical losses to fisheries and aquaculture industries (Jin et al., 2008; Park et al., 2013). Recently, HABs have occurred more frequently due to trends in global warming and increased anthropogenic nutrient inputs to aquatic systems (Padmakumar et al., 2012; Lee et al., 2013; Griffith and Gobler, 2020). Although many research directions have been pursued to better understand their dynamics, collectively they show that HABs are one of the most complex coastal ecosystem processes that links biogeochemical and hydrodynamical characteristics of the ambient environment (Lee, 2008; Kim et al., 2016; Zhou et al., 2017; Baek et al., 2020).

Modeling approaches are frequently used as powerful tools to resolve the complexity of HABs. In many laboratories culturing experiments, single-equation models are simply regressed against measured culturing results (Lee et al., 2001; Cho and Cho, 2014; Lim et al., 2014). Adding to the complexity, interaction between HABs and other phytoplankton groups including diatom are common and can have a wide variety of outcomes (Kwon et al., 2014; Lim et al., 2014; Oh et al., 2015). Several culturing experiments explicitly show that the presence of diatoms inhibits growth of the HABs group (Lim et al.,2014; Mitra and Flynn, 2006), and frequently results in negative correlation between diatoms and HABs (Lee, 2008; Kang et al., 2009; Lim et al., 2014). Allelopathy or physical contract of diatoms are often pointed out as the mechanism suppressing growth of HABs (Fistarol et al., 2004; Tang and Gobler, 2010; Lim et al., 2014). Furthermore, nutrient uptake ability by the HABs group, estimated by laboratories experiments, implies that the HABs group is defeated by the diatoms in the resource competition (Eppley et al., 1969; Lee et al., 2001; Kudela et al., 2010; Cho and Cho, 2014; Oh et al., 2015), and thus plays a primal role in suppressing growth of one

phytoplankton group relative to the other (Tilman, 1977).

Various mechanisms have been suggested to explain how the HABs group (suppressed by the presence of the diatom group) can bloom, including mixotrophic behavior (Jeong et al., 2004), swimming ability (Lim et al., 2014l Jeong et al., 2017), and multi-resource competition (Gilbert and Burkholder, 2011; Zhou et al., 2017), as well as predation avoidance by the HABs group (Solé et al., 2006; Mitra and Flynn, 2006; Flynn, 2008; Harvey and Menden-Deuer, 2011 and 2012). Mitra and Flynn (2006) developed a simple ecosystem model that consists of two phytoplankton groups (one HAB and one non-HAB), one nutrient, and one zooplankton species. Their model considered allelopathy, prey switching, and prey rejection of the HAB group, and through sensitivity experiments concluded that prey rejection plays the most important role in the formation of HABs. Although these studies explicitly consider interactions between HABs and the ambient system, most analyses and discussion are focused on how well numerical solutions reproduce the observations. Theoretical analysis of the system of governing equations are generally not considered even though the internal dynamics are determined by the mathematical characteristics of the governing equations. In addition, the models designed to reconstruct laboratory experiments are difficult to extrapolate to the field.

In this work we conduct theoretical analysis of a HAB model coupled with the simple Nutrient-Phytoplankton-Zooplankton-Detritus (NPZD) model, one of the most basic models used to describe the marine ecosystem, to study internal dynamics of the ecosystem including HABs. To focus on the internal dynamics governed by prey-predation interaction between components of the ecosystem, physical transport terms are ignored in the theoretical development. In addition, the system of equations is analyzed using steady-state solutions so time-dependent behavior of HABs is not considered in the theory; however, it will be qualitatively addressed when HABs group can be sustained by the system without extinction in the model and when equilibrium conditions favor HAB development. In doing so, details of

the resource competition between two different phytoplankton groups and top-down control mechanisms through prey avoidance are examined and discussed.

2.2. Method

2.2.1. Ecosystem model

We use a Nutrient-Phytoplankton-Zooplankton-Detritus (NPZD) system of equations for the marine ecosystem model. Although there are more sophisticated models, NPZD model is one of the most popular models and contains sufficient complexity to describe realistic marine ecosystems (Onitsuka et al., 2007; Xu et al., 2008; Perruche et al., 2010; Priester et al., 2017; Cruz-Rico and Rivas, 2018). Furthermore, the NPZD system has been theoretically scrutinized (Busenberg et al., 1990; Edwards, 2001; Heinle and Slawig, 2013a and 2013b) and can be easily modified and expanded to resolve additional ecological dynamics (Newberger et al., 2003; Lima and Doney, 2004; Koné et al., 2005; Fennel et al., 2006; Kishi et al., 2007; Fiechter et al., 2009). Governing equations for the NPZD system are slightly different in each study; equations suggested by Powell et al. (2006) are used in this study because their model is coupled with the publicly available Regional Ocean Modeling System (ROMS; Haidvogel et al., 2008) and easily accessible. In our work, to resolve the resource competition between two specific phytoplankton groups, we include one additional phytoplankton group representing the HAB group. The governing equations of our modified NPZD system including a HAB group are given by

$$\frac{dN}{dt} = \delta D + \gamma GZ - U_1 P_1 - U_2 P_2$$

$$\frac{dP_1}{dt} = U_1 P_1 - (1 - \Pi) GZ - \sigma_1 P_1$$

$$\frac{dP_2}{dt} = U_2 P_2 - \Pi GZ - \sigma_2 P_2 \qquad (2.1)$$

$$\frac{dZ}{dt} = (1-\gamma)GZ - \xi Z$$

$$\frac{dD}{dt} = \sigma_1 P_1 + \sigma_2 P_2 + \xi Z - \delta D$$

where t is time, and N, P_1, P_2, Z, and D indicate nutrient, normal phytoplankton, HAB group, zooplankton, and detritus, respectively. U_1 U_2, G, and Π are growth rates of each phytoplankton group, the zooplankton, and predation probability function, respectively, and defined as

$$U_n(N) = V_n \frac{N}{N + k_n}$$

$$G(P_1, P_2) = R_m\left(1 - e^{-\Lambda(P_1 + \psi P_2)}\right)$$

$$\Pi(P_1, P_2) = \frac{\psi P_2}{P_1 + \psi P_2}$$

where subscript *n* takes on values of 1 or 2. The concept of predation probability function and grazing term is described in Fennel and Neumann (2014). For the sake of simplicity, U_n is defined as a function of only nutrient concentration and influence from other environmental factors, such as light intensity, is merged with the maximum growth rate coefficient V_n. The other variables (δ, γ, ξ, σ_1, σ_2, k_1, k_2, Λ) are constant model coefficients defined and specified from the literature in Table 2.1. The coefficients shared with traditional NPZD model are defaults setting of the model (Powell et al., 2006; Fiechter et al., 2009). The maximum growth rate and half saturation concentration of HAB group are those of *C. polykrikoides* based on laboratory experiments (Lee et al., 2001; Cho and Cho, 2014). In this study, the critical element of the ecosystem model (2.1) is nitrogen, so unit of the variables and half saturation concentration coefficients are given in $\mu M - N$.

ψ is a non-dimensional number indicating the HAB group feeding preference by zooplankton. When $\psi < 1$, the zooplankton group prefers to consume P_1, whereas $\psi > 1$

indicates more P_2 preference than P_1. $\psi = 1$ represents that the zooplankton group does not have preference for either phytoplankton group. The value of ψ is arbitrary in this study but the sensitivity of the system for the parameter will be discussed in section 2.3.2.2.

Figure 2.1 shows a schematic for the ecosystem model showing the various processes cycling nitrogen, such as uptake of nutrients by phytoplankton, grazing by zooplankton, excretion of nutrients from phytoplankton, mortality of phytoplankton and zooplankton, and remineralization of detritus. The ecosystem model can be considered as a NP2ZD type having two different phytoplankton functional groups, P_1 and P_2. Characteristics of each phytoplankton group are identical to that used by Mitra and Flynn (2006) where P_1 has better nutrient uptake ability (represented by higher maximum growth rate U_1 and lower half saturation nutrient concentration k_1 than those of P_2), whereas P_2 is better able to avoid predation ($\psi \ll 1$).

2.2.2. Equilibrium points

Steady-state solutions of the ecosystem model are frequently used to analyze characteristics and internal dynamics of the system (Tilman, 1977; Newberger et al., 2003; Heinle and Slawig, 2013a and b; Perruche et al., 2010). Although system (2.1) is nonlinear, steady-state solutions are easily obtained. Negative or imaginary solutions are non-physical and not discussed further. Because system (2.1) is closed and conserves mass, the five equations in (2.1) with steady state are undetermined. The last equation needed to solve the system can be obtained by summing all of equations in (2.1) and requiring that $d(N + P_1 + P_2 + Z + D)/dt = 0$, and can be written as

$$N + P_1 + P_2 + Z + D = N_T$$

where N_T indicates the total nitrogen concentration determined by the sum of all the state variable initial conditions. The steady-state solutions are expressed as function of model

coefficients (Table 2.1) and N_T. To represent the state of the system, state variables are notated as a vector $E^{(m)} = (N^{(m)}, P_1^{(m)}, P_2^{(m)}, Z^{(m)}, D^{(m)})$, similar to Heinle and Slawig (2013a), where superscript m indicates index of each steady-state solution. In addition to the steady-state solutions, the stability condition of each steady-state solution is discussed. It is worth noting given initial condition move toward the stable solution, and the stability condition determines the feasibility of the solution. The stability condition can be determined by linearization of the ordinary differential equation system (Heinle and Slawig, 2013a), but here we focus on the ecological consequences of the stability condition similar to Busenberg et al. (1990).

It must be noted that the system (2.1) does not always converge toward the steady-state solution. To be specific, when total nitrogen in the system is sufficiently high, the steady-state solution can change from a stable focal point toward a neutral stability point where the state of the system oscillates around the steady-state solution (Busenberg et al., 1990). However, the steady-state solution for a neutral stability point attracts the system away from other unstable solutions and remains close to the center of oscillation. In this study, the steady-state solution as neutral stability point is not discussed further, and the focus is on the transition of stable steady-states from one solution to another, useful for determining the conditions that result in the presence (or absence) of a functional group.

2.3. Results

2.3.1. Shared solutions with NPZD system ($P_2 = 0$)

Because system (2.1) converges to the general NPZD model when $P_2 = 0$, steady-state solutions of the general NPZD model are also considered as one of the solutions. In this section, equilibriums of general NPZD model are revisited to highlight transition of stable solution as total nitrogen level and role of zooplankton in the eutrophic limit. The first solution of the

general NPZD system requires that all nitrogen in the system exist as nutrient N and all the other state variables are zeros, so $E^{(1)} = (N^{(1)}, 0, 0, 0, 0)$ where $N^{(1)} = N_T$. This solution occurs when the initial concentration of phytoplankton groups is zero or when nutrient concentrations are not enough to sustain the phytoplankton group, $U_1(N_T) < \sigma_1$, which can be written as

$$N_T < {U_1}^{-1}(\sigma_1) = \frac{\sigma_1 k_1}{V_1 - \sigma_1} \tag{2.2}$$

where ${U_n}^{-1}(\sigma_n)$ indicates the nutrient concentration that makes the growth rate of the phytoplankton balanced by the mortality rate; in other words, the minimum nutrient concentration needed for the phytoplankton group to be sustained. For the oligotrophic conditions that satisfy (2.2), all state variables except N exponentially decrease and converge to zero (Figure 2.2).

A second solution occurs when the zooplankton group does not exist, such that $E^{(2)} = (N^{(2)}, P_1^{(2)}, 0, 0, D^{(2)})$. The components of the second equilibrium $E^{(2)}$ are given as

$$N^{(2)} = {U_1}^{-1}(\sigma_1)$$

$$P_1^{(2)} = \frac{\delta}{\delta + \sigma_1}\left(N_T - {U_1}^{-1}(\sigma_1)\right)$$

$$D^{(2)} = \frac{\sigma_1}{\delta + \sigma_1}\left(N_T - {U_1}^{-1}(\sigma_1)\right).$$

This solution is feasible both when zooplankton initially do not exist, or when nutrient concentrations are high enough to sustain the phytoplankton but the phytoplankton concentration itself is not enough to maintain a viable zooplankton population, such that $\sigma_1 < U_1(N_T)$ and $(1-\gamma)G(P_1^{(2)}, 0) < \xi$. This condition can be written as

$${U_1}^{-1}(\sigma_1) < N_T < {U_1}^{-1}(\sigma_1) + \frac{\delta + \sigma_1}{\delta} P_1^{(3)} \tag{2.3}$$

where $P_1^{(3)}$ indicates the minimum phytoplankton concentration needed to sustain zooplankton,

and corresponds to the phytoplankton concentration that results in a balance between growth and mortality of the zooplankton, and is defined as

$$P_1^{(3)} = G^{-1}\left(\frac{\xi}{1-\gamma}\right) = \frac{1}{\Lambda}\ln\left[\left(1-\frac{\xi}{R_m(1-\gamma)}\right)^{-1}\right].$$

When condition (2.3) is satisfied, numerical solutions show that N, P_1, and D converge to non-zero (constant) values, whereas P_2 and Z converge to zero (Figure 2.3).

When the steady-state phytoplankton concentration is enough to sustain zooplankton, or equivalently, the total nitrogen concentration is high enough to sustain both phytoplankton and zooplankton, a third steady-state solution, $E^{(3)} = (N^{(3)}, P_1^{(3)}, 0, Z^{(3)}, D^{(3)})$, results with all non-zero state variables except for P_2. Components of $E^{(3)}$ are determined by

$$N^{(3)^2} + \left(k_1 + V_1 P_1^{(3)}(1-\gamma)\left(\frac{1}{\xi}+\frac{1}{\delta}\right) + \left[P_1^{(3)}\left(1-\frac{\sigma_1}{\xi}(1-\gamma)+\frac{\sigma_1}{\delta}\gamma\right) - N_T\right]\right)N^{(3)}$$

$$+\left[P_1^{(3)}\left(1-\frac{\sigma_1}{\xi}(1-\gamma)+\frac{\sigma_1}{\delta}\gamma\right) - N_T\right]k_1 = 0$$

$$Z^{(3)} = \frac{1-\gamma}{\xi}\left(U_1\left(N^{(3)}\right) - \sigma_1\right)P_1^{(3)}$$

$$D^{(3)} = \frac{1}{\delta}\left((1-\gamma)U_1\left(N^{(3)}\right) + \gamma\sigma_1\right)P_1^{(3)}.$$

It is worth noting that the quadratic equation for $N^{(3)}$ induces two solutions, but one is negative and non-physical. $P_1^{(3)}$ is independent of N_T and determined by coefficients related to the zooplankton (as mentioned above); all other state variables are dependent on N_T. The condition that allows the zooplankton group to be present is $(1-\gamma)G(P_1^{(2)}, 0) > \xi$, and can be written as

$$U_1{}^{-1}(\sigma_1) + \frac{\delta}{\delta+\sigma_1}P_1^{(3)} < N_T. \tag{2.4}$$

when N_T is sufficiently high and satisfies condition (2.4), numerical solutions show that all state variables, except for P_2, converge to non-zero constant values (Figure 2.4).

Figure 2.5 shows components of the steady-state solution to the general NPZD system varying with N_T; that is, feasible steady-state solutions are transited from $E^{(1)}$ to $E^{(2)}$, and $E^{(2)}$ to $E^{(3)}$ whenever N_T becomes higher than the threshold conditions (2.3) and (2.4). For $E^{(3)}$, all state variables except for phytoplankton increase with increasing N_T. When N_T is sufficiently high, nutrient concentration $N^{(3)}$ linearly increases, whereas $Z^{(3)}$ and $D^{(3)}$ are saturated and converge to constant values (Figure 2.5). It is worth noting that $Z^{(3)}$ and $D^{(3)}$ solutions are Monod functions with non-zero intercept. The slope of $N^{(3)}$ and saturated concentration of $Z^{(3)}$ and $D^{(3)}$ can be analytically determined as N_T gets large, and are given in the limit by

$$\lim_{N_T \to \infty} \frac{\partial N^{(3)}}{\partial N_T} = 1$$

$$\lim_{N_T \to \infty} Z^{(3)} = \frac{1-\gamma}{\xi}(V_m - \sigma)P_1^{(3)}$$

$$\lim_{N_T \to \infty} D^{(3)} = \frac{1}{\delta}\big((1-\gamma)V_m + \gamma\sigma\big)P_1^{(3)}.$$

Consequently, in the eutrophic limit, nutrient concentration converges to a linear polynomial function with slope one, and all the other state variables become constant. This implies that once the system is sufficiently eutrophic, additional nitrogen will not influence the steady-state values of phytoplankton, zooplankton, and detritus. Any additional nitrogen is stored in nutrient pools.

The steady-state solutions of the general NPZD system with only one functional phytoplankton group are discussed by Heinle and Slawig (2013a). The governing equations of NPZD system used by Heinle and Slawig (2013a) are different with those of this study. In their model, mortality of zooplankton increases nutrient concentrations and the inefficiency of zooplankton grazing increases detritus. The opposite occurs in our work where zooplankton

mortality increases detritus and the inefficiency of grazing increases nutrient. Regardless, qualitative characteristics of steady-state solutions are the same because detritus acts as an intermediate state between mortality and remineralization in the closed system, and the presence of a zooplankton group intrinsically plays a role in pumping nitrogen from the phytoplankton pool to the nutrient pool.

2.3.2. HAB group presence solutions ($P_2 \neq 0$)

2.3.2.1. Resource competition between two phytoplankton groups ($Z = 0$)

The presence of a HAB phytoplankton group, $P_2 \neq 0$, induces additional steady-state solutions. However, it is worth noting first that steady-state solutions do not exist for situations where P_1 and P_2 coexist without zooplankton ($Z = 0$). This is because system (2.1) represents two different phytoplankton groups that compete for only one resource (Tilman, 1977). That is, when $P_1 \neq 0$, $P_2 \neq 0$, and $Z = 0$, each governing equation for the phytoplankton groups drives two different steady-state nutrient concentrations, ${U_1}^{-1}(\sigma_1)$ and ${U_2}^{-1}(\sigma_2)$, and thus has no solution. As a result, the phytoplankton group that can survive under conditions with lower nutrient concentration (i.e., lower $U^{-1}(\sigma)$) defeats the other phytoplankton group. The winner of the resource competition is generally P_1 because of its higher maximum growth rate and lower half saturation coefficient that contributes to lower ${U_1}^{-1}(\sigma_1) \approx 0.07\ \mu M$ compared to that from P_2 with ${U_2}^{-1}(\sigma_2) \approx 0.52\ \mu M$.

There does exist a steady-state solution $E^{(4)} = (N^{(4)}, 0, P_2^{(4)}, 0, D^{(4)})$ of which components are given by

$$N^{(4)} = {U_2}^{-1}(\sigma_2)$$

$$P_2^{(4)} = \frac{\delta}{\delta + \sigma_2}\left(N_T - {U_2}^{-1}(\sigma_2)\right)$$

$$D^{(4)} = \frac{\sigma_1}{\delta + \sigma_2}\left(N_T - {U_2}^{-1}(\sigma_2)\right).$$

However, $E^{(4)}$ sustained by the defeated functional group is an unstable saddle point (van Opheusden et al., 2015). The presence of P_1 rapidly moves the state of the system from solution $E^{(4)}$ to $E^{(2)}$. As the state of the system approaches solution $E^{(2)}$, P_2 converges to zero because the growth rate of P_2 around $E^{(2)}$ is less than the mortality, $U_2(N_2) < \sigma_2$, equivalent to ${U_1}^{-1}(\sigma_1) < {U_2}^{-1}(\sigma_2)$. In other words, for the solution $E^{(4)}$ to become viable, the initial concentration of P_1 must be strictly zero. Otherwise, the presence of a minute amount of P_1 moves the state of the system from solution $E^{(4)}$ to $E^{(2)}$. This result is in agreement with laboratory experiments by Oh et al. (2015) and indicates that the model system (2.1) in this study incorporates resource competition dynamics between normal phytoplankton and a HAB group. However, this resource competition does not explain how a HAB group can bloom in the system because P_1 represents normal phytoplankton that are ubiquitous and not likely to be absent in the natural ocean.

2.3.2.2. Equilibrium with $P_2 \neq 0$

As mentioned above, P_2 cannot exist when zooplankton do not exist because nutrient concentration in the steady-state solution contributes to negative net growth rate of the HAB group. However, the presence of zooplankton increases the nutrient concentration as total nitrogen level in the system increases (Figure 2.5). Once nutrient concentration – increased by zooplankton – is sufficient to cause larger growth rates than the sum of sink terms (including mortality and predation rate), a steady-state solution with non-zero P_2, $E^{(5)} = (N^{(5)}, P_1^{(5)}, P_2^{(5)}, Z^{(5)}, D^{(5)})$, is feasible. The components of solution $E^{(5)}$ are determined by

$$U_2\left(N^{(5)}\right) - \sigma_2 = \psi\left(U_1\left(N^{(5)}\right) - \sigma_1\right)$$

$$Z^{(5)} = \frac{1-\gamma}{\xi}\left(U_1(N^{(5)}) - \sigma_1\right)P_1^{(3)}$$

$$P_1^{(5)} = \frac{\psi\left(\delta\left(N_T - N^{(5)} - Z^{(5)}\right) - \xi Z^{(5)}\right) - (\sigma_2 + \delta)P_1^{(3)}}{\psi(\sigma_1 + \delta) - (\sigma_2 + \delta)}$$

$$P_2^{(5)} = \frac{\delta\left(N_T - N^{(5)} - Z^{(5)}\right) - \xi Z^{(5)} - (\sigma_2 + \delta)P_1^{(3)}}{(\sigma_1 + \delta) - \psi(\sigma_2 + \delta)}$$

$$D^{(5)} = N_T - N^{(5)} - P_1^{(5)} - P_2^{(5)} - Z^{(5)}.$$

It is worth noting that the first equation above for nutrient concentration can be rewritten in quadratic form with one of the two solutions non-physical, similar to $E^{(3)}$. The condition necessary for $E^{(5)}$ is $U_2(N^{(3)}) > \sigma_2 + \psi/P_1^{(3)}GZ^{(3)}$, which can be rewritten as $U_2(N^{(3)}) - \sigma_2 > \psi(U_1(N^{(3)}) - \sigma_1)$ and $N^{(3)} > N^{(5)}$. The second form of the condition shows that net growth of P_2 should be larger than that of P_1 weighted by ψ. When P_2 cannot gain an advantage from prey avoidance, the net growth rate of P_2 is unconditionally less than those of P_1 whose nutrient uptake ability outperforms P_2, in which case $E^{(5)}$ is not possible. Therefore, the coefficient ψ should be sufficiently small for the model to trigger HABs. The maximum ψ which can resolve HABs is also analytically determinable; the former becomes $V_2 - \sigma_2 > \psi(V_1 - \sigma_1)$ in the eutrophic limit where $N_T \to \infty$ and $N^{(3)} \to \infty$, so $(V_2 - \sigma_2)/(V_1 - \sigma_1) > \psi$ is required. Because $N^{(3)}$ is a function of total nitrogen N_T, and $N^{(5)}$ is a constant determined by coefficients V_n, k_n, and ψ, the condition necessary for $E^{(5)}$, $N^{(3)} > N^{(5)}$, can be rewritten again as

$$N^{(3)^{-1}}\left(N^{(5)}\right) < N_T \tag{2.5}$$

showing that the total nitrogen must be larger than a threshold determined by coefficients. Explicit form of the thresholds is given in Appendix. If $\psi > (V_2 - \sigma_2)/(V_1 - \sigma_1)$, condition of $E^{(5)}$ never be satisfied even if $N_T \to \infty$. When N_T is less than $N^{(3)^{-1}}(N^{(5)})$, numerical

solutions show that P_2 cannot be sustained in the system and converges to zero (Figures 2.2-2.4), whereas P_2 converges to non-zero constant when condition (2.5) is satisfied (Figure 2.6).

When $\psi = 0$, indicating that P_2 is not subject to predation, complexity of the governing equations (2.1) is significantly reduced because Π becomes zero, and the steady-state solution $E^{(5)}$ is also simplified. Figure 2.7a shows steady-state concentration of each state variables expressed as function of N_T with $\psi = 0$. It is worth noting that solutions of the general NPZD system occur when N_T is less than ${N^{(3)}}^{-1}(N^{(5)})$. Once N_T is larger than ${N^{(3)}}^{-1}(N^{(5)})$, P_2 and D linearly increase with N_T, and the other state variables become independent of N_T. In this case, the dynamics described by the system are straightforward: P_2 that are not consumed by zooplankton uptake surplus nutrients converted from P_1 by the zooplankton.

When ψ is sufficiently small and positive so that condition (2.5) is satisfied, P_2 increases as N_T increases, similar to the case where $\psi = 0$; however, at the same time P_1 slowly decreases (Figure 2.7b). Eventually, once N_T is high enough, a steady-state solution occurs without P_1, $E^{(6)} = (N^{(6)}, 0, P_2^{(6)}, Z^{(6)}, D^{(6)})$. The components of $E^{(6)}$ are given as

$$P_2^{(6)} = \frac{1}{\psi\Lambda}\ln\left[\left(1 - \frac{\xi}{R_m(1-\gamma)}\right)^{-1}\right]$$

$$N^{(6)^2} + \left(k_2 + V_2 P_2^{(6)}(1-\gamma)\left(\frac{1}{\xi}+\frac{1}{\delta}\right) + \left[P_2^{(6)}\left(1 - \frac{\sigma_2}{\xi}(1-\gamma) + \frac{\sigma_2}{\delta}\gamma\right) - N_T\right]\right)N^{(6)}$$

$$+ \left[P_2^{(6)}\left(1 - \frac{\sigma_2}{\xi}(1-\gamma) + \frac{\sigma_2}{\delta}\gamma\right) - N_T\right]k_2 = 0$$

$$Z^{(6)} = \frac{1-\gamma}{\xi}\left(U_2\left(N^{(6)}\right) - \sigma_2\right)P_2^{(6)}$$

$$D^{(6)} = \frac{1}{\delta}\left((1-\gamma)U_2\left(N^{(6)}\right) + \gamma\sigma_2\right)P_2^{(6)}.$$

$E^{(6)}$ has identical mathematical characteristics as $E^{(3)}$; $Z^{(6)}$ and $D^{(6)}$ depend on N_T but are saturated and converge to constant values in the eutrophic limit. On the other hand, $N^{(6)}$

linearly increases with N_T in the limit. The condition necessary for $E^{(6)}$ is the absence of P_1 which occurs when the growth rate of P_1 is less than sum of sink terms, $U_1(N^{(6)}) < \sigma_1 + 1/P_1^{(3)} GZ^{(6)}$ (where $\psi P_2^{(6)} = P_1^{(3)}$). This condition, similar to condition (2.5), is given by $\psi(U_1(N^{(6)}) - \sigma_1) < U_2(N^{(6)}) - \sigma_2$ and $N^{(5)} < N^{(6)}$, which can be written as

$$N^{(6)^{-1}}\left(N^{(5)}\right) < N_T. \tag{2.6}$$

Figure 2.8 shows that P_1 exponentially decreases and converges to zero when condition (2.6) is satisfied. This steady-state solution shows that P_1 cannot survive in environments where P_2 sustains a large enough zooplankton group. It is interesting that both P_1 and P_2 coexist in the eutrophic limit if P_2 is not subject to predation. Conversely, P_1 is not sustained when predation for P_2 is allowed. This implies that the niche of a functional group must be provided and present within the functional group. When P_2 is not consumed, P_1 has a unique niche that sustains a zooplankton group that is required by P_2. However, once P_2 is available as prey for the zooplankton group, P_2 itself can sustain zooplankton group even without P_1. As a consequence, the role of P_1 in sustaining a zooplankton group is replaced by P_2 in the eutrophic limit.

The preference coefficient ψ plays a crucial role in the behavior of the equilibrium when $P_2 \neq 0$ (Figure 2.7). Figure 2.9 shows that the analytically determined thresholds of $E^{(5)}$ and $E^{(6)}$ expressed as function of ψ. If P_2 is not subject to predation ($\psi = 0$), the threshold of $E^{(5)}$, given by $N^{(3)^{-1}}(N^{(5)})$, becomes minimum. On the other hand, the threshold of $E^{(6)}$, given by $N^{(6)^{-1}}(N^{(5)})$, increases infinitely as $\psi \to 0$, and thus $E^{(6)}$ cannot be feasible if $\psi = 0$. As before, P_1 is necessary to sustain the zooplankton group that is required by P_2 when $\psi = 0$. As ψ increases, $N^{(3)^{-1}}(N^{(5)})$ increases and steady-state concentration of P_2 decreases because the predation for P_2 is allowed and acts as a sink of P_2. At the same time $N^{(6)^{-1}}(N^{(5)})$

decreases because P_2 itself can efficiently sustain zooplankton irrespective of P_1. There is another singularity at $\psi = (V_2 - \sigma_2)/(V_1 - \sigma_1)$ where both ${N^{(3)}}^{-1}(N^{(5)})$ and ${N^{(6)}}^{-1}(N^{(5)})$ become infinite. In this situation predation for P_2 is too intense and P_2 cannot gain an advantage as the functional group with better predation avoidance. As a result, P_2 does not exist and only $E^{(3)}$ become feasible.

2.4. Discussions

In this study, steady-state solutions of a coupled NPZD system that includes a second functional HAB species are proposed and theoretically discussed. The feasible steady-state solution is determined by the total nitrogen level, similar to the general NPZD system (Heinle and Slawig, 2013a). The steady-state solutions of the coupled system show that there is a threshold that triggers HAB blooms through a top-down control mechanism in which the ecosystem must be sufficiently eutrophic for the total nitrogen level to exceed a threshold. This result agrees with the observations that HAB species coincide with events that increase nutrient supply, such as inflow of a eutrophic riverine water mass (Yang et al., 2000; Hwang et al., 2005; Lee, 2006; Lee et al., 2007; Lee et al., 2010; Lee et al., 2016; Kwon et al., 2019). The presence of thresholds may explain the regime shift of the dominant species causing HABs off the coast of Korea where most blooms in the 1970s were caused by the diatom *Skeletonema costatum*, but over the past few decades *C. polykrikoides* phytoplankton blooms have become much more dominant than the diatom (Lee et al., 2013). Interestingly, anthropogenic nutrient loading caused by industrialization has accelerated since 1970s (Lee et al., 2018). The coincidence of increasing nutrient loading and HABs was also reported of the coast of China (Heisler et al., 2008; Glibert, 2014). Our theoretical results suggest that increased nitrogen levels from nutrient loading can alter the coastal ecosystem from conditions that cannot trigger HABs to condition

which can (i.e., from $E^{(3)}$ to $E^{(5)}$). It is worth noting that several ad hoc assumptions (e.g., steady-state and ignoring transport terms) are made in the discussion; still, the solutions highlight basic dynamics of the ecosystem including results from resource competition, how resource competition can be overcome by predation avoidance, and conditions favorable to sustaining HABs.

2.5. Conclusions

In this study, a modified NPZD system of equations that highlights different predation pressure for the two phytoplankton functional group is suggested and the steady-state solutions are discussed. The feasible steady-state solution is transited from one to another whenever total nitrogen level in the system N_T is higher than the thresholds determined by model coefficients (Figure 2.5 and 2.7). If $N_T < {N^{(3)}}^{-1}(N^{(5)})$, the predation of zooplankton is not considerable and steady-state solutions shared with traditional NPZD ($P_2 = 0$) are appeared as consequence of resource competition where normal phytoplankton defeats HAB group. When ${N^{(3)}}^{-1}(N^{(5)}) < N_T < {N^{(6)}}^{-1}(N^{(3)})$, zooplankton can sufficiently pump nitrogen from normal phytoplankton to nutrient pool and equilibrium coexisting two phytoplankton group is appeared. When ${N^{(6)}}^{-1}(N^{(3)}) < N_T$, HAB group itself can sustain zooplankton group without P_1, as a result, steady-state solution without normal phytoplankton ($P_1 = 0$) is shown.

The feasibility of steady-state solutions resolving HABs are sensitive to parameter ψ indicating HAB group feeding preference by zooplankton (Figure 2.9). When $\psi = 0$, steady-state solution where HAB group outperforms normal phytoplankton group is not feasible because HAB group cannot sustain zooplankton group. As ψ increase, threshold for the solution without normal phytoplankton group decrease because HAB group become efficient to sustain zooplankton but the steady-state concentration of HAB is also decrease by increasing

predation. When $\psi > (V_2 - \sigma_2)/(V_1 - \sigma_1)$, both equilibria resolving HABs are not feasible because HAB group cannot gain advantage as functional group having better predation avoidance.

Here we show theoretically that increased nitrogen levels from anthropogenic nutrient loading can alter the coastal ecosystem from conditions that cannot trigger HABs to conditions that can (that is, steady state solutions move from one equilibrium state to another). The thresholds may explain the dynamics of regime shift, which switch the dominant species to the HAB group. This theoretical study elucidates details of top-down control dynamics and the development of a coupled ecosystem model resolving HABs. Results show that (1) HABs can be suppressed because of resource competition with normal phytoplankton, and (2) HABs having better predation avoidance can be triggered when total nitrogen exceeds a threshold by using nutrients pumped by zooplankton from normal phytoplankton pools.

2.6. Appendix

Explicit forms of the thresholds of $P_2 \neq 0$ steady-state solutions are given as

$$N^{(3)^{-1}}\left(N^{(5)}\right) = \frac{(k_1 + \epsilon_1 + \epsilon_2 - \epsilon_3)^2 - (k_1 + \epsilon_2 - \epsilon_3)^2 + 4k_1\epsilon_2}{4k_1 + 2\epsilon_1}$$

$$N^{(6)^{-1}}\left(N^{(3)}\right) = \frac{\left(k_2 + \epsilon_1 + \epsilon_2{}' - \epsilon_3{}'\right)^2 - \left(k_2 + \epsilon_2{}' - \epsilon_3{}'\right)^2 + 4k_1\epsilon_2{}'}{4k_2 + 2\epsilon_1}$$

where

$$\epsilon_1 = \frac{\sqrt{\left((\sigma_2 - \sigma_1\psi)(k_1 + k_2) - V_2k_1 + \psi V_1k_2\right)^2 - 4k_1k_2(\sigma_2 - \psi\sigma_1)\left(\sigma_2 - V_2 - \psi(V_1 - \sigma_1)\right)} - V_2k_1 + (\sigma_2 - \psi\sigma_1)(k_1 + k_2) + \psi V_1k_2}{V_2 - \sigma_2 - (V_1 - \sigma_1)}$$

$$\epsilon_2 = \frac{1}{\Lambda}\ln\left[\left(1 + \frac{\xi}{R_m(\gamma - 1)}\right)^{-1}\psi\right]\left(\frac{\sigma_1(\gamma - 1)}{\xi} + \frac{\gamma\sigma_1}{\delta} + 1\right)$$

$$\epsilon_2{}' = \frac{1}{\psi\Lambda}\ln\left[\left(1 + \frac{\xi}{R_m(\gamma - 1)}\right)^{-1}\right]\left(\frac{\sigma_2(\gamma - 1)}{\xi} + \frac{\gamma\sigma_2}{\delta} + 1\right)$$

$$\epsilon_3 = \frac{1}{\Lambda}\ln\left[\left(1+\frac{\xi}{R_m(\gamma-1)}\right)^{-1}\right]V_1(\gamma-1)\left(\frac{1}{\delta}+\frac{1}{\xi}\right)$$

$$\epsilon_3{}' = \frac{1}{\psi\Lambda}\ln\left[\left(1+\frac{\xi}{R_m(\gamma-1)}\right)^{-1}\right]V_2(\gamma-1)\left(\frac{1}{\delta}+\frac{1}{\xi}\right).$$

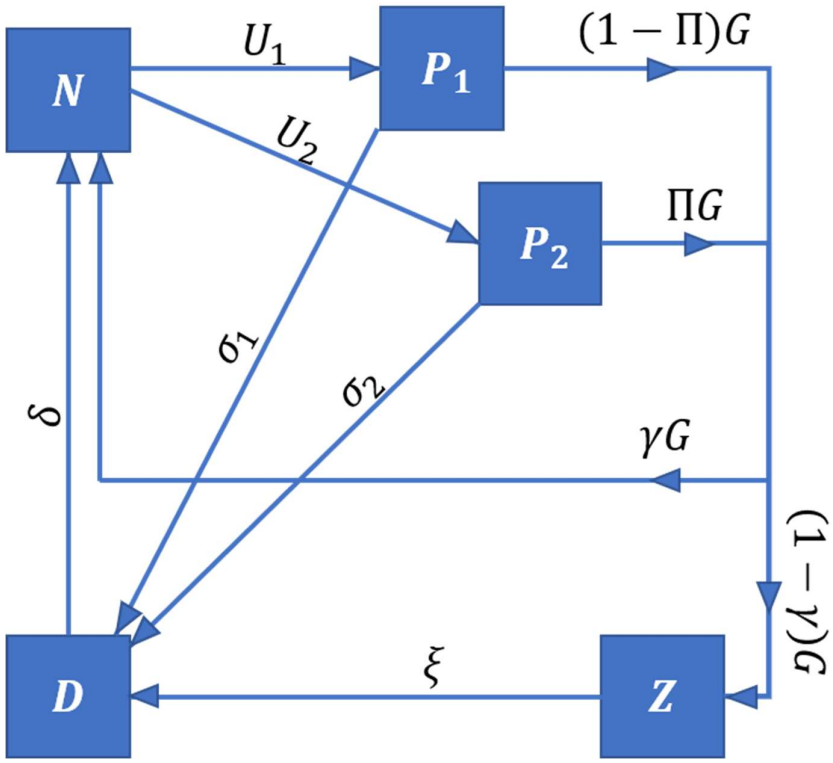

Figure 2.1. Schematics of HABs model coupled with NPZD system. Variables are defined in the text and in Table 2.1.

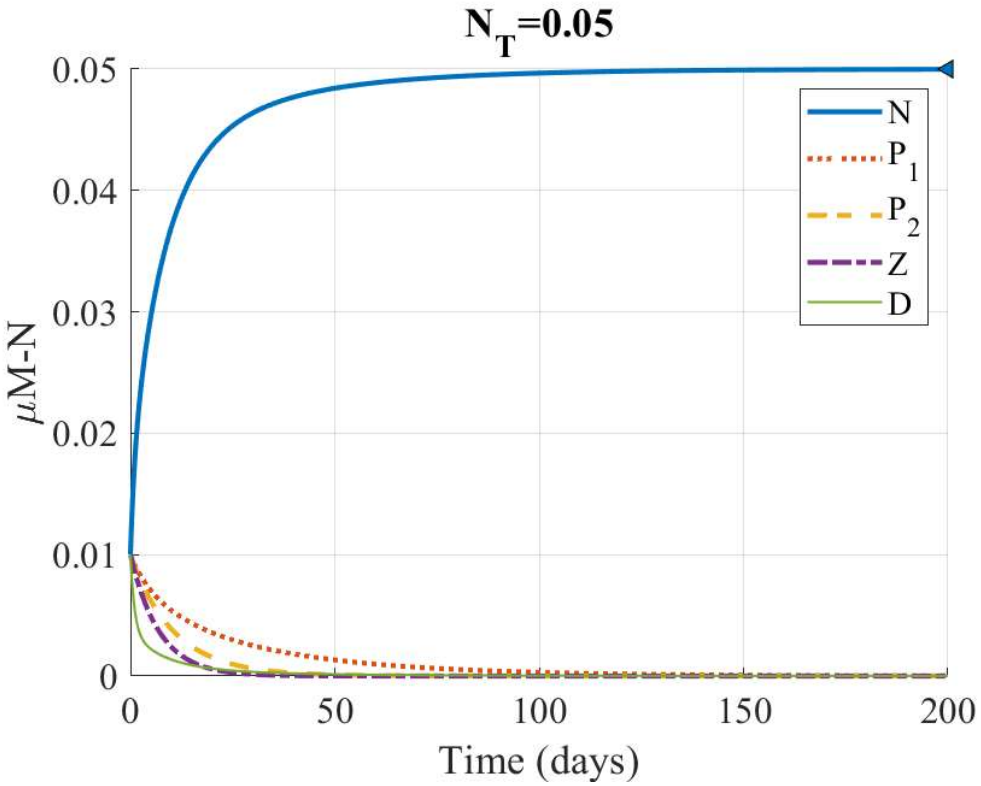

Figure 2.2. Numerical solution of the coupled system with N_T satisfy condition (2). Left-pointing triangles indicate analytically determined steady-state concentrations of each state variables.

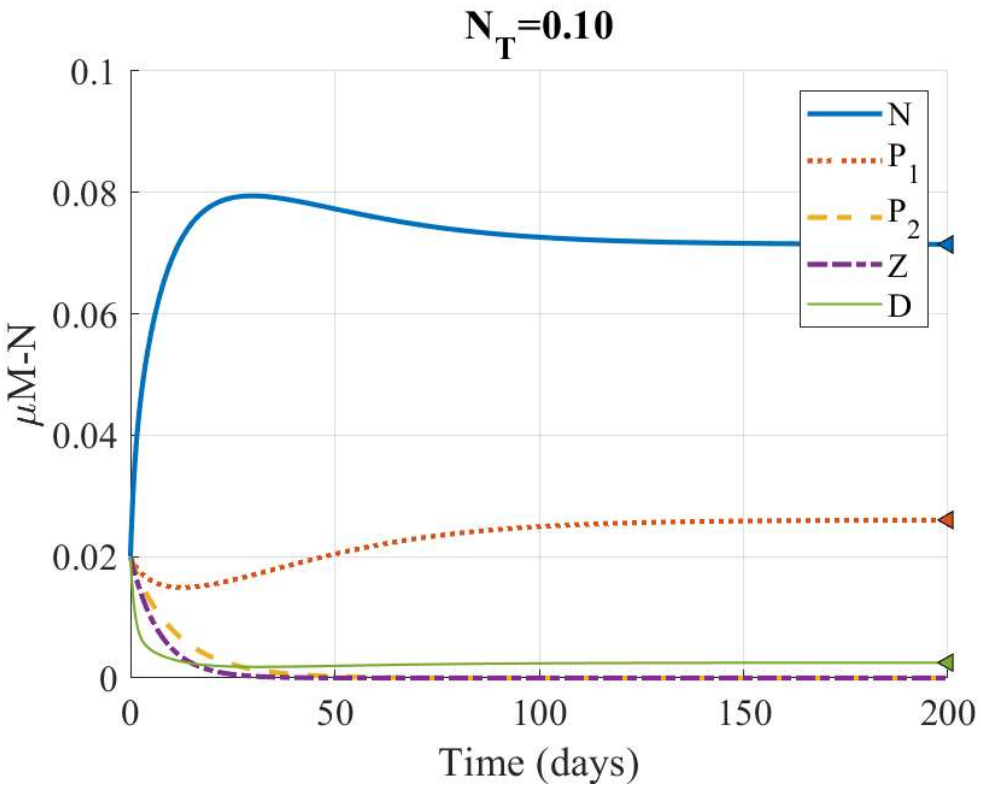

Figure 2.3. Numerical solution of the coupled system with N_T satisfy condition (3). Left-pointing triangles indicate analytically determined steady-state concentrations of each state variables.

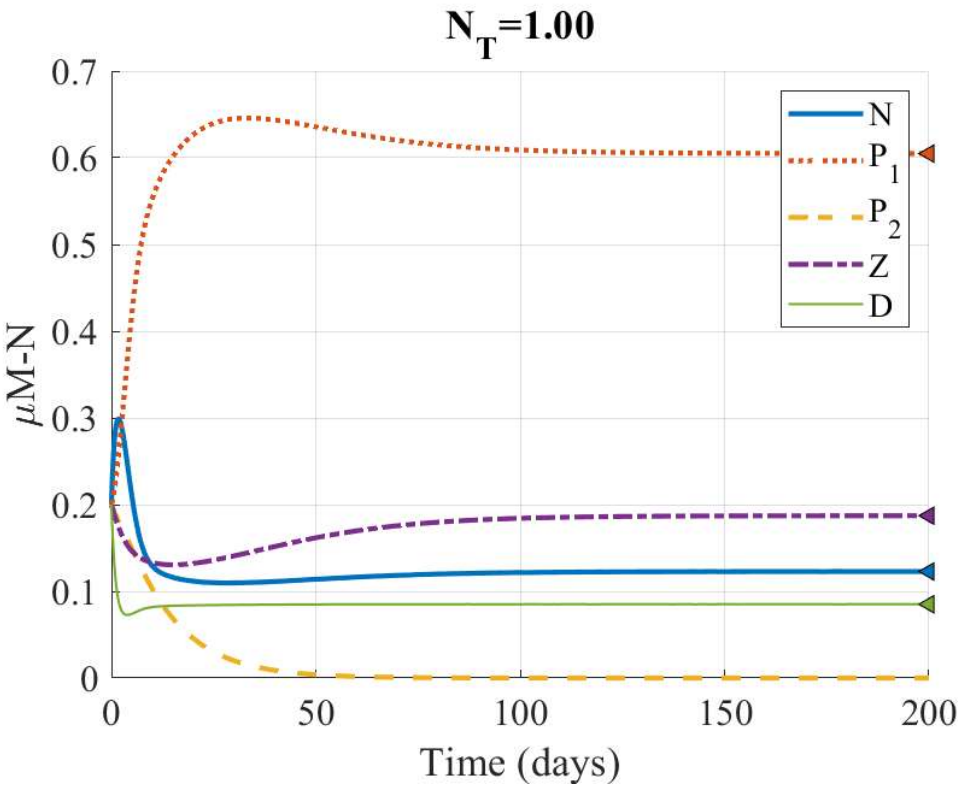

Figure 2.4. Numerical solution of the coupled system with N_T satisfy condition (4). Left-pointing triangles indicate analytically determined steady-state concentrations of each state variables.

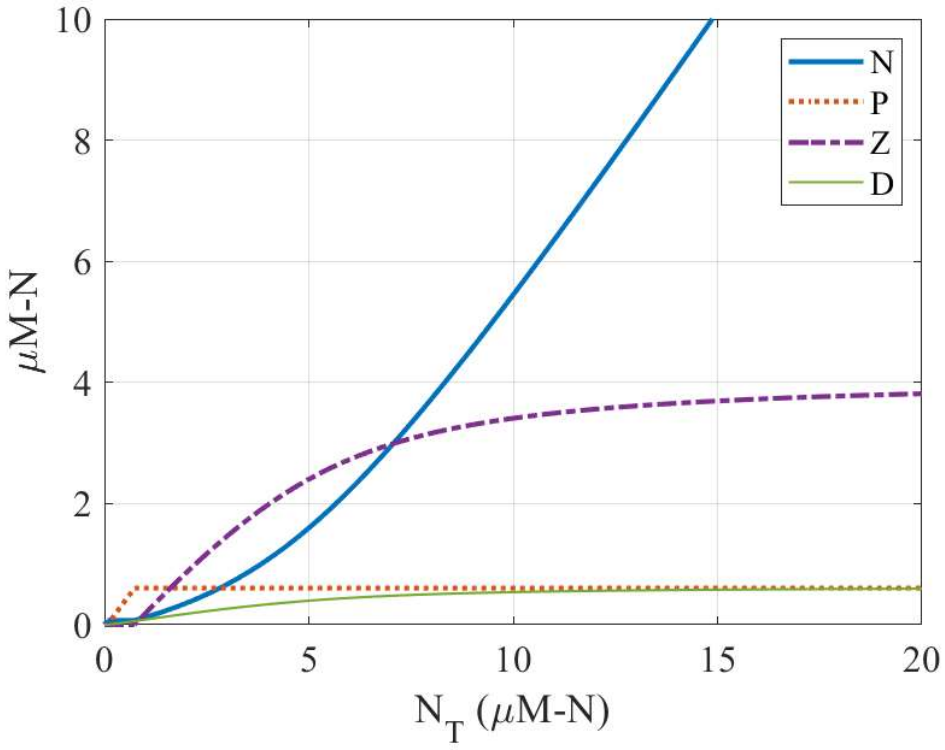

Figure 2.5. Steady-state solutions of general NPZD system varying with N_T. In the eutrophic limit, all state variable except for nutrients converge to constant and nutrient linearly increase with slope one.

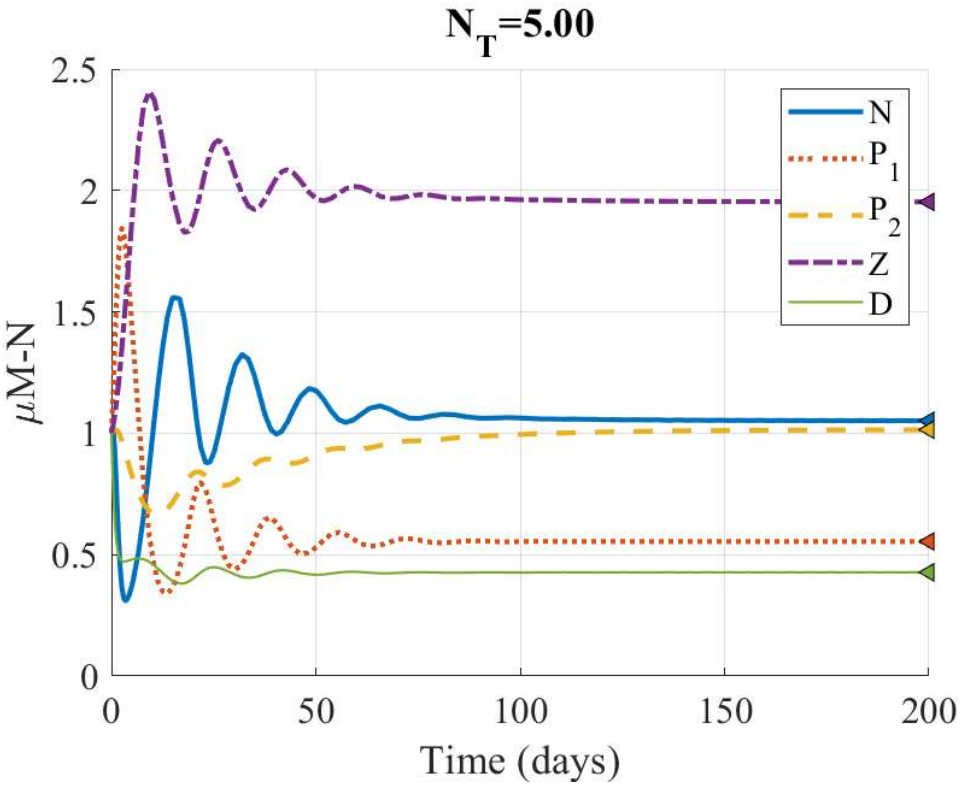

Figure 2.6. Numerical solution of the coupled system with N_T satisfy condition (5). Left-pointing triangles indicate analytically determined steady-state concentrations of each state variables.

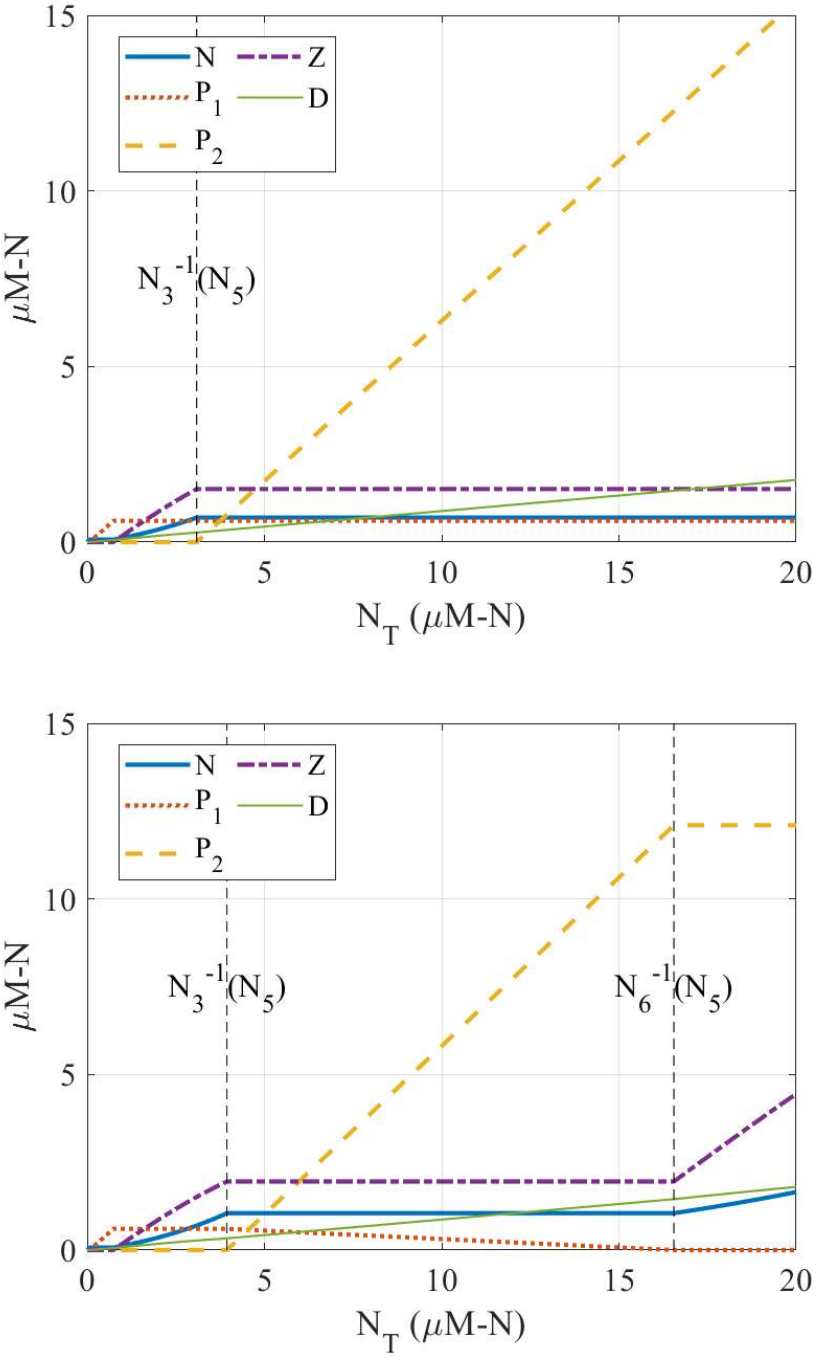

Figure 2.7. Steady-state solutions of NPZD system with HAB group varying with N_T in case of (A) $\psi = 0$ and (B) $\psi \neq 0$. Vertical dashed line indicates thresholds of equilibriums with $P_2 \neq 0$, before the threshold of P_2 presence, solutions are identical with general NPZD system.

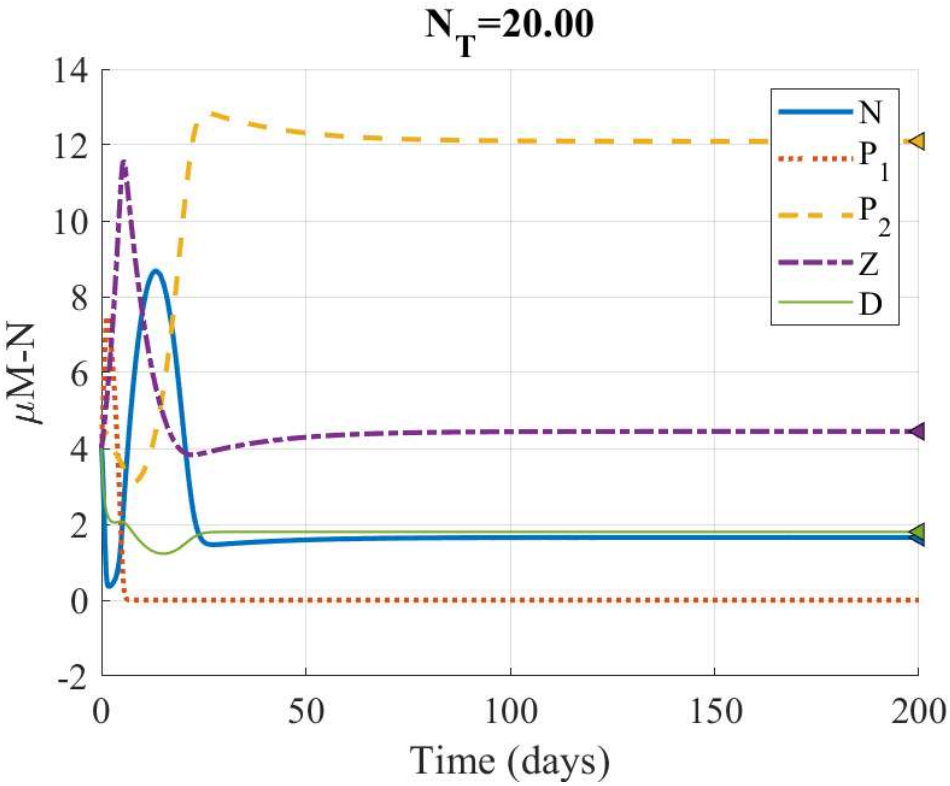

Figure 2.8. Numerical solution of the coupled system with N_T satisfy condition (6). Left-pointing triangles indicate analytically determined steady-state concentrations of each state variables.

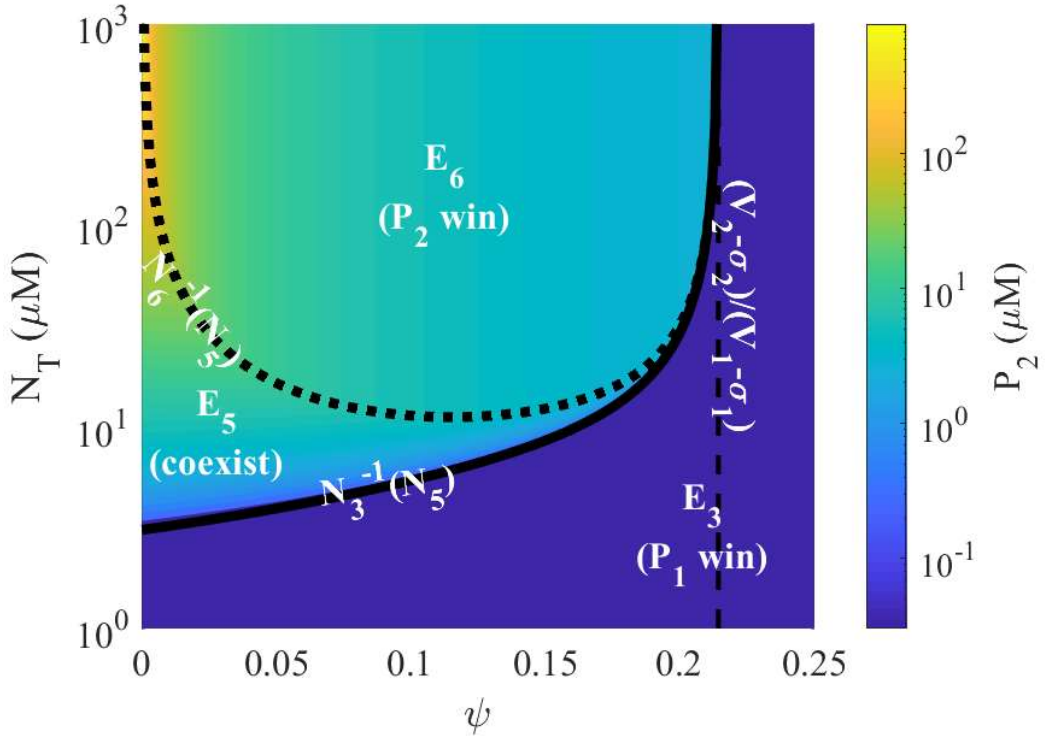

Figure 2.9. Sensitivity of thresholds for E_5 and E_6 to the coefficient ψ. When $\psi \approx 0$, E_6 is not feasible because the threshold increases infinitely. When ψ is sufficiently large, P_2 cannot survive in the system and only E_3, indicating $P_2 = 0$, is feasible.

Coefficient name	symbol	value	Unit
P_1 maximum growth rate	V_1	1.5	1/day
P_1 nitrate half saturation concentration	k_1	1.0	μM-N
P_1 natural mortality rate	σ_1	0.1	1/day
P_2 maximum growth rate	V_2	0.4	1/day
P_2 nitrate half saturation concentration	k_2	2.1	μM-N
P_2 natural mortality rate	σ_2	0.1	1/day
Z maximum grazing rate	R_m	0.52	1/day
Z Ivlev constant	Λ	0.84	1/μM-N
Z excretion efficiency	γ	0.3	-
Z mortality rate	ξ	0.145	1/day
Z prey preference of P_2	ψ	0.05	-
D remineralization rate	δ	1.03	1/day

Table 2.1. Model coefficients of the modified NPZD system.

CHAPTER 3

DEVELOPMENT OF OPTIMAL COMPLEXITY MARINE ECOSYSTEM MODEL FOR COASTAL OCEAN: INTERNAL DYNAMICS AND ROLE OF NON-REDFIELD BEHAVIORS

Abstract

Many ecosystem models have chronic issues that result in unrealistic oligotrophic conditions in the shallow coastal regions. This problem is attributed to the poorly resolved bottom boundary condition for ecological tracers; detritus reaching bottom boundary in shallow water escapes the model domain resulting in continuously decreasing total nitrogen levels. The scaling for the problem is determined by a vertical length scale w_d/δ where w_d is detritus sinking speed and δ is remineralization rate. To alleviate the problem, traditional Nutrient-Phytoplankton-Zooplankton-Detritus (NPZD) models are expanded to consider denitrification and nitrogen fixation which result in non-Redfield nutrient ratios. Internal dynamics of the expanded model are examined through steady-state solutions. The intensity of denitrification, scaled as the ratio between w_d/δ and water depth, plays an important role sustaining nitrogen fixers by regulating phosphorous competition with normal phytoplankton. The theoretical equilibriums of the expanded model well represent characteristics of estuarine, pelagic, and freshwater ecosystems. The expanded ecosystem model is used to simulate the coastal ecosystem of the Yellow Sea and shows that the unrealistic oligotrophic conditions along the coast are not present when non-Redfield dynamics are considered.

3.1. Introduction

Various marine ecosystem models have been developed to quantify ocean productivity

and its contribution to the global carbon cycle. In general, ocean productivity is considered to be limited by separation of euphotic and eutrophic layers; sinking of organic matter forces the euphotic surface layer to become oligotrophic and vice versa for the aphotic subsurface layer. Consequently, the productivity is governed by physical transport of nutrients into the surface layer (Sigman and Hain, 2012), and most ecosystem models are coupled with a hydrodynamics model to resolve the eco-physical interactions. For example, the Regional Ocean Modeling System (ROMS; Shchepetkim and McWilliams, 2005) is coupled with various ecosystem models having different complexities, such as the Nutrient-Phytoplankton-Zooplankton-Detritus model (NPZD; Powell et al., 2006), North Pacific Ecosystem Model for Understanding Regional Oceanography (NEMURO; Kishi et al., 2007), and Fennel ecosystem model (Fennel et al., 2006).

Although the ecosystem models successfully reproduce the behavior of large-scale pelagic ecosystems, they do not work well in the shallower coastal ocean. Generally, the coastal ocean is more productive than in pelagic regions, yet most ecosystem models chronically simulate oligotrophic conditions in shallow water and considerably underestimate phytoplankton concentration (Xu et al., 2008; Fiechter et al., 2009; Hofmann et al., 2011; Xue et al., 2013; Thushara and Vinayachandran, 2016; Uchiyama et al., 2017; Hoshiba et al., 2018). Interestingly, the problem is also present in models that consider realistic river discharge. Furthermore, data assimilation schemes and coefficient optimization techniques seldom alleviate the problem (Xu et al., 2008; Hoshiba et al., 2018). The problem might be caused by structure error within the ecosystem model originating from unresolved ecological or biogeochemical processes in the shallow regions.

Traditionally, marine ecosystems are considered to be limited by nitrogen (Howarth, 1988; Howarth and Marino, 2006), and thus most models have been designed to focus on the

nitrogen cycle; essentially it has been implicitly assumed that phosphorous does not limit the growth of phytoplankton and follows a pelagic Redfield ratio. However, recent studies have shown that the marine ecosystem is frequently co-limited by both nitrogen and phosphorous, and occasionally limited by phosphorous (Arrigo, 2005; Elser et al., 2007; Mills et al., 2008). In addition, denitrification and nitrogen fixation, omitted by many traditional ecosystem models, could be considerable in the marine ecosystem (Voss et al., 2013; Pajares and Ramos, 2019). Furthermore, coastal marine ecosystems are closely connected with freshwater ecosystems that are primarily controlled by phosphorous limitation and dominant nitrogen fixation (Hecky and Kilham, 1988; Turner et al., 2003; Elser et al., 2007). Because the coastal system is much shallower than pelagic environments, components of the marine ecosystem easily interact with the bottom sediment layer which plays a role accelerating remineralization and denitrification processes (Devol, 2015; Lin et al., 2017; Zhu et al., 2018). Because denitrification and nitrogen fixation act as an additional sink and source for only nitrogen and do not influence phosphorous, these processes result in deviations of the nutrient Redfield ratio that has been implicitly assumed by the traditional ecosystem models. Consequently, coastal ecosystem models need to resolve benthic biogeochemical, phosphorous cycles, and non-Redfield dynamics (denitrification and nitrogen fixation).

A few modern ecosystem models, such as European Regional Seas Ecosystem Model (ERSEM) and Ecological Regional Ocean Model (ERGOM), try to describe all possible biogeochemical cycles that contribute to the marine ecosystem (Neumann et al., 2002; Butenschön et al., 2016; Radtke et al., 2019). However, these models consist of numerous state variables and parameters that are too complex to elucidate details of the ecological dynamics. In this study, we describe a new coastal marine ecosystem model that includes optimal complexity by modifying a traditional NPZD model to consider both denitrification and nitrogen fixation, which cause non-Redfield behavior of nutrients. The purpose of this study is

to explain why traditional ecosystem models render oligotrophic water masses in shallow regions and how consideration of non-Redfield dynamics alleviates the problem. The models with and without non-Redfield dynamics are analyzed theoretically using steady-state solutions and compared to examine the role of the non-Redfield dynamics. In the theoretical analysis, steady-state solutions are found under the following assumptions: no zooplankton in order to focus on primal production that sustains the system, no physical transport (advection and diffusion), and no vertical variation of ecological transport (well mixed environments). The latter two assumptions are defined to solve the equations analytically. However, it will be shown that characteristics and dynamics elucidated by the simplified system (phosphorous competition between nitrogen fixers and normal phytoplankton) also appear in the numerical modeling results that resolve bloom behavior in well-mixed coastal areas.

In section 3.2, we summarize traditional NPZD ecosystem model equations and introduce an expanded version of the model that considers non-Redfield dynamics. In section 3.3.1 and 3.3.2, differences between the traditional and modified NPZD ecosystem models are discussed, and in particular how unrealistic oligotrophic water masses predicted by traditional NPZD in shallow regions are avoided with the modified model that includes non-Redfield dynamics. In section 3.3.3, details of internal dynamics of the expanded model are theoretically investigated with steady-state solutions. In section 3.4, the expanded ecosystem model is applied to simulate realistic conditions of the Yellow Sea and compared with results from the traditional model. Finally, discussion with qualitative evidence to support the expanded model and conclusions from this study are presented in sections 3.5 and 3.6.

3.2. Ecosystem models

3.2.1. Traditional NPZD model

We use the traditional NPZD ecosystem model proposed by Powell et al. (2006) to

examine the unrealistic oligotrophic water masses predicted for the coastal region. The governing equations are given by

$$\frac{\partial DIN}{\partial t} = \delta D + \gamma GZ - U_1 P_1 \tag{3.1}$$

$$\frac{\partial P_1}{\partial t} = U_1 P_1 - GZ - \sigma_1 P_1 \tag{3.2}$$

$$\frac{\partial Z}{\partial t} = (1-\gamma)GZ - \xi Z \tag{3.3}$$

$$\frac{\partial D}{\partial t} = \sigma_1 P_1 + \xi Z - \delta D + \frac{\partial (w_d D)}{\partial z} \tag{3.4}$$

where DIN , P_1 , Z , and D indicate nutrient (dissolved inorganic nitrogen), normal phytoplankton, zooplankton, and detritus concentration in μM-N, respectively. U_1 is normal phytoplankton growth rate defined by

$$U_1 = V_1 \frac{N}{N + k_{1,DIN}} \frac{\alpha_1 I}{\sqrt{\alpha_1 I^2 + {V_1}^2}} \tag{3.5}$$

where I is light intensity in W/m^2. G is zooplankton growth rate defined by

$$G = R_m (1 - e^{-\Lambda P}) \tag{3.6}$$

All the other symbols in equation (3.1) – (3.6) are constant parameters defined in Table 3.1. In the governing equations, physical transport terms including advection and diffusion not considered.

3.2.2. Expanded model considering non-Redfield dynamics

Here we expand the traditional NPZD model by considering the phosphorous cycle, denitrification, and nitrogen fixation to examine the role of non-Redfield dynamics in coastal regions. The governing equations are given by

$$\frac{\partial DIN}{\partial t} = \delta D + \gamma GZ - U_1 P_1 + (1-\phi)\frac{\partial (w_d' D)}{\partial z} \tag{3.7}$$

$$\frac{\partial DIP}{\partial t} = r_{P/N}\left(\delta D + \gamma GZ - U_1 P_1 - U_2 P_2 + \frac{\partial (w_d' D)}{\partial z}\right) \tag{3.8}$$

$$\frac{\partial P_1}{\partial t} = U_1 P_1 - \Pi_1 GZ - \sigma_1 P_1 \tag{3.9}$$

$$\frac{\partial P_2}{\partial t} = U_2 P_2 - \Pi_2 GZ - \sigma_2 P_2 \tag{3.10}$$

$$\frac{\partial Z}{\partial t} = (1-\gamma)GZ - \xi Z \tag{3.11}$$

$$\frac{\partial D}{\partial t} = \sigma_1 P_1 + \sigma_2 P_2 + \xi Z - \delta D - \frac{\partial (w_d D)}{\partial z} \tag{3.12}$$

where DIP and P_2 indicate phosphorous (dissolved inorganic phosphorous) nutrient concentration in μM-P and nitrogen fixer group concentration in μM-N, respectively. Physical transport terms, including advection and diffusion, are omitted in the equations. Although the transport terms are ignored in the theoretical analysis (section 3.3), they are considered (and assessed) in numerical experiments where the ecosystem model is implemented into ROMS (section 3.4). In the expanded model, the growth rate of each phytoplankton functional group U_i, growth rate of the zooplankton group G, and the predation preference term Π_i are defined as

$$U_1 = V_1 \min\left(\frac{DIN}{DIN + k_{1,DIN}}, \frac{DIP}{DIP + k_{1,DIP}}\right)\frac{\alpha_1 I}{\sqrt{\alpha_1 I^2 + {V_1}^2}} \tag{3.13}$$

$$U_2 = V_2 \frac{DIP}{DIP + k_{2,DIP}}\frac{\alpha_2 I}{\sqrt{\alpha_2 I^2 + {V_2}^2}} \tag{3.14}$$

$$G = R_m\left(1 - e^{-\Lambda(P_1+P_2)}\right) \tag{3.15}$$

$$\Pi_i = \frac{P_i}{P_1 + P_2}. \tag{3.16}$$

where $i = 1$ or 2 indicating parameters for normal phytoplankton or nitrogen fixers,

respectively. Figure 3.1 shows schematics of the traditional NPZD model and the expanded model resolving non-Redfield dynamics. The description for nitrogen fixation is included following Fennel and Neumann (2014) where the growth of normal phytoplankton P_1 in (3.13) can be limited by both nitrogen and phosphorous, whereas nitrogen fixing plankton P_2 in (3.14) depend only on phosphorous. The nitrogen fixing group produces organic matter, including both nitrogen and phosphorous with Redfield ratio $r_{P/N}$, without any consumption of nitrogen within the system. This formulation assumes that nitrogen fixers obtain nitrogen from outside of the system, for example, atmospheric nitrogen gas. Eventually, their growth imports additional nitrogen into the system corresponding to the nitrogen fixation. The last terms in (3.7) and (3.8) indicate a coupled remineralization-denitrification process within the sediment layer (proposed by Fennel et al., 2006 and Laurent and Fennel, 2014), where w_d' is defined as

$$w_d' = \begin{cases} w_d & if\ z = -h \\ 0 & otherwise. \end{cases} \tag{3.17}$$

where h is the water depth. The coupled sediment processes remove a certain portion, ϕ, of nitrogen in the detritus reaching bottom boundary, with the remaining portion of nitrogen, $1 - \phi$, spontaneously changed into DIN and transported back to the water column. The former indicates sediment denitrification and latter represents sediment remineralization from oxygen reduction. Because phosphorous is not subject to denitrification, it is entirely changed into DIP without any loss by similar processes. Additional model coefficients used in the expanded model are defined in Table 3.2.

The parameters for the nitrogen fixer group in Table 3.2 are based roughly on Neumann et al. (2002) but modified so that nitrogen fixers have qualitatively poorer nutrient uptake ability than normal phytoplankton. Situations where parameters for the nitrogen fixer group define higher nutrient uptake potential relative to normal phytoplankton are discussed in section 3.3.3.2.

3.3. Internal dynamics of the model

3.3.1. Problem of bottom boundary condition in the traditional model

In this section, we systematically revisit the structure of the traditional ecosystem model and show that predicted (but unrealistic) oligotrophic water masses in coastal areas are a result of the poorly resolved bottom boundary condition for ecological tracers. The governing equation for total nitrogen of the traditional NPZD system is found by summing all equations, (3.1) – (3.4), for state variables associated with nitrogen, yielding

$$\frac{\partial N_T}{\partial t} = \frac{\partial (w_d D)}{\partial z} \tag{3.18}$$

where $N_T = DIN + P_1 + Z + D$ indicates the total nitrogen concentration. Although the system of governing equations is different for various other ecosystem models, an identical equation for total nitrogen can be derived by assuming a closed nitrogen cycle associated with ecological activities; prey-predation interaction terms between each state variable are intrinsically designed to cancel each other to conserve mass. Equation (3.18) shows that total nitrogen in a control volume is conserved if there is no change in detritus with depth (i.e., no sinking). As one of the simplest ecosystem models which can describe realistic properties of the marine ecosystem, NPZD has been well studied theoretically to show that total nitrogen is the most important quantity determining stable equilibriums of the closed system (Busenberg et al., 1990; Heinle and Slawig, 2013). However, those theoretical studies do not consider a loss of detritus through the bottom boundary and focus on a closed nitrogen cycle governed by prey-predation relationships and population dynamics between each functional group within the water column. On the other hand, inclusion of a detritus sinking term in the physical-ecological coupled model (3.18) allows situations where total nitrogen in the water column is not conserved. Vertical integration of (3.18) through water column gives

$$\frac{\partial}{\partial t}\left(\int_{-h}^{\eta} N_T \, dz\right) = w_d D|_{z=\eta} - w_d D|_{z=-h} \tag{3.19}$$

where η is the sea surface elevation, shows that total amount of nitrogen in the water column is determined by surface and bottom boundary conditions for detritus. Most ecosystem models apply only one boundary condition which assumes no detritus flux through surface boundary and do not specify a bottom boundary condition. As a result, the detritus in the model continues to sink even if it reaches the bottom boundary and escapes the model domain. This process continuously decreases the nitrogen level in the water column, resulting in unrealistic oligotrophic water along marginal coastal regions by models that do not consider denitrification in the bottom boundary. In essence, most traditional ecosystem models intrinsically assume permanent and instantaneous sedimentation of detritus that reaches the bottom boundary, a process that is too intense to sustain a realistic nitrogen balance in the coastal ecosystem.

The governing equation (3.4) shows that the fate of detritus, rendered by mortality of plankton, is determined by two processes: remineralization and vertical sinking. For the shallower regions, it is easier for detritus to reach the bottom boundary without being remineralized within the water column, so detritus rapidly escapes model domain. On the other hand, in the deep ocean, detritus has sufficient time to be transformed into dissolved inorganic form and is not subject to loss through the bottom boundary. The amount of detritus that reaches the seabed is negligible in the pelagic region, and as a result makes total nitrogen conservative and a closed nitrogen cycle in the deep water column. Consequently, total nitrogen is determined by the relative dominance between detritus remineralization and vertical sinking. Scale analysis between the last two terms in (3.4) shows that the length scale

$$h_c = \frac{w_d}{\delta} \tag{3.20}$$

is determined by the relative dominance between remineralization and vertical sinking. If the water depth is shallower than h_c, then the detritus sinks and is transported out of the domain;

when the water depth is greater than h_c, detritus is remineralized within the water column. Therefore, the depth scale in (3.20) determines the region where oligotrophic water will occur in the model.

3.3.2. Mass conservativity of the expanded model

In the expanded ecosystem model resolving non-Redfield dynamics (section 3.2.2), the governing equation for total nitrogen within the water column is derived by summing all equations that include substances containing nitrogen; equation (3.8) governing dissolved inorganic phosphorous does not contain nitrogen and should be excluded in the summation. Summing equations (3.7) and (3.9) – (3.12) and then vertically integrating from the bottom to the surface gives

$$\frac{\partial}{\partial t}\left(\int_{-h}^{\eta} N_T \, dz\right) = \int_{-h}^{\eta} U_2 \, P_2 dz - \phi w_d D|_{z=-h} \tag{3.21}$$

where $N_T = DIN + P_1 + P_2 + Z + D$ and there is no flux of detritus through the surface boundary. The first term on the right-hand side indicates the vertically integrated nitrogen fixation rate and the second term describes the denitrification rate at the bottom boundary. Equation (3.21) shows that the total amount of nitrogen in the system is governed by non-Redfield behavior and implies that the nitrogen level in shallow regions can be sustained by nitrogen fixation. In addition, flux of detritus through the bottom boundary can be controlled by the denitrification ratio parameter ϕ.

Similarly, the governing equation for total phosphorous can be obtained by summing equations for substances that include phosphorous, and assuming Redfield stoichiometry where 16 μM-N of organic matter (P_1, P_2, Z, and D) corresponds to 1 μM-P. In the expanded model, the governing equation for total phosphorous concentration in the water column is given by

$$\frac{\partial}{\partial t}\left(\int_{-h}^{\eta} P_T \, dz\right) = 0 \tag{3.22}$$

where $P_T = DIP + r_{P/N}(P_1 + P_2 + Z + D)$. Phosphorous in the system is conservative because it is not subject to either nitrogen fixation or denitrification by bottom remineralization process. Nitrogen in the system is dissipative and depends on newly fixed nitrogen, whereas, phosphorous is conservative because it is instantaneously regenerated in the sediments in the model. The continuous regeneration of phosphorous maintains the production from the nitrogen fixer group which does not require dissolved inorganic nitrogen.

3.3.3. Equilibriums of expanded model

Primary production in the expanded model is controlled by two phytoplankton functional groups (normal phytoplankton and nitrogen fixer) and two different resources (dissolved inorganic nitrogen and phosphorous); resource competition between the two functional groups plays an important role in the net primary production. Population dynamics in the ecosystem are examined with steady-state solutions to the governing equations. The vertical advection terms related to vertical sinking of detritus can be scaled as

$$\frac{\partial(w_d D)}{\partial z} \approx -\frac{w_d}{h} D \tag{3.23}$$

which simplifies the governing equations into a system of ordinary differential equations. It is worth noting that this simplification well represents a sediment process that becomes negligible in deep regions. The simplified governing equations are given by

$$\frac{\partial DIN}{\partial t} = \delta D - U_1 P_1 + (1 - \phi)\frac{w_d}{h} D \tag{3.24}$$

$$\frac{\partial DIP}{\partial t} = r_{P/N}\left(\delta D - U_1 P_1 - U_2 P_2 + \frac{w_d}{h} D\right) \tag{3.25}$$

$$\frac{\partial P_1}{\partial t} = U_1 P_1 - \sigma_1 P_1 \tag{3.26}$$

$$\frac{\partial P_2}{\partial t} = U_2 P_2 - \sigma_2 P_2 \tag{3.27}$$

$$\frac{\partial D}{\partial t} = \sigma_1 P_1 + \sigma_2 P_2 - \delta D - \frac{w_d}{h} D \tag{3.28}$$

where zooplankton have been ignored to focus on primary production which sustains the ecosystem and the relative dominance between normal phytoplankton and nitrogen fixer groups. In addition, light limitations on growth rate for each phytoplankton group, equations (3.13) and (3.14), are not included because light intensity is an independent forcing variable and can be accounted for by assigning a different maximum growth rate coefficient.

It should be noted that the simplified system of equations (3.24) to (3.28) cannot resolve the vertical structure of the ecological tracers or the stratification, and is thus only applicable to well mixed environments that allow recycling of nutrients from deeper waters to the surface. When stratification is considerable and mixing between the surface euphotic layer and subsurface eutrophic later is limited (e.g., summertime in pelagic ocean), the simplified system cannot properly resolve the ecological dynamics. The simplified system is designed to examine the relative dominance between nitrogen fixers and normal phytoplankton when the phytoplankton group is sufficiently maintained by vertical mixing of nutrients and the importance of including a dominant bottom boundary process (i.e., denitrification). The simplified system consistently resolves the dynamics discussed in the previous section; the bottom boundary process is more dominant in the shallow regions than in deeper regions. In addition, total nitrogen is dissipative and determined by nitrogen fixation and denitrification, whereas total phosphorous is conservative and completely regenerated by remineralization of the bottom boundary process (also well resolved by the simplification).

3.3.3.1. Coexistent solution and limits for shallow and deep environments

Steady-state solutions that coexist with different functional groups can be established

when each species is limited by different resources (Tilman, 1977). Because nitrogen fixers are not limited by nitrogen, they should be limited by phosphorous, and normal phytoplankton should be limited by nitrogen to satisfy the coexistent condition. The nitrogen limitation for normal phytoplankton group can be mitigated by considerable denitrification. Steady-state concentrations of the coexistent equilibrium of the simplified system are given by

$$DIN = \frac{\sigma_1 k_{1,DIN}}{V_1 - \sigma_1} \tag{3.29}$$

$$DIP = \frac{\sigma_2 k_{2,DIP}}{V_2 - \sigma_2} \tag{3.30}$$

$$P_1 = \frac{\sigma_2 \left(1 + (1-\phi)\frac{w_d}{\delta h}\right)}{\sigma_2 \left(\frac{\sigma_1}{\delta} + 1 + (1-\phi)\frac{w_d}{\delta h}\right) + \sigma_1 \phi \frac{w_d}{\delta h}} \widetilde{N} \tag{3.31}$$

$$P_2 = \frac{\sigma_1 \phi \frac{w_d}{\delta h}}{\sigma_2 \left(\frac{\sigma_1}{\delta} + 1 + (1-\phi)\frac{w_d}{\delta h}\right) + \sigma_1 \phi \frac{w_d}{\delta h}} \widetilde{N} \tag{3.32}$$

$$D = \frac{\frac{\sigma_1 \sigma_2}{\delta}}{\sigma_2 \left(\frac{\sigma_1}{\delta} + 1 + (1-\phi)\frac{w_d}{\delta h}\right) + \sigma_1 \phi \frac{w_d}{\delta h}} \widetilde{N} \tag{3.33}$$

where $\widetilde{N} = (P_T - DIP)/r_{P/N}$. Steady-state equations for normal phytoplankton and nitrogen fixer concentration, (3.31) and (3.32), can be considered as Monod-type functions with $w_d/(\delta h)$ rewritten as h_c/h. It is worth noting that multiplying by the nondimensional denitrification ratio ϕ induces the nondimensional number $\phi w_d/(\delta h)$ that explicitly represents the relative dominance between denitrification rate $\phi w_d/h$ and remineralization rate δ. Equation (3.32) shows that the concentration of nitrogen fixers is zero when that nondimensional number is zero and increases as the ratio increases until the concentration is saturated (Figure 3.2). Normal phytoplankton concentration behaves in an opposite fashion, but the concentration does not converge to zero when the nondimensional number is infinitely large (Figure 3.2). The steady-state solutions clearly show that denitrification intensity

indicated by $\phi w_d/(\delta h)$ determines the relative dominance by the nitrogen fixer or normal phytoplankton.

In the shallow coastal ocean limit where h is much smaller than h_c and the nondimensional number $\phi w_d/(\delta h)$ goes to infinity (indicating considerable denitrification due to the shallow depth), nitrogen fixers can overcome phosphorous limitations because the growth of normal phytoplankton is suppressed by nitrogen limitation. In this scenario, nitrogen fixers increase and supply additional nitrogen to the system. The added nitrogen by the fixation process sustains the normal phytoplankton group by alleviating the nitrogen limitation. Consequently, the ecosystem in shallow regions contains negative feedback mechanisms that sustain both phytoplankton functional groups; nitrogen limitation of normal phytoplankton caused by denitrification triggers nitrogen fixation, and in turn the fixation decreases the nitrogen limitation.

In the deep pelagic ocean limit where h is much greater than h_c (the nondimensional number $\phi w_d/(\delta h)$ goes to zero), nitrogen loss from sediment denitrification processes becomes negligible and total nitrogen in the system is conservative. As a result, the growth of normal phytoplankton is seldom limited by nitrogen but phosphorous, thus both phytoplankton groups compete for phosphorous. When two different functional groups compete for one resource, they cannot coexist and only one group having better nutrient uptake ability can survive (Tilman, 1977).

The steady-state solutions above intrinsically assume that normal phytoplankton wins the phosphorous competition. For the normal phytoplankton group to be limited by nitrogen, that is condition for the coexistence, equation (3.13) requires that the condition

$$\frac{DIN}{DIN + k_{1,DIN}} < \frac{DIP}{DIP + k_{1,DIP}}. \tag{3.34}$$

is satisfied. Based on steady-state concentrations of nutrients, equations (3.29) and (3.30),

condition (3.34) can be rewritten as

$$\frac{\sigma_1 k_{1,DIP}}{V_1 - \sigma_1} < \frac{\sigma_2 k_{2,DIP}}{V_2 - \sigma_2}. \tag{3.35}$$

which indicates that normal phytoplankton wins based on the resource competition theory (Tilman, 1977). Condition (3.34) and (3.35) imply that normal phytoplankton must win phosphorous competition for themselves to be limited by nitrogen and to coexist with nitrogen fixer. The quantities on the left- and right-side hand of condition (3.35) represent the minimum phosphorous nutrient concentrations needed to sustain each functional group and are driven by the steady state balance between growth and mortality rates in the governing equations of each phytoplankton group, equation (3.26) and (3.27). The assumption that normal phytoplankton can survive in lower phosphorous nutrient environments than nitrogen fixers indicates that the normal phytoplankton will defeat nitrogen fixers in phosphorous competition. This is a reasonable assumption because normal phytoplankton functional groups are usually described as having overwhelming nutrient uptake ability but require both nitrogen and phosphorous; on the other hand, nitrogen fixers are described as being independent of nitrogen instead of on their competitive nutrient uptake ability (Neumann et al., 2002).

In this model, nitrogen fixers cannot be sustained in the deep pelagic limit where denitrification is negligible because normal phytoplankton outcompetes nitrogen fixers in the phosphorous competition. The absence of both nitrogen fixation and denitrification in the pelagic region implies that nutrients follow the Redfield ratio. It is worth noting that the governing equations of the expanded model converge onto those of the traditional NPZD model when denitrification and nitrogen fixations are absent, corresponding to dominant Redfield stoichiometry in the pelagic ocean.

3.3.3.2. Equilibriums for freshwater system

It is worthwhile to examine what happens if the nitrogen fixers defeat the normal phytoplankton in the phosphorous competition. If normal phytoplankton are defeated ($P_1 = 0$), steady-state concentrations of nitrogen fixers and detritus are given as

$$P_2 = \frac{1 + \frac{w_d}{\delta h}}{1 + \frac{\sigma_2}{\delta} + \frac{w_d}{\delta h}} \widetilde{N} \tag{3.36}$$

$$D = \frac{\frac{\sigma_2}{\delta}}{1 + \frac{\sigma_2}{\delta} + \frac{w_d}{\delta h}} \widetilde{N} \tag{3.37}$$

where phosphorous nutrient concentration of this equilibrium is identical with equation (3.30). Steady-state concentration of nitrogen nutrients are not determined. However, substitution of equations (3.36) and (3.37) into the governing equation of nitrogen nutrient, (3.24), yields

$$\frac{\partial DIN}{\partial t} = \frac{\left(1 + (1 - \phi)\frac{w_d}{\delta h}\right)}{1 + \frac{\sigma_2}{\delta} + \frac{w_d}{\delta h}} \sigma_2 \widetilde{N}. \tag{3.38}$$

Equation (3.38) indicates that nitrogen nutrient concentration linearly increases with time when the other state variables reach the steady-state condition. Figure 3.3 shows numerical solutions to the system; nitrogen nutrient concentration linearly increases and does not reach steady-state when condition (3.35) is not satisfied (in this case by decreasing V_1 from 1.5 to 0.2 day^{-1}). The equilibrium represents a phosphorous-limited and fixer-dominant environment with anomalously high nitrogen nutrient concentration, a situation that is rarely observed in the marine ecosystem but a common characteristic of freshwater ecosystems (Howarth et al., 1988; Doering et al., 1995; Turner et al., 2003). Because the model describes more competitive nutrient uptake ability by normal phytoplankton than by nitrogen fixers, additional limiting mechanisms are required in (3.13) for the freshwater equilibrium to be feasible as a stable solution, such as a salinity limitation for the normal phytoplankton group. In addition, a better description for the sink of nitrogen may be needed to prevent nitrogen nutrient concentrations

from increasing infinitely.

3.4. Application

3.4.1. Model configuration

The circulation system and biogeochemical cycle in marginal ocean of the northwest Pacific, including the Yellow Sea, a semi-closed marginal coastal ocean between China and Korea, are modeled with the Regional Ocean Modeling System (ROMS; Shchepetkim and McWilliams, 2005), that is one of the most popular ocean hydrodynamics models using the Boussinesq approximation, hydrostatic assumption, and sigma coordinate system. The expanded ecosystem model described in the previous section is implemented into ROMS and fully coupled with the hydrodynamics model, so the transport processes and vertical structures of ecological tracers are resolved (e.g., 3-dimensional advection and diffusion of the tracers and vertical decay of light intensity). Figure 3.4 shows the model domain and bathymetry. All model inputs and configurations are made by preprocessing toolbox provided by the Coastal and Regional Ocean Community (CROCO; both toolbox and datasets are available at https://www.croco-ocean.org/download/croco-project/). To be specific, horizontal and vertical resolution of the model are 1/4º and 20 sigma layers, respectively. Topography is interpolated from the ETOPO 2 dataset. Surface boundary conditions are obtained from the COADS monthly climatological dataset which includes momentum flux from wind stress, surface heat and freshwater fluxes (Woodruff et al., 1987). The monthly WOA2009 dataset is used as a lateral boundary condition (Boyer et al., 2009). Tidal forcing is resolved based on the TPXO7 dataset (Egbert and Erofeeva, 2002). We consider 14 major rivers in the study area, including the Yangtze River where discharge is several orders of magnitude larger than any of the other rivers (circles in Figure 3.4), based on dataset from Dai and Trenberth (2002). The Mellor-Yamada level 2.5 turbulence closure scheme is used. Simulations are initialed from a static

condition and run four years.

We also model ecosystem behavior with the traditional NPZD model (without denitrification in the bottom boundary) to compare with the expanded model that resolves non-Redfield dynamics. Rather than quantitative reconstruction of the ecological variables, the objective of the numerical experiments is to assess the qualitative difference between model with and without consideration of non-Redfield dynamics and determine whether the expanded models can properly resolve the productive coastal ecosystem.

3.4.2. Simulated ecosystem with and without non-Redfield dynamics

Figure 3.5a shows the simulated annual mean surface phytoplankton concentration in the last year obtained with the traditional NPZD model. The model renders an unrealistic oligotrophic water mass in the coastal region of the Yellow Sea. Anomalously high phytoplankton concentration is predicted to occur around the Yangtze River Estuary, but it is constrained locally and quickly dissipated. The other rivers rarely contribute to a productive coastal ecosystem. Coastal regions adjacent to the pelagic ocean are relatively productive because nutrients are upwelled from the subsurface aphotic layer. However, most marginal regions separated from the larger scale current system (except for the Changjiang Estuary) show low phytoplankton concentration. Figure 3.5b (inset) shows the time series of the integrated phytoplankton concentration from the pelagic regions where $h \geq 3h_c$ (solid blue line) and those from the shallow regions (but excluding the Changjiang Estuary region) where $h < 3h_c$ (dashed red line). High phytoplankton concentrations given by the initial conditions decay quickly and are not sustained by the model in the shallow coastal region (dashed red line in Figure 3.5b). On the other hand, in the pelagic region the traditional model shows a realistic variation of phytoplankton concentration associated with spring blooms (solid blue line in Figure 3.5b).

In contrast with traditional NPZD model, the expanded model considering non-Redfield dynamics (described herein) successfully resolves the productive water mass along shallow margins of the Yellow Sea (Figure 3.6a and b). Temporal variability of phytoplankton concentration for the pelagic region is nearly the same as with that predicted by the traditional NPZD model. This corresponds to the limit for the deep region in the coexistence equilibrium. In addition, the fraction of nitrogen fixers is higher in the shallow coastal regions than the deep ocean where the fraction trends toward zero (Figure 3.7), also in agreement with the coexistence equilibrium (Figure 3.2).

3.5. Discussion

In this study, it is shown that traditional NPZD ecosystem models predict unrealistic oligotrophic water masses in shallow regions where $h < h_c$ because of the absence of bottom boundary condition for the detritus. The traditional NPZD model is expanded by considering non-Redfield dynamics, including both denitrification and nitrogen fixation, that better accounts for productive coastal waters. The ecosystem of the Yellow Sea is chosen as an example to show how consideration of non-Redfield dynamics improves system behavior and shows realistic productive water mass along the marginal coastal region (Figures 3.5 and 3.6). Numerical simulation results agree with analytical steady-state equilibrium solutions and highlight how denitrification controls the relative the dominance between normal phytoplankton and nitrogen fixers through phosphorous resource competition. That is, the nitrogen fixing group can be sustained by denitrification processes which suppress the growth of the normal phytoplankton group; otherwise, the normal phytoplankton defeats the nitrogen fixer through phosphorous competition.

Assumptions are needed in order to solve the system of equations (e.g., ignoring advection and diffusion, and applied to unstratified, well-mixed environments). It is recognized

that it is possible that coastal ecosystems adjacent to the pelagic ocean (e.g., east coast of the Korean Peninsula) can be sustained by advection and diffusion of nutrients from the pelagic ocean even without nitrogen fixation (Figure 3.5). Nevertheless, the solutions using the simplifying assumptions highlight phosphorous competition between nitrogen fixers and normal phytoplankton under different intensities of denitrification (e.g., dominant nitrogen fixers in the shallow regions occur where there is strong denitrification), consistent with numerical simulation results that resolving the mechanisms ignored in the solutions (Figure 3.2 and 3.7). Many previous studies have reported significant phosphorous limitation in the Yellow Sea (Liu et al., 2003; Wang et al., 2003; Jang et al., 2018). Liu et al. (2003) showed that an additional phosphorous source is required to explain the primal production of the Yellow Sea and suggested a rapid recycling of phosphorous that corresponds to the bottom boundary condition of the expanded model. Recent observations also show that the shallow coastal region can be hotspot of nitrogen fixation (Tang et al., 2019), consistent with the expanded ecosystem model.

Equilibriums of the expanded model well reflect characteristics of estuarine, pelagic, and freshwater ecosystems. Figures 3.8, 3.9, and 3.10 show the phosphate-nitrate relationship based on in situ observations around the Korean Peninsula. The observations are obtained from three different datasets: Fisheries Environment Monitoring System dataset (available at http://www.nifs.go.kr/femo/), Serial Oceanographic Observation dataset (http://www.nifs.go.kr/kodc/soo_list.kodc), and Water Environment Information System (available at http://water.nier.go.kr/). The observations from the eastern ocean off the Korean Peninsula, connected to the deep pelagic system of the East Sea, show a linear relation between phosphate and nitrate approximating the well-known Redfield ratio (Figure 3.8) that corresponds with the deep pelagic limit for equilibrium. On the other hand, nitrate concentrations off the shallow western and southern regions of the Yellow Sea are frequently

over- and undersaturated than the Redfield ratio (Figure 3.9) implying the presence of both denitrification and nitrogen fixation processes. The coexistence equilibrium condition in the shallow region influenced by the non-Redfield dynamics agrees with the observations. Figure 3.10 shows observations from the riverine freshwater ecosystem. The extremely oversaturated nitrate concentration implies dominant nitrogen fixation and corresponds with the equilibrium condition when nitrogen fixers defeat normal phytoplankton in phosphorous competition.

3.6. Conclusions

In this work we describe a simple expanded ecosystem model that considers non-Redfield ratio dynamics and show that the expanded model alleviates chronic issue of traditional ecosystem models rendering unrealistic oligotrophic water in shallow region. Existing models that resolve non-Redfield dynamics are too complex to be discussed theoretically and it is difficult to ascertain the underlying dynamics. The theoretical approach of the expanded model in this study shows how the general marine ecosystem model is influenced by consideration of the non-Redfield dynamics (denitrification and nitrogen fixing) and reveals the underlying internal dynamics of the system; denitrification in the shallow region sustains nitrogen fixers by suppressing growth of normal phytoplankton, otherwise, normal phytoplankton defeats nitrogen fixers in phosphorous competition. The simple expanded model reveals important scale of depth h_c , determined by detritus sinking speed w_d and remineralization rate δ, which distinguish estuary ecosystem where non-Redfield dynamics are dominant and pelagic ecosystem where Redfield stoichiometry are dominant. It is worth noting that the simple expanded model uses fewer state variables and model coefficients than the more complex models, and thus has lower uncertainties induced by model parameters and is easily adaptable to other coastal regions. We highlight that the expanded model is readily incorporated into ROMS and can be provided to other researchers.

The model is appliable in the ocean where dominant non-Redfield dynamics occur, either through denitrification or nitrogen fixation. Furthermore, the solutions in this study elucidate important ecological dynamics: (1) nitrogen fixers can be sustained where there is considerable denitrification, such as in shallow coastal regions, because they can be successful in phosphate competition with normal phytoplankton whose growth is limited by denitrification; (2) normal phytoplankton defeat the nitrogen fixers in the pelagic region where there is negligible denitrification, and as a result, denitrification and nitrogen fixation become unimportant and nutrient concentrations follow the Redfield ratio; and (3) when nitrogen fixers defeat normal phytoplankton in phosphorous competition, nitrogen nutrients are accumulated and extremely oversaturated relative to phosphorous concentration, a situation that occurs in freshwater ecosystems.

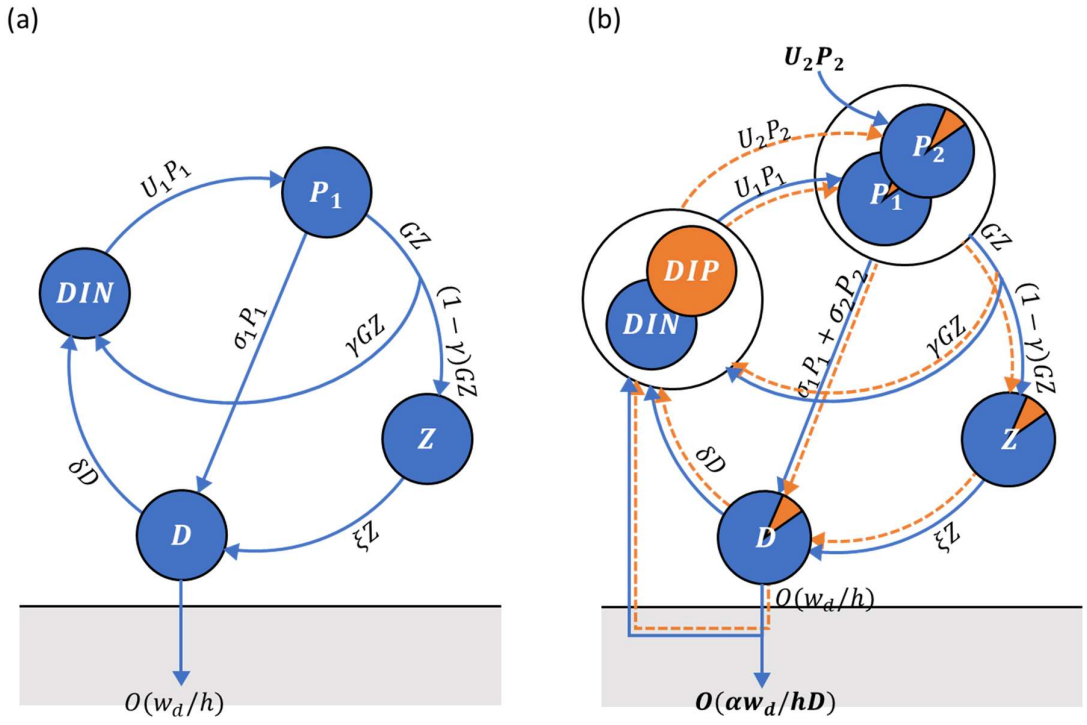

Figure 3.1. Schematics of traditional NPZD model (a) and expanded model considering non-Redfield dynamics (b). Blue solid arrow and orange dashed arrows in (b) indicates flow of nitrogen and phosphorous, respectively. Nitrogen fixers make organic matter including nitrogen without any consumption of nitrogen in the system, so their growth supply additional nitrogen into the system. Bottom sediment plays a role instantaneously remineralizing detritus and removing a portion of nitrogen in the detritus by denitrification.

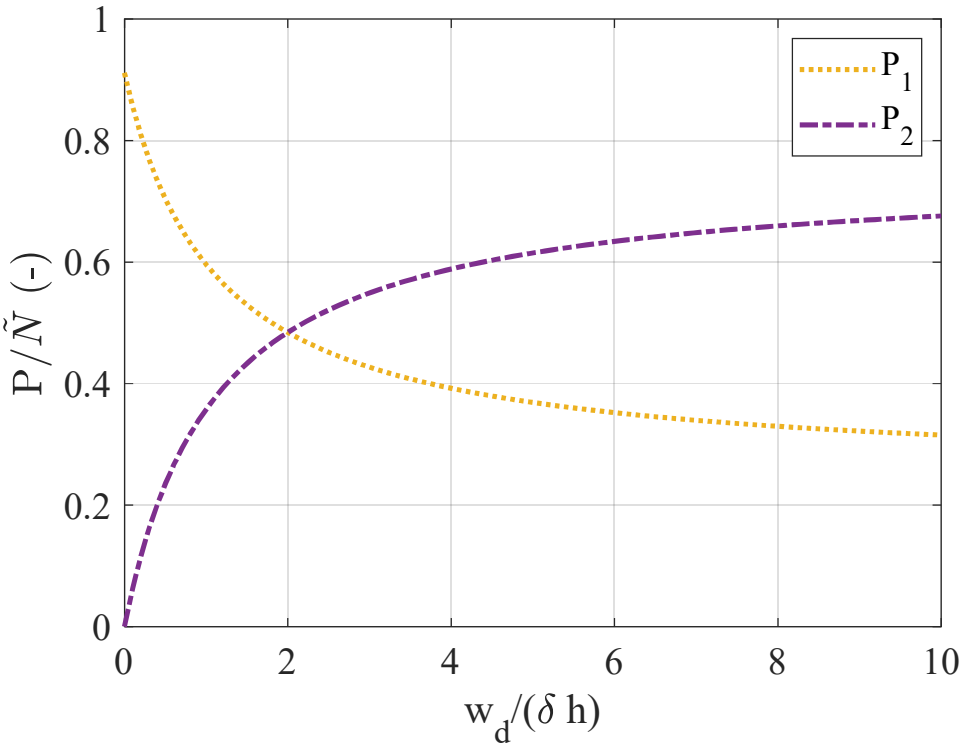

Figure 3.2. Steady-state concentrations of normal phytoplankton (blue) and nitrogen fixer (red) of coexistent equilibrium as nondimensional number h_c/h, which are normalized by $\widetilde{N}$. In the deep limit, nitrogen fixers concentration become zero. As depth decreases, fraction of nitrogen fixer increases and is saturated into maximum.

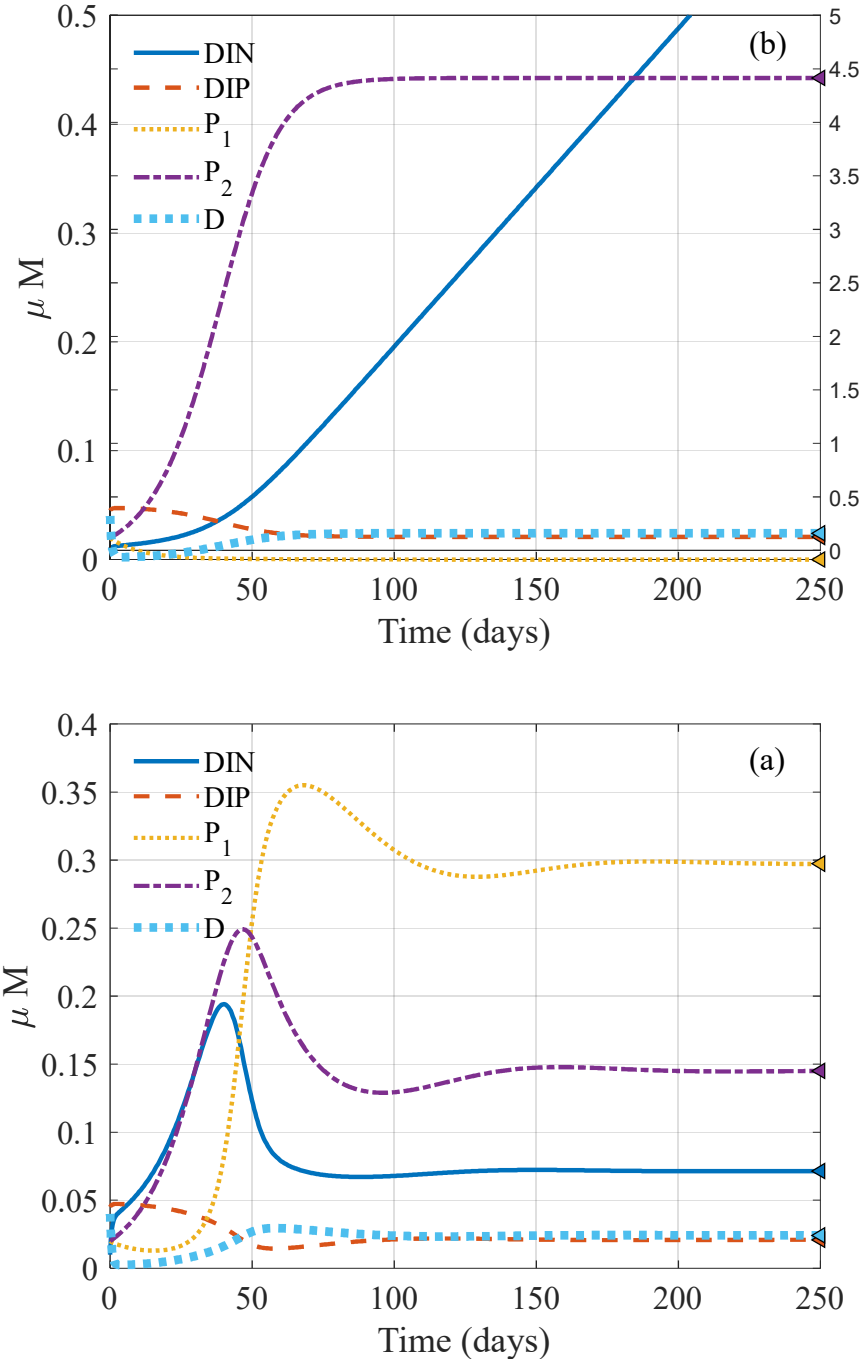

Figure 3.3. Numerical solution of system (21) when normal phytoplankton win phosphorous competition (a) and when nitrogen fixer win (b). The latter shows that DIN linearly increases when the other state variables reach steady-state condition.

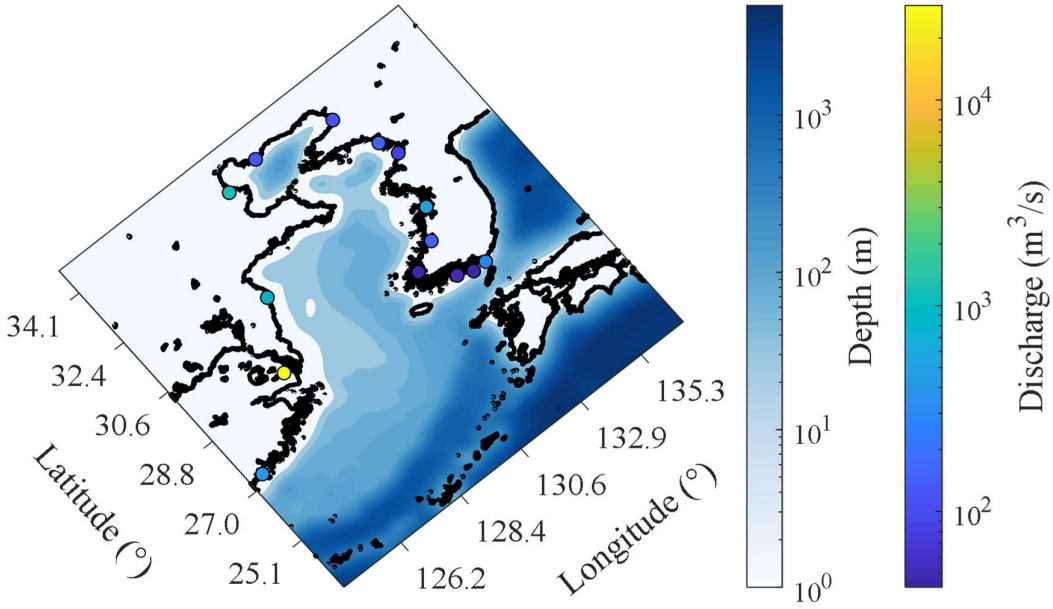

Figure 3.4. Model domain and bathymetry of the study area. Circles and their color indicate location of rivers considered by the model and discharge of the river, respectively.

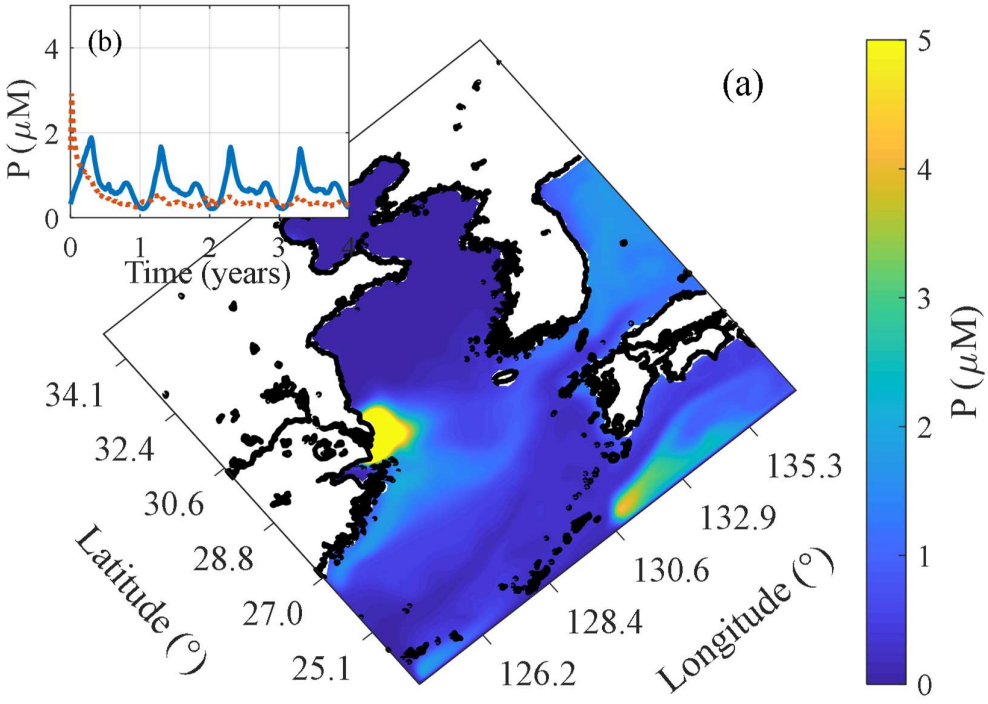

Figure 3.5. Simulated surface phytoplankton concentration by traditional NPZD model. The annual averaged spatial field during last year from operation (a) shows unrealistic oligotrophic water mass. Temporal variances of the concentration are reasonable in the pelagic region (solid blue line in (b)) but those in the shallow region excluding the Changjiang estuary region (dashed red line in (b)) is not properly sustained by the model.

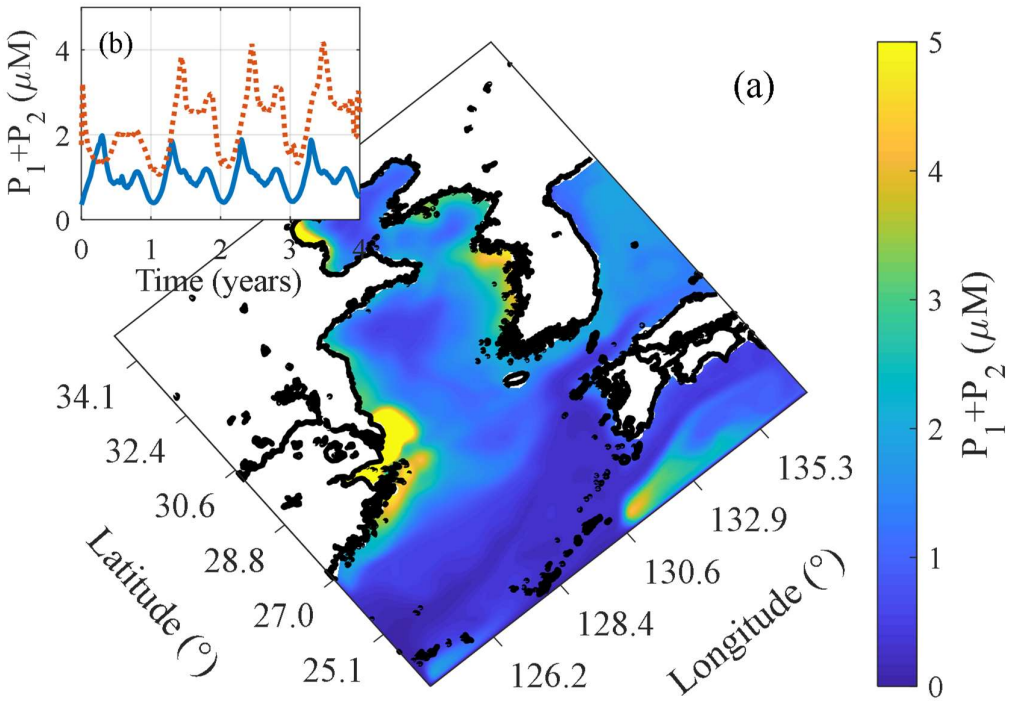

Figure 3.6. Simulated surface phytoplankton concentration by the expanded model resolving non-Redfield dynamics. The annual averaged spatial field during last year from operation (a) shows realistic productive water mass. Temporal variances of the concentration in the pelagic region are mostly identical with traditional NPZD model (solid blue line in (b)) and those in the shallow region excluding the Changjiang estuary region (dashed red line in (b)) is properly sustained by the model with reasonable order of magnitude what is higher than offshore region.

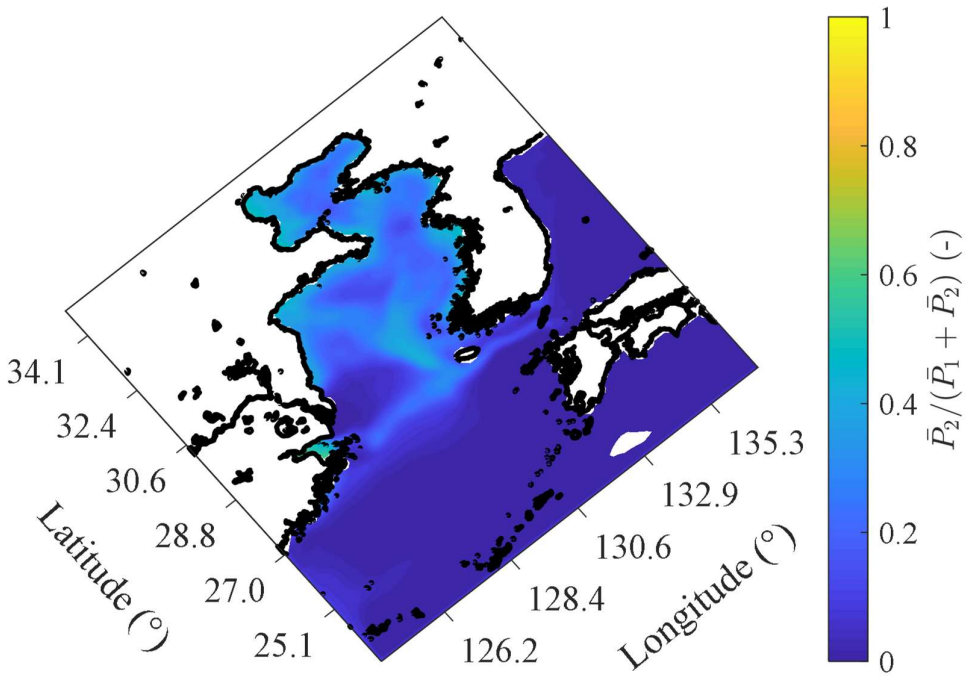

Figure 3.7. Fraction of nitrogen fixer concentration calculated by annual mean phytoplankton concentrations. Nitrogen fixers are relatively dominant in shallow region but not sustained in the pelagic region where denitrification is negligible.

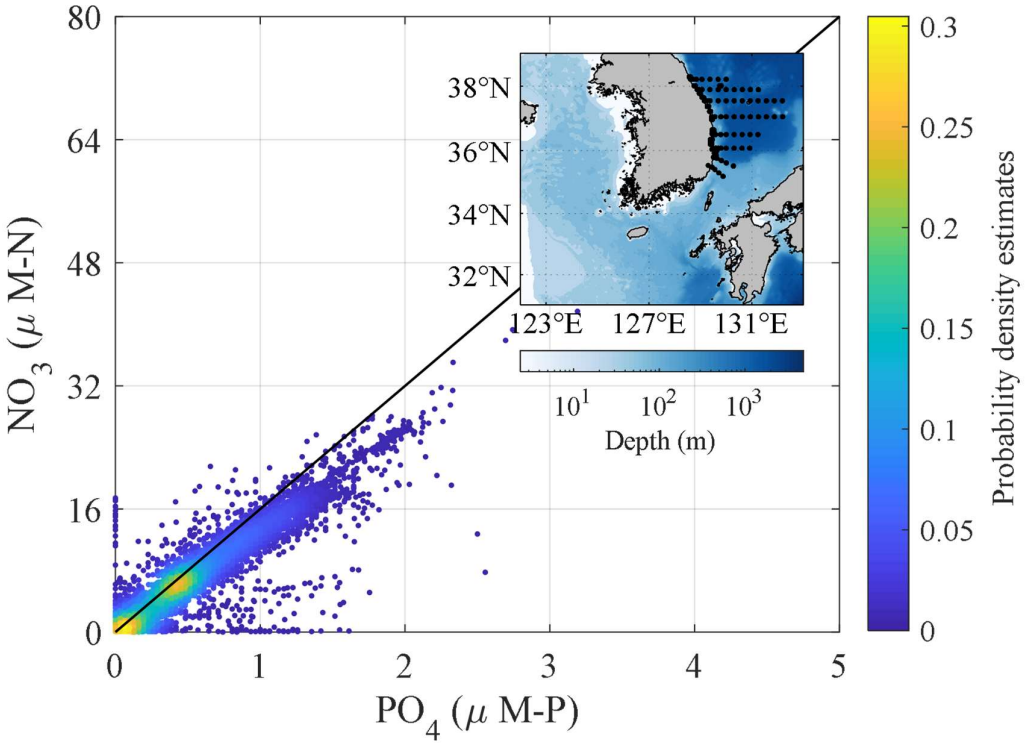

Figure 3.8. Phosphate-nitrate plot based on in situ measurements off the pelagic region (eastern ocean of the Korea; black dots). Black solid line indicates Redfield ratio (1:16). The observations show the Redfield ratio which corresponds deep pelagic limit of the coexistence equilibrium.

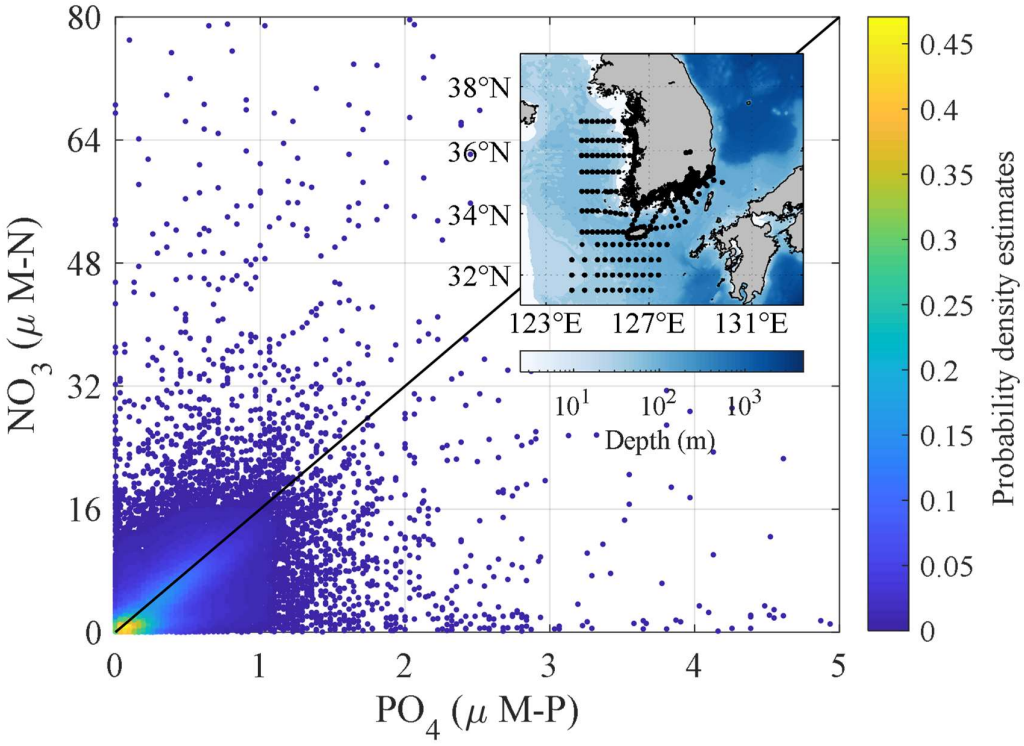

Figure 3.9. Phosphate-nitrate plot based on in situ measurements off the shallow region (western and southern oceans of the Korea; black dots). Black solid line indicates Redfield ratio (1:16). The observations imply presence of non-Redfield dynamics corresponding the shallow depth limit of equilibrium.

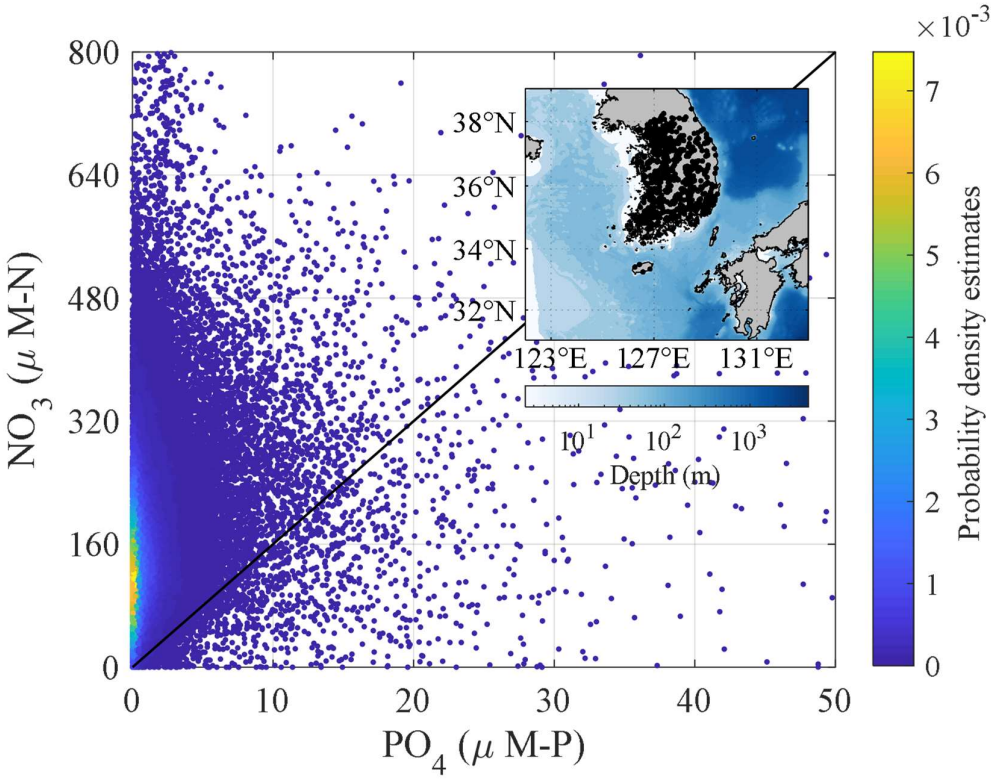

Figure 3.10. Phosphate-nitrate plot based on in situ measurements for freshwater environments of the Korean Peninsula. Black solid line indicates Redfield ratio (1:16). Nitrate concentrations are extremely oversaturated, that corresponds the equilibrium that can be established when nitrogen fixers win the phosphorous competition.

Coefficient name	Symbol	value	Unit
P_1 maximum growth rate	V_1	1.5	1/day
P_1 *DIN* half saturation concentration	$k_{1,DIN}$	1.0	μM-N
P_1 mortality rate	σ_1	0.1	1/day
P_1 initial slope of light sensitivity	α_1	0.025	$m^2W^{-1}\text{day}^{-1}$
Z maximum grazing rate	R_m	0.52	1/day
Z Ivlev constant	Λ	0.84	1/μM-N
Z excretion efficiency	γ	0.3	-
Z mortality rate	ξ	0.145	1/day
D remineralization rate	δ	1.03	1/day
D sinking speed	w_d	8.0	m/day

Table 3.1. Model coefficients of traditional NPZD model

Coefficient name	Symbol	value	Unit
P_1 DIP half saturation concentration	$k_{1,DIP}$	6.25×10^{-2}	μM-N
P_2 maximum growth rate	V_2	0.3	1/day
P_2 DIP half saturation concentration	$k_{2,DIP}$	1.25×10^{-1}	μM-N
P_2 initial slope of light sensitivity	α_2	0.008	$m^2W^{-1}\text{day}^{-1}$
P_2 mortality rate	σ_2	0.1	1/day
Phoshorous-nitrogen ratio	$r_{P/N}$	6.25×10^{-2}	mol-P/mol-N
Denitrification ratio	ϕ	0.75	-

Table 3.2. Additional coefficients of expanded model resolving non-Redfield dynamics

CONCLUSIONS

In this study, various models to describe HABs are developed. In chapter 1, diagnostic models based on observations are developed and used to quantify contributions to HABs by physical transport and environmental factors. The model consists of single equations where the influence of complex ecological dynamics are implicitly considered by direct usage of observations. Consequently, the governing equation for HABs are given as simple advection-diffusion-reaction equations where reaction rates are positive in shallow coastal region and negative in the deep pelagic region. The dynamics described by the system of equations are simple; if HABs dwell for a long time on the coastal region where there is a positive net growth rate, large HABs are triggered, whereas if HABs are quickly transported toward offshore net growth rates become negative then HABs decay and no bloom occurs. The modeling results show that contributions of physical transport and biological activities are of the same order, implying that the coupled ecosystem models that include hydrodynamic transport (as an additional sink term accounting for plankton advected laterally out of the system) are required to properly describe HAB behavior. Qin and Shen (2019) conducted similar numerical experiments and analytical analysis for *C. polykrikoides* bloom in the James River and concluded that the physical transport has identical or more significant contribution to the HABs than the biological processes, consistent with this study (Table 1.2). Similarly, previous studies argued that downwelling-favorable wind triggers HABs by aggregating cells (Lee, 2008; He et al., 2008), an example of where physical transport processes may outweigh biological processes. Among the environmental factors that contribute to HABs, nutrient concentration is pointed out as the most important factor limiting HABs. The model shows that limitation from phosphate and ammonium concentrations are more considerable than those from nitrate. These results using simple diagnostic model provides strategy for development of realistic HABs

model; the model is required to be coupled with hydrodynamics and biogeochemical model to resolve physical transport and nutrient environments.

Although the diagnostic model alludes to the importance of the nutrient concentration, one of the key limitations of the model is that it cannot explicitly resolve nonlinear prey-predation interactions between each state variable, such as nutrient depletion as phytoplankton grow, zooplankton predation, or resource competition with other functional group. In chapter 2, an ecosystem model is developed that modifies the traditional NPZD models by inclusion of HAB species and used to examine the nonlinear interactions between ambient ecosystem conditions and the HABs. To focus on the nonlinear interactions between components of the ecosystem, physical transports are ignored, and a closed system is assumed. In the model, HABs groups are designed to be functional groups having worse nutrient uptake ability and better predation avoidance than normal (non HAB) phytoplankton. The predation avoidance of HABs have been pointed out as a strong candidate mechanism triggering HABs by previous studies (Solé et al., 2006; Mitra and Flynn, 2006; Flynn, 2008; Harvey and Menden-Deuer, 2011 and 2012). In chapter 2 details of ecological dynamics caused by predation avoidance of HABs group are discussed. Theoretical studies show that HABs group cannot be sustained because they are defeated by normal phytoplankton in resource competition when predation pressure is weak. However, once predation pressure is considerable and zooplankton pumps significant nitrogen from the normal phytoplankton to the nutrient pool, HABs groups having better predation avoidance can be sustained by consuming nutrients increased by the zooplankton. Conditions for the predation pressure to sustain HABs group can be expressed as the total amount of currency (nitrogen) in the system that must exceed a threshold.

In the model proposed in chapter 2, NPZD model is induced as background ecosystem model and dynamics of closed cycle is discussed by ignoring detritus sinking term. However, the model is too simple to resolve complexity of the coastal ecosystem. In chapter 3, the

traditional NPZD model is expanded to better simulate realistic coastal ecosystem behavior by allowing for non-Redfield dynamics. Numerical experiments, which simulate a realistic coastal ecosystem resolving physical transport and biogeochemical cycles, show that consideration of non-Redfield dynamics revises the chronic problem inherent to traditional ecosystem models that render unrealistic oligotrophic water masses in shallow coastal waters of marginal ocean environments. The unrealistic oligotrophic water mass is a result of nitrogen in detritus that reaches the bottom boundary being transported out by a detritus sinking term. Consideration of the nitrogen fixation in the expanded model plays a role offsetting the nitrogen sinking mechanism and results in realistic productive water in the shallow region, consistent with observations.

The considerable nitrogen fixation does not appear in the pelagic region where bottom boundary processes are neglibile (including denitrification removing nitrogen) because the fixers are defeated by normal phytoplankton group in phosphate competition. As a result, in the pelagic region both nitrogen fixation and denitrification are greatly reduced, so nutrients follow Redfield ratios. On the other hand, in the shallow region where there is considerable denitrification, growth of normal phytoplankton is suppressed by nitrogen limitation, so nitrogen fixers become more competitive in phosphate competition. As a consequence, the two phytoplankton groups can coexist and contribute to productive water mass in the shallow regions. If nitrogen fixers defeat normal phytoplankton in the phosphate competition due to certain unresolved mechanisms not considered by the model (e.g., salinity limitation for normal phytoplankton), nitrogen nutrient in the system becomes extremely high, and corresponds with characteristics of a freshwater ecosystem. Consequently, the expanded model yields equilibrium conditions for pelagic, estuarine, and freshwater ecosystems. In addition, the model implies important ecological dynamics of non-Redfield processes; denitrification plays an important role determining nitrogen fixation by controlling phosphorous competition with

normal phytoplankton.

Several additional steps are needed before the models can simulate realistic HABs events that quantitatively compare with observations. The HABs model suggested in chapter 2 should be coupled with the expanded model in chapter 3 allowing for dynamics that link HABs species to shallow water effects (denitrification and nitrogen fixing) to be studied. In addition, refinement and adjustment of coefficients are needed. Although qualitative agreement between the models in this study and observations are discussed, the models cannot be used to hindcast or forecast real coastal ecosystems with HABs due to uncertainties associated with model coefficients. Systematic coefficient optimization techniques should be used to determine coefficients that are hard to estimate with observations. Nevertheless, the steady-state solutions and stability conditions – expressed as function of model coefficients – explicitly reveals the sensitivity of state variables to changes in model coefficients. More simple ecosystem models with fewer model coefficients are expected to be much efficient in the coefficient optimization.

The models herein are designed to be as simple as possible so that they may be analyzed theoretically. Excessive complexities do not guarantee high performance owing to errors associated with multiple inputs including model coefficients and initial/boundary conditions for each state variable. Furthermore, complexities obscure the important components of the internal dynamics of the system. The simple models that can be theoretically analyzed enhance understanding of system behavior and provide insight to the ecological processes even if performance of the simple model is worse than that of the complex model. Modeling approaches that incrementally add complexities step by step are useful and allow for improved understanding of the system itself and to find the best model with optimal complexity. The ecological dynamics of HABs and coastal ecosystem examined by simple models provide useful information to understand the driving phenomenon and can guide the development of complex models.

LIST OF REFERENCES

Anderson, D. M. (1995). Toxic red tides and harmful algal blooms: A practical challenge in coastal oceanography. Reviews of Geophysics, 33(S2), 1189–1200.

Anderson, D. M., Cembella, A. D., & Hallegraeff, G. M. (2012). Progress in Understanding Harmful Algal Blooms: Paradigm Shifts and New Technologies for Research, Monitoring, and Management. Annual Review of Marine Science, 4, 143–176.

Arrigo, K. R. (2005). Marine microorganisms and global nutrient cycles. Nature, 437(7057), 349–355.

Baek, S. H., Kim, Y., Lee, M., Ahn, C.-Y., Cho, K. H., & Park, B. S. (2020). Potential Cause of Decrease in Bloom Events of the Harmful Dinoflagellate Cochlodinium polykrikoides in Southern Korean Coastal Waters in 2016. Toxins, 12(6), 390.

Boyer, T. P., Antonov, J. I., Baranova, O. K., Garcia, H. E., Johnson, D. R., Mishonov, A. V., ... & Zweng, M. M. (2009). World ocean database 2009. NOAA Atlas NESDIS 66.

Brussaard, C. P. D. (2004). Viral control of phytoplankton populations - A review. Journal of Eukaryotic Microbiology, 51(2), 125–138.

Busenberg, S., Kumar, S. K., Austin, P., & Wake, G. (1990). The dynamics of a model of a plankton-nutrient interaction. Bulletin of Mathematical Biology, 52(5), 677–696.

Butenschön, M., Clark, J., Aldridge, J. N., Icarus Allen, J., Artioli, Y., Blackford, J., et al. (2016). ERSEM 15.06: A generic model for marine biogeochemistry and the ecosystem dynamics of the lower trophic levels. Geoscientific Model Development, 9(4), 1293–1339.

Cho, H.-Y., & Cho, B. J. (2014). Optimal Growth Model of the Cochlodinium Polykrikoides. Journal of Korean Society of Coastal and Ocean Engineers, 26(4), 217–224.

Choi, D. H., Yang, S. R., Hong, G. H., Chung, C. S., Kim, S. H., Park, J. S., & Cho, B. C.

(2005). Different interrelationships among phytoplankton, bacterial and environmental variables in dumping and reference areas in the East Sea. Aquatic Microbial Ecology, 41(2), 171–180.

Choi, J. K., Min, J. E., Noh, J. H., Han, T. H., Yoon, S., Park, Y. J., et al. (2014). Harmful algal bloom (HAB) in the East Sea identified by the Geostationary Ocean Color Imager (GOCI). Harmful Algae, 39, 295–302.

Cruz-Rico, J., & Rivas, D. (2018). Physical and biogeochemical variability in Todos Santos Bay, northwestern Baja California, derived from a numerical NPZD model. Journal of Marine Systems, 183, 63–75.

Cushman-Roisin, B., & Beckers, J.-M. (2011). Introduction to Geophysical Fluid Dynamics, Academic Press.

Dai, A., & Trenberth, K. E. (2002). Estimates of freshwater discharge from continents: Latitudinal and seasonal variations. Journal of hydrometeorology, 3(6), 660-687.

Davidson, K., Gowen, R. J., Harrison, P. J., Fleming, L. E., Hoagland, P., & Moschonas, G. (2014). Anthropogenic nutrients and harmful algae in coastal waters. Journal of Environmental Management, 146, 206–216.

Devol, A. H. (2015). Denitrification, anammox, and N2 production in marine sediments. Annual Review of Marine Science, 7, 403–423.

Doering, P. H., Oviatt, C. A., Nowicki, B. L., Klos, E. G., & Reed, L. W. (1995). Phosphorus and nitrogen limitation of primary production in a simulated estuarine gradient. Marine Ecology Progress Series, 124(1–3), 271–287.

Edwards, A. M. (2001). Adding Detritus to a Nutrient-Phytoplankton-Zooplankton Model: A Dynamical-Systems Approach. Journal of Plankton Research, 23(4), 389–413.

Elser, J. J., Bracken, M. E. S., Cleland, E. E., Gruner, D. S., Harpole, W. S., Hillebrand, H., et al. (2007). Global analysis of nitrogen and phosphorus limitation of primary producers in

freshwater, marine and terrestrial ecosystems. Ecology Letters, 10(12), 1135–1142.

Egbert, G. D., & Erofeeva, S. Y. (2002). Efficient inverse modeling of barotropic ocean tides. Journal of Atmospheric and Oceanic technology, 19(2), 183-204.

Eppley, R. W., Rogers, J. N., & McCarthy, J. J. (1969). Half-saturation constants for uptake of nitrate and ammonium by marine phytoplankton 1. Limnology and oceanography, 14(6), 912-920.

Fennel, K., Wilkin, J., Levin, J., Moisan, J., O'Reilly, J., & Haidvogel, D. (2006). Nitrogen cycling in the Middle Atlantic Bight: Results from a three-dimensional model and implications for the North Atlantic nitrogen budget. Global Biogeochemical Cycles, 20(3).

Fennel, W., & Neumann, T. (2004). Introduction to the Modelling of Marine Ecosystems.

Fiechter, J., Moore, A. M., Edwards, C. A., Bruland, K. W., Di Lorenzo, E., Lewis, C. V. W., et al. (2009). Modeling iron limitation of primary production in the coastal Gulf of Alaska. Deep-Sea Research Part II: Topical Studies in Oceanography, 56(24), 2503–2519.

Fistarol, G. O., Legrand, C., Selander, E., Hummert, C., Stolte, W., & Granéli, E. (2004). Allelopathy in Alexandrium spp.: effect on a natural plankton community and on algal monocultures. Aquatic Microbial Ecology, 35(1), 45–56.

Franks, P. J. S. (1997). Models of harmful algal blooms. Limnology and Oceanography, 42(5), 1273–1282.

Fulton, E. A., Smith, A. D. M., & Johnson, C. R. (2003). Effect of complexity on marine ecosystem models. Marine Ecology Progress Series, 253, 1–16.

Glibert, P. M. (2014). Harmful Algal Blooms in Asia: an insidious and escalating water pollution phenomenon with effects on ecological and human health. ASIANetwork Exchange: A Journal for Asian Studies in the Liberal Arts, 21(1), 52.

Glibert, P. M., & Burkholder, J. M. (2011). Harmful algal blooms and eutrophication:"strategies" for nutrient uptake and growth outside the Redfield comfort

zone. Chinese Journal of Oceanology and Limnology, 29(4), 724-738.

Gobler, C. J., Burson, A., Koch, F., Tang, Y., & Mulholland, M. R. (2012). The role of nitrogenous nutrients in the occurrence of harmful algal blooms caused by Cochlodinium polykrikoides in New York estuaries (USA). Harmful Algae, 17, 64–74.

Gobler, C. J., Doherty, O. M., Hattenrath-Lehmann, T. K., Griffith, A. W., Kang, Y., & Litaker, R. W. (2017). Ocean warming since 1982 has expanded the niche of toxic algal blooms in the North Atlantic and North Pacific oceans. Proceedings of the National Academy of Sciences, 114(19), 4975–4980.

Griffith, A. W., & Gobler, C. J. (2020, January 1). Harmful algal blooms: A climate change co-stressor in marine and freshwater ecosystems. Harmful Algae. Elsevier B.V.

Haidvogel, D. B., Arango, H., Budgell, W. P., Cornuelle, B. D., Curchitser, E., Di Lorenzo, E., et al. (2008). Ocean forecasting in terrain-following coordinates: Formulation and skill assessment of the Regional Ocean Modeling System. Journal of Computational Physics, 227(7), 3595–3624.

Hallegraeff, G. M. (1993). A review of harmful algal blooms and their apparent global increase. Phycologia, 32(2), 79–99.

Harvey, E. L., & Menden-Deuer, S. (2011). Avoidance, movement, and mortality: the interactions between a protistan grazer and Heterosigma akashiwo, a harmful algal bloom species. Limnology and oceanography, 56(1), 371-378.

Harvey, E. L., & Menden-Deuer, S. (2012). Predator-induced fleeing behaviors in phytoplankton: a new mechanism for harmful algal bloom formation?.

He, R., McGillicuddy, D. J., Keafer, B. A., & Anderson, D. M. (2008). Historic 2005 toxic bloom of Alexandrium fundyense in the western Gulf of Maine: 2. Coupled biophysical numerical modeling. Journal of Geophysical Research: Oceans, 113(7), 7040.

Hecky, R. E., & Kilham, P. (1988). Nutrient limitation of phytoplankton in freshwater and

marine environments: A review of recent evidence on the effects of enrichment. Limnology and Oceanography, 33(4part2), 796–822.

Heinle, A., & Slawig, T. (2013a). Internal dynamics of NPZD type ecosystem models. Ecological Modelling, 254, 33–42.

Heinle, A., & Slawig, T. (2013b). Impact of parameter choice on the dynamics of NPZD type ecosystem models. Ecological Modelling, 267, 93–101.

Heisler, J., Glibert, P. M., Burkholder, J. M., Anderson, D. M., Cochlan, W., Dennison, W. C., et al. (2008). Eutrophication and harmful algal blooms: A scientific consensus. Harmful Algae, 8(1), 3–13.

Hofmann, E. E., Cahill, B., Fennel, K., Friedrichs, M. A. M., Hyde, K., Lee, C., et al. (2011). Modeling the dynamics of continental shelf carbon. Annual Review of Marine Science, 3, 93–122.

Hoshiba, Y., Hirata, T., Shigemitsu, M., Nakano, H., Hashioka, T., Masuda, Y., & Yamanaka, Y. (2018). Biological data assimilation for parameter estimation of a phytoplankton functional type model for the western North Pacific. Ocean Science, 14(3), 371–386.

Howarth, R. W. (1988). Nutrient Limitation of Net Primary Production in Marine Ecosystems. Annual Review of Ecology and Systematics, 19(1), 89–110.

Howarth, R. W., & Marino, R. (2006). Nitrogen as the limiting nutrient for eutrophication in coastal marine ecosystems: Evolving views over three decades. Limnology and Oceanography, 51(1 II), 364–376.

Howarth, R. W., Marino, R., Lane, J., & Cole, J. J. (1988). Nitrogen fixation in freshwater, estuarine, and marine ecosystems. 1. Rates and importance. Limnology and Oceanography, 33(4part2), 669–687.

Hwang, D. W., Kim, G., Lee, Y. W., & Yang, H. S. (2005). Estimating submarine inputs of groundwater and nutrients to a coastal bay using radium isotopes. Marine Chemistry, 96(1–2),

61–71.

Jang, H. K., Kang, J. J., Lee, J. H., Kim, M., Ahn, S. H., Jeong, J. Y., et al. (2018). Recent Primary Production and Small Phytoplankton Contribution in the Yellow Sea during the Summer in 2016. Ocean Science Journal, 53(3), 509–519.

Jeong, H. J., Lim, A. S., Franks, P. J. S., Lee, K. H., Kim, J. H., Kang, N. S., et al. (2015). A hierarchy of conceptual models of red-tide generation: Nutrition, behavior, and biological interactions. Harmful Algae, 47, 97–115.

Jeong, H. J., Lim, A. S., Lee, K., Lee, M. J., Seong, K. A., Kang, N. S., et al. (2017). Ichthyotoxic Cochlodinium polykrikoides red tides offshore in the South Sea, Korea in 2014: I. temporal variations in three-dimensional distributions of red-tide organisms and environmental factors. Algae, 32(2), 101–130.

Jeong, H. J., Shim, J. H., Kim, J. S., Park, J. Y., Lee, C. W., & Lee, Y. (1999). Feeding by the mixotrophic thecate dinoflagellate Fragilidium cf. mexicanum on red-tide and toxic dinoflagellates. Marine Ecology Progress Series, 176, 263–277.

Jeong, H. J., Yoo, Y. Du, Kim, J. S., Kim, T. H., Kim, J. H., Kang, N. S., & YIH, W. (2004). Mixotrophy in the Phototrophic Harmful Alga Cochlodinium polykrikoides (Dinophycean): Prey Species, the Effects of Prey Concentration, and Grazing Impact. The Journal of Eukaryotic Microbiology, 51(5), 563–569.

Jin, D., Thunberg, E., & Hoagland, P. (2008). Economic impact of the 2005 red tide event on commercial shellfish fisheries in New England. Ocean and Coastal Management, 51(5), 420–429.

Kang, Y.-S., Park, Y.-T., Lim, W.-A., Cho, E.-S., Lee, C.-K., & Kang, Y.-S. (2009). A comparative study on outbreak scale of Cochlodinium polykrikoides blooms. The Sea, 14(4), 229–239.

Kim, C. J., Kim, H. G., Kim, C. H., & Oh, H. M. (2007). Life cycle of the ichthyotoxic

dinoflagellate Cochlodinium polykrikoides in Korean coastal waters. Harmful Algae, 6(1), 104–111.

Kim, C.-H., & Shin, J.-B. (1997). Harmful and Toxic Red Tide Algal Development and Toxins Production in Korean Coastal Waters. Algae, 12(4), 269–276.

Kim, D. Il, Matsuyama, Y., Nagasoe, S., Yamaguchi, M., Yoon, Y.-H., Oshima, Y., et al. (2004). Effects of temperature, salinity and irradiance on the growth of the harmful red tide dinoflagellate Cochlodinium polykrikoides Margalef (Dinophyceae). Journal of Plankton Research, 26(1), 61–66.

Kim, D. W., Jo, Y. H., Choi, J. K., Choi, J. G., & Bi, H. (2016). Physical processes leading to the development of an anomalously large Cochlodinium polykrikoides bloom in the East sea/Japan sea. Harmful Algae, 55, 250–258.

Kim, H. C., Lee, C. H., Lee, S. G., Kim, H. G., & Park, C. K. (2001). Physico-chemical factors on the growth of Cochlodinium polykrikoides and nutrient utilization. Korean Journal of Fisheries and Aquatic Sciences, 34(5), 445–456.

Kim, T. W., Lee, K., Lee, C. K., Jeong, H. D., Suh, Y. S., Lim, W. A., et al. (2013). Interannual nutrient dynamics in Korean coastal waters. Harmful Algae, 30(SUPPL.1), S15–S27.

Kishi, M. J., Kashiwai, M., Ware, D. M., Megrey, B. A., Eslinger, D. L., Werner, F. E., et al. (2007). NEMURO-a lower trophic level model for the North Pacific marine ecosystem. Ecological Modelling, 202(1–2), 12–25.

Koné, V., Machu, E., Penven, P., Andersen, V., Garçon, V., Fréon, P., & Demarcq, H. (2005). Modeling the primary and secondary productions of the southern Benguela upwelling system: A comparative study through two biogeochemical models. Global Biogeochemical Cycles, 19(4).

Kudela, R. M., Ryan, J. P., Blakely, M. D., Lane, J. Q., & Peterson, T. D. (2008). Linking the physiology and ecology of Cochlodinium to better understand harmful algal bloom events: A

comparative approach. Harmful Algae, 7(3), 278–292.

Kudela, R. M., Seeyave, S., & Cochlan, W. P. (2010). The role of nutrients in regulation and promotion of harmful algal blooms in upwelling systems. Progress in Oceanography, 85(1-2), 122-135.

Kwon, C. H., & Cho, K. D. (2002). Numerical Model for Spreading of Cochlodinium Bloom in the Southern Coastal Waters in Korea. Korean Journal of Fisheries and Aquatic Sciences, 35(6), 568–577.

Kwon, H. K., Kim, G., Han, Y., Seo, J., Lim, W. A., Park, J. W., et al. (2019). Tracing the sources of nutrients fueling dinoflagellate red tides occurring along the coast of Korea using radium isotopes. Scientific Reports, 9(1), 1–9.

Kwon, H.-K., Kim, H.-J., Yang, H.-S., & Oh, S.-J. (2014). Non-Outbreak Cause of Cochlodinium Bloom in the Western Coast of Jaran Bay in Summer, 2013 : On the Basis of Nutrient Data. Journal of the Korean Society of Marine Environment and Safety, 20(4), 372–381.

Laurent, A., Fennel, K., Hu, J., & Hetland, R. (2012). Simulating the effects of phosphorus limitation in the Mississippi and Atchafalaya river plumes. Biogeosciences, 9(11), 4707–4723.

Lee, C. K., Kim, H. C., Lee, S.-G., Jung, C. S., Kim, H. G., & Lim, W. A. (2001). Abundance of harmful algae, Cochlodinium polykrikoides, Gyrodinium impudicum and Gymnodinium catenatum in the coastal area of South Sea of Korea and their effects of temperature, salinity, irradiance and nutrient on the growth in culture. Korean Journal of Fisheries and Aquatic Science, 34(5), 536–544.

Lee, C. K., Park, T. G., Park, Y. T., & Lim, W. A. (2013). Monitoring and trends in harmful algal blooms and red tides in Korean coastal waters, with emphasis on Cochlodinium polykrikoides. Harmful Algae, 30(SUPPL.1), S3–S14.

Lee, D. K. (2008). Cochlodinium polykrikoides blooms and eco-physical conditions in the

South Sea of Korea. Harmful Algae, 7(3), 318–323. https://doi.org/10.1016/j.hal.2007.12.014

Lee, J., Park, K. T., Lim, J. H., Yoon, J. E., & Kim, I. N. (2018). Hypoxia in Korean coastal waters: A case study of the natural Jinhae Bay and artificial Shihwa Bay. Frontiers in Marine Science, 5, 70.

Lee, M. O., Choi, J. H., & Park, I. H. (2010). Outbreak conditions for Cochlodinium polykrikoides blooms in the southern coastal waters of Korea. Marine Environmental Research, 70(2), 227–238.

Lee, M. O., Kim, J. K., & Kim, B. K. (2016). Factors controlling the origin of Cochlodinium polykrikoides blooms along the Goheung coast, South Korea. Marine Pollution Bulletin, 113(1–2), 165–175.

Lee, Y. S. (2006). Factors affecting outbreaks of high-density Cochlodinium polykrikoides red tides in the coastal seawaters around Yeosu and Tongyeong, Korea. Marine Pollution Bulletin, 52(10), 1249–1259.

Lee, Y.-S., Lim, W.-A., & Lee, S.-G. (2007). Horizontal Distributions of Salinity and the Concentrations of DIN and DIP After Heavy Rainfall Events in Areas of Cochlodinium Polykrikoides Bloom Occurrence. The Korean Environmental Sciences Society, 16(10), 1119–1125.

Lewitus, A. J., Horner, R. A., Caron, D. A., Garcia-Mendoza, E., Hickey, B. M., Hunter, M., et al. (2012). Harmful algal blooms along the North American west coast region: History, trends, causes, and impacts. Harmful Algae, 19, 133–159.

Lim, A. S., Jeong, H. J., Jang, T. Y., Jang, S. H., & Franks, P. J. S. (2014). Inhibition of growth rate and swimming speed of the harmful dinoflagellate Cochlodinium polykrikoides by diatoms: Implications for red tide formation. Harmful Algae, 37, 53–61.

Lima, I. D., & Doney, S. C. (2004). A three-dimensional, multinutrient, and size-structured ecosystem model for the North Atlantic. Global Biogeochemical Cycles, 18(3).

Lin, X., Liu, M., Hou, L., Gao, D., Li, X., Lu, K., & Gao, J. (2017). Nitrogen Losses in Sediments of the East China Sea: Spatiotemporal Variations, Controlling Factors, and Environmental Implications. Journal of Geophysical Research: Biogeosciences, 122(10), 2699–2715.

Liu, S. M., Zhang, J., Chen, S. Z., Chen, H. T., Hong, G. H., Wei, H., & Wu, Q. M. (2003). Inventory of nutrient compounds in the Yellow Sea. Continental Shelf Research, 23(11–13), 1161–1174.

Mills, M. M., Moore, C. M., Langlois, R., Milne, A., Achterberg, E., Nachtigall, K., et al. (2008). Nitrogen and phosphorus co-limitation of bacterial productivity and growth in the oligotrophic subtropical North Atlantic. Limnology and Oceanography, 53(2), 824–834.

Mitra, A., & Flynn, K. J. (2006). Promotion of harmful algal blooms by zooplankton predatory activity. Biology Letters, 2(2), 194–197.

Neumann, T., Fennel, W., & Kremp, C. (2002). Experimental simulations with an ecosystem model of the Baltic Sea: A nutrient load reduction experiment. Global Biogeochemical Cycles, 16(3), 7-1-7–19.

Newberger, P. A., Allen, J. S., & Spitz, Y. H. (2003). Analysis and comparison of three ecosystem models. Journal of Geophysical Research: Oceans, 108(3).

Noh, J. H., Kim, W., Son, S. H., Ahn, J. H., & Park, Y. J. (2018). Remote quantification of cochlodinium polykrikoides blooms occurring in the East Sea using geostationary ocean color imager (GOCI). Harmful Algae, 73, 129–137.

Oh, S. J., Kim, H. J., Kwon, H. K., Yang, H.-S., & Kim, S. Y. (2015). Effect of Nutrients on Competition among the Harmful Dinoflagellates Cochlodinium polykrikoides and the Diatom Skeletonema sp. in Jaran Bay Using a Mathematical Model. The Sea, 20(2), 92–101.

Oh, S.-J., Kim, C.-H., Kwon, H.-K., & Yang, H.-S. (2010). Effects of Water Temperature, Salinity and Irradiance on the Growth of Harmful Dinoflagellate Cochlodinium polykrikoides

Margelef isolated from South Sea of Korea in 2008. Korean Journal of Fisheries and Aquatic Sciences, 43(6), 715–722.

Onitsuka, G., Miyahara, K., Hirose, N., Watanabe, S., Semura, H., Hori, R., et al. (2010). Large-scale transport of Cochlodinium polykrikoides blooms by the Tsushima Warm Current in the southwest Sea of Japan. Harmful Algae, 9(4), 390–397.

Onitsuka, G., Yanagi, T., & Yoon, J.-H. (2007). A numerical study on nutrient sources in the surface layer of the Japan Sea using a coupled physical-ecosystem model. Journal of Geophysical Research, 112(C5), C05042.

Padmakumar, K. B., Menon, N. R., & Sanjeevan, V. N. (2012). Is Occurrence of Harmful Algal Blooms in the Exclusive Economic Zone of India on the Rise? International Journal of Oceanography, 1–7.

Pajares, S., & Ramos, R. (2019). Processes and Microorganisms Involved in the Marine Nitrogen Cycle: Knowledge and Gaps. Frontiers in Marine Science, 6, 739.

Park, T. G., Lim, W. A., Park, Y. T., Lee, C. K., & Jeong, H. J. (2013). Economic impact, management and mitigation of red tides in Korea. Harmful Algae, 30(SUPPL.1), S131–S143.

Perruche, C., Rivière, P., Pondaven, P., & Carton, X. (2010). Phytoplankton competition and coexistence: Intrinsic ecosystem dynamics and impact of vertical mixing. Journal of Marine Systems, 81(1–2), 99–111.

Powell, T. M., Lewis, C. V. W., Curchitser, E. N., Haidvogel, D. B., Hermann, A. J., & Dobbins, E. L. (2006). Results from a three-dimensional, nested biological-physical model of the California Current System and comparisons with statistics from satellite imagery. Journal of Geophysical Research, 111(C7), C07018.

Priester, C. R., Melbourne-Thomas, J., Klocker, A., & Corney, S. (2017). Abrupt transitions in dynamics of a NPZD model across Southern Ocean fronts. Ecological Modelling, 359, 372–382.

Radtke, H., Lipka, M., Bunke, D., Morys, C., Woelfel, J., Cahill, B., et al. (2019). Ecological ReGional Ocean Model with vertically resolved sediments (ERGOM SED 1.0): Coupling benthic and pelagic biogeochemistry of the south-western Baltic Sea. Geoscientific Model Development, 12(1), 275–320.

Shchepetkin, A. F., & McWilliams, J. C. (2005). The regional oceanic modeling system (ROMS): A split-explicit, free-surface, topography-following-coordinate oceanic model. Ocean Modelling, 9(4), 347–404.

Sigman, D. M., & Hain, M. P. (2012). The Biological Productivity of the Ocean. Nature Education Knowledge, 3(6), 1–16.

Soetaert, K., & Herman, P. M. J. (2009). A Practical Guide to Ecological Modelling - Using R as a Simulation Platform. Springer Netherlands.

Solé, J., Garcia-Ladona, E., & Estrada, M. (2006). The role of selective predation in harmful algal blooms. Journal of Marine Systems, 62(1-2), 46-54.

Son, Y. B., Ishizaka, J., Jeong, J. C., Kim, H. C., & Lee, T. (2011). Cochlodinium polykrikoides red tide detection in the South Sea of Korea using spectral classification of MODIS data. Ocean Science Journal, 46(4), 239–263.

Stock, C. A., McGillicuddy, D. J., Solow, A. R., & Anderson, D. M. (2005). Evaluating hypotheses for the initiation and development of Alexandrium fundyense blooms in the western Gulf of Maine using a coupled physical-biological model. Deep-Sea Research Part II: Topical Studies in Oceanography, 52(19-21 SPEC. ISS.), 2715–2744.

Tang, D. L., Kester, D. R., Ni, I. H., Qi, Y. Z., & Kawamura, H. (2003). In situ and satellite observations of a harmful algal bloom and water condition at the Pearl River estuary in late autumn 1998. Harmful Algae, 2(2), 89–99.

Tang, W., Wang, S., Fonseca-Batista, D., Dehairs, F., Gifford, S., Gonzalez, A. G., et al. (2019). Revisiting the distribution of oceanic N 2 fixation and estimating diazotrophic contribution to

marine production. Nature Communications, 10(1), 1–10.

Tang, Y. Z., & Gobler, C. J. (2010). Allelopathic effects of Cochlodinium polykrikoides isolates and blooms from the estuaries of Long Island, New York, on co-occurring phytoplankton. Marine Ecology Progress Series, 406, 19–31.

Thushara, V., & Vinayachandran, P. N. (2016). Formation of summer phytoplankton bloom in the northwestern Bay of Bengal in a coupled physical-ecosystem model. Journal of Geophysical Research: Oceans, 121(12), 8535–8550.

Tilman, D. (1977). Resource Competition between Plankton Algae: An Experimental and Theoretical Approach. Ecology, 58(2), 338–348.

Turner, R. E., Rabalais, N. N., Justic, D., & Dortch, Q. (2003). Global patterns of dissolved N, P and Si in large rivers. Biogeochemistry, 64(3), 297–317.

Uchiyama, Y., Suzue, Y., & Yamazaki, H. (2017). Eddy-driven nutrient transport and associated upper-ocean primary production along the Kuroshio. Journal of Geophysical Research: Oceans, 122(6), 5046–5062.

van Opheusden, J. H. J., Hemerik, L., van Opheusden, M., & van der Werf, W. (2015). Competition for resources: complicated dynamics in the simple Tilman model. SpringerPlus, 4(1), 1–31.

Voss, M., Bange, H. W., Dippner, J. W., Middelburg, J. J., Montoya, J. P., & Ward, B. (2013). The marine nitrogen cycle: Recent discoveries, uncertaintiesand the potential relevance of climate change. Philosophical Transactions of the Royal Society B: Biological Sciences, 368(1621).

Wang, B. D., Wang, X. L., & Zhan, R. (2003). Nutrient conditions in the Yellow Sea and the East China Sea. Estuarine, Coastal and Shelf Science, 58(1), 127–136.

Wang, J., & Wu, J. (2009). Occurrence and potential risks of harmful algal blooms in the East China Sea. Science of the Total Environment, 407(13), 4012–4021.

Woodruff, S. D., Slutz, R. J., Jenne, R. L., & Steurer, P. M. (1987). A comprehensive ocean-atmosphere data set. Bulletin of the American meteorological society, 68(10), 1239-1250.

Xu, Q., Lin, H., Liu, Y., Lv, X., & Cheng, Y. (2008). Data assimilation in a coupled physical-biological model for the Bohai Sea and the Northern Yellow Sea. Marine and Freshwater Research, 59(6), 529.

Xue, Z., He, R., Fennel, K., Cai, W.-J., Lohrenz, S., & Hopkinson, C. (2013). Modeling ocean circulation and biogeochemical variability in the Gulf of Mexico. Biogeosciences, 10, 7219–7234.

Yamatogi, T., Sakaguti, M., Takagi, N., Iwataki, M., & Matsuoka, K. (2005). Effects of temperature, salinity and light intensity on the growth of a harmful dinoflagellate Cochlodinium polykrikoides Margalef occuring in coastal waters of West Kyushu, Japan. Bulletin of the Plankton Society of Japan, 52(1), 4–10.

Yang, J.-S., Choi, H.-Y., Jeong, H.-J., Jeong, J.-Y., & Park, J.-K. (2000). The Outbreak of Red Tides in the Coastal Waters off Kohung, Chonnam, Korea: 1. Physical and Chemical Characteristics in 1997. The Sea, 5(1), 16–26.

Zhou, Y., Zhang, Y., Li, F., Tan, L., & Wang, J. (2017). Nutrients structure changes impact the competition and succession between diatom and dinoflagellate in the East China Sea. Science of the Total Environment, 574, 499–508.

Zhu, W., Wang, C., Hill, J., He, Y., Tao, B., Mao, Z., & Wu, W. (2018). A missing link in the estuarine nitrogen cycle?: Coupled nitrification-denitrification mediated by suspended particulate matter. Scientific Reports, 8(1), 1–10.